Article:

Bacon, S.N., Jayko, A.S., Owen, L.A. et al. (4 more authors) (2020) A 50,000-year record of lake-level variations and overflow from Owens Lake, eastern California, USA. Quaternary Science Reviews, 238. 106312. ISSN 0277-3791

https://doi.org/10.1016/j.quascirev.2020.106312

A 50,000-year record of lake-level variations and overflow from Owens Lake, eastern California, USA

Steven N. Bacon†

Desert Research Institute, Reno, Nevada 89512, USA

Angela S. Jayko

U.S. Geological Survey, U.C. White Mountain Research Station, Bishop, California 93514, USA

Lewis A. Owen

Department of Marine, Earth, and Atmospheric Sciences, North Carolina State University, Raleigh, North Carolina 27695, USA

Scott C. Lindvall

Lettis Consultants International, Inc., Valencia, California 91335, USA

Edward J. Rhodes

Department of Geography, University of Sheffield, Sheffield, United Kingdom

David L. Decker

Rina A. Schumer

Desert Research Institute, Reno, Nevada 89512, USA

†Corresponding author. Tel.: +1 775 673 7473; fax.: +1 775 673 7485.

E-mail address: Steven.Bacon@dri.edu (S.N. Bacon).

Abstract

New stratigraphic and geotechnical studies were used to refine the lake-level and overflow history of Owens Lake in eastern California. A continuous lake-level curve, defined by 47 ^{14}C and 24 luminescence ages, was constructed by integrating lake-core data and wind-wave and sediment entrainment modeling of lake core sedimentology. The elevations of stratigraphic sites, plus lake bottom and spillway positions were corrected for vertical tectonic deformation using a differential fault-block model to estimate the absolute hydrologic change of the watershed-lake system. New studies include ^{14}C dating of mollusk shells in shoreline deposits, plus post-IR-IRSL dating of a suite of 5 beach ridges and OSL dating of spillway alluvial and deltaic deposits in deep boreholes. Geotechnical data show the overflow area is an entrenched channel that had soft sill elevations at ~1113–1165 m above sea level (asl). Owens Lake spilled most of the time at or near minimum sill levels controlled by a hard sill at ~1113 m asl developed on bedrock. Nine major transgressions at ~40.0, 38.7, 23.3, 19.3, 15.6, 13.8, 12.8, 11.6, and 10.5 ka reached levels ~10–45 m above the hard sill. Several major regressions at or below the hard sill from 36.9–28.5 ka, and at ~17.8, 13.1, and 10.5–8.8 ka indicate little to no overflow during these times. The latest period of overflow occurred ~8–20 m above the hard sill between ~8.4 and 6.4 ka that was followed by closed basin conditions after ~6.4 ka. Discrepancies in the timing of millennial-scale Northern Hemisphere climate-change signals between the shoreline record and lake-core proxies of Owens Lake were resolved through revising lake-core age-depth models by accounting for sediment compaction and applying a reservoir correction of 1 ka. Our integrated analysis provides a continuous 50 ka lake-level record of hydroclimate variability along the south-central Sierra Nevada that is consistent with other shoreline and speloethem records in the southwestern U.S.

Keywords: Late Pleistocene; Holocene; Owens Lake; Sierra Nevada; Paleoclimatology; Hydroclimatic variability; Lake-level reconstruction; Shorelines

1. Introduction

Paleo-lakes in the Great Basin of the western U.S. provide geomorphic and sedimentological records of climate and drainage-basin change. Lake levels in closed basins fluctuate in response to the balance between precipitation and evapotranspiration in the watershed and evaporation from the lake (Street-Perrott and Harrison, 1985). The sediments and landforms of pluvial lakes are sensitive recorders of these balances, thereby provide information on the magnitudes and rates of climatic change that influence lake level. Numerous geomorphic and exposure-based sedimentological studies in the Great Basin have focused on developing lake-level reconstructions (e.g., Reheis et al., 2014). These types of studies are commonly used to infer regional paleohydroclimate variability at multiple time scales (e.g., Mifflin and Wheat, 1979; Enzel et al., 1989; 2003; Broeker et al., 2009). The spatiotemporal distribution of paleolakes and lake-level histories in the southwestern U.S. have also been used as a proxy for migration of the North American polar jet stream (NAPJS) and associated hydroclimatic conditions between 35°N and 43°N to infer North Pacific atmospheric circulation patterns across the western U.S. during the late Quaternary (e.g., Enzel et al., 1989; 2003; Benson et al., 1990, 1995, 2003; Negrini, 2002; Zic et al., 2002; Lyle et al., 2012; Antinao and McDonald, 2013; Munroe and Laabs, 2013; Garcia et al., 2014; Kirby et al., 2014, 2015; Oster et al., 2015; Hatchett et al., 2019; McGee et al., 2018; Knott et al., 2019).

The Owens River-Lake system includes Owens Valley, an ~15–40 km wide and 200 km long tectonic graben within the southwestern Great Basin in eastern California (Fig. 1). The river-lake system is on the eastern escarpment of the south-central Sierra Nevada that forms one of the principal rain shadows in the western U.S. The highest part of the Sierra Nevada (crest elevations of 3400–4300 m) lies between ~36°N and 38°N and snowmelt runoff accounts for most of the annual streamflow in the watershed (Hollet et al., 1991). The entire range was heavily glaciated during the Pleistocene, and many small glaciers and snowfields persist in sheltered cirques at high elevations (Gillespie and Clark, 2011; Moore and Moring, 2013). A recent analysis of combining shoreline and lake-core proxy records of Owens Lake linked the hydrologic response of the Owens River-Lake system to two general patterns of hydroclimatic forcing during the Late Holocene. The analysis demonstrated that sand deposition (i.e., low stands) and glacial maxima occurred mostly during periods with persistent and higher hydroclimate variability, whereas mud deposition (i.e., high stands) occurred primarily during times with persistent and lower hydroclimate variability, that collectively have good temporal correspondence with global-scale climate change (Bacon et al., 2018). The physiographic and hydrologic setting of the Owens River-Lake system is optimally located in the southwestern U.S. to record long-term atmospheric circulation patterns that modulate streamflow and lake-level variations in the region (e.g., Redmond et al., 1991; Dettinger et al., 1998). Combining the older geomorphic and lacustrine sediment archives of Owens Lake into an integrated record of hydrologic change will provide a long-term dataset that can be used to validate and/or refine atmospheric circulation models developed from the spatiotemporal extent of paleolakes in the western U.S. (e.g., Lyle et al., 2012; Oster et al., 2015; Lachniet et al., 2014; McGee et al., 2018).

The primary goal of this investigation is to refine the Middle–Early Holocene to late Pleistocene portion of the lake-level record of Owens Lake previously developed by Bacon et al. (2006) and included in Reheis et al. (2014) to improve assessments of late Quaternary hydroclimate variability along the south-central Sierra Nevada (Fig. 1). This information is combined with improved shoreline and paleo-spillway reconstructions to better understand the influence of surface flow inputs to downstream basins that contained China and Searles Lakes within the paleo Owens River system (Fig. 1). Our objectives are five-fold: (1) to present new radiocarbon (^{14}C) and luminescence ages for beach ridges and shoreline stratigraphic sites in Owens Lake basin; (2) to use previously unpublished subsurface geotechnical data and luminescence ages from the overflow channel of Owens Lake to directly link shoreline and spillway levels; (3) to reconstruct the elevation of shorelines, spillway channels and lake bottoms to absolute positions by applying a differential fault-block model; (4) to estimate lake levels in the absence of shoreline evidence by applying wind-wave and sediment entrainment modeling of lake-core sedimentology to estimate threshold lake-water depth and produce a continuous lake-level curve; and (5) to evaluate temporal correspondence between the shoreline record and lake-core proxies of Owens Lake in identifying trends of hydroclimatic variability related to climate change over the past 50 ka at both watershed- and global-scales.

One of the significant new observations in our study is the occurrence of latest Pleistocene and Early Holocene shorelines that can be directly linked to spillway channel incision and show younger episodes of Owens Lake overflow during the Middle–Early Holocene than previously recognized. Gaining a better understanding of the spatiotemporal hydrologic connections between Owens Lake and downstream lakes of the paleo-Owens River system is the first step in assessing the hydroclimate variability of the south-central Sierra Nevada and region prior to watershed-lake paleohydrological modeling.

2. Background of paleo-Owens River system

2.1. Geologic and hydrologic settings

The Owens River watershed has a drainage area of ~8515 km^2 and is bounded by the crests of the Sierra Nevada on the west, White-Inyo Mountains on the east, and the Coso Range on the south and east. Crests of the Sierra Nevada and White-Inyo Mountains rise >3000 m above sea level (asl) above southern Owens Valley, with Mount Whitney (at an elevation of 4421 m asl) rising ~3280 m asl above the valley floor. The northern and southern parts of the watershed share drainage divides with the watersheds of Mono and China Lake basins, respectively. The northern reach of the Owens River is within the Long Valley caldera and its southern extent drains into Owens Lake (Fig. 1). During the period AD 1872–1878, Owens Lake was a perennial, closed-basin lake that covered >280 km^2 with a historical maximum lake level at 1096.4 m asl and a water depth of 14.9 m (Gale, 1914; Lee, 1915). Major water diversions in Owens Valley began after AD 1913 with construction of the Los Angeles aqueduct system that transported surface water from the Owens River watershed and Mono Lake basin (since AD 1941) >320 km to the south for distribution (Hollett et al., 1991). Owens Lake first began depositing salts onto the lake floor in AD 1921 because of these diversions, and by AD ~1931, Owens Lake had desiccated and become a playa (Smith and Bischoff, 1997).

Owens Lake occupies a topographically closed basin contained by a modern spillway across its drainage divide (i.e., sill) at the south end of the basin. During much of the Pleistocene, Owens Lake was a perennial freshwater lake that periodically overflowed its sill to form a chain of pluvial lakes occupying one or more of four successively lower-elevation lake basins during periods with greater moisture flux and cooler temperatures across the region (Gale, 1914; Smith and Street-Perrott, 1983; Jannik et al., 1991; Menking, 1995; Phillips, 2008; Knott et al., 2019) (Fig. 1). Shoreline and sediment-core records from lakes in the paleo-Owens River system indicate that pluvial Owens Lake had relatively high water levels during the late Pleistocene coinciding with deglaciations and exceptionally wet periods in the Sierra Nevada. Owens Lake has previously been inferred to have overflowed into China-Searles and Panamint Lakes, as many as 2 to 3 times between 15 and 12 ka (Benson et al., 1996, 1997; 1998; 2002; Phillips et al., 1996; Smith et al., 1997; Bishoff and Cummins, 2001; Jayko et al., 2008; Orme and Orme, 2008; Phillips, 2008; Rosenthal et al., 2017; Knott et al., 2019) (Fig. 1). Previous research also inferred that overflow from Owens Lake to support downstream lakes likely ceased after 11–12 ka based on shoreline stratigraphic studies in China Lake basin (Rosenthal et al., 2017). Owens Lake was considered to be the terminal lake in the system during the Holocene with mostly moderate to shallow water levels into historical times according to geomorphic shoreline records (Bacon et al., 2006; 2018) and lake-core evidence (Newton, 1991; Smith et al., 1997; Li et al., 2000; Smoot et al., 2000; Benson et al., 2002).

2.2. Neotectonic setting

Tectonic forces in extensional regimes generally act to create internally drained basins separated by highlands or mountain ranges (e.g., Peterson, 1981). Orographic focusing of precipitation on uplands creates runoff that supports lakes or wetlands in basins during periods with greater moisture flux (e.g., Cohen, 2003). Drainage-basin integration can be thought of as the balance between climate and tectonics, with climate-driven processes acting to fill a basin with sediment and tectonics acting to create both accommodation space through subsidence in depocenter areas and either uplift or subsidence of spillways (e.g., Reheis et al., 2014). The physiography of the paleo-Owens River drainage reflects active tectonic processes associated with several north- to northwest-striking principal strike-slip faults and northeast-striking connecting normal faults that collectively accommodate ~20–25% of right-lateral shear inboard of the San Andreas plate boundary along a regional zone at the western edge of the extensional Basin and Range Province (e.g., Argus and Gordon, 1991; Wernicke et al., 2000; Fig. 2). This zone of right-lateral shear is locally accommodated by clockwise rotation of crustal blocks that has produced structural basins and oblique components of slip that are commonly partitioned into subparallel strike-slip and dip-slip faults (Wesnousky, 2005a,b). The regional zone north of the Garlock fault is known as the southern Walker Lane belt (WLB) and consists of three major subparallel strike-slip fault systems that have helped formed lake basins: the Death Valley-Fish Lake Valley, Hunter Mountain-Panamint Valley, and Owens Valley-Little Lake fault zones (e.g., Dokka and Travis, 1990; Wesnousky, 2005a; Fig. 2).

Owens Valley is a region of active tectonics, as demonstrated by the M_w7.5–7.9 AD 1872 Owens Valley earthquake (Beanland and Clark, 1994; Hough and Hutton, 2008; Haddon et al., 2016). Owen Lake basin is crossed by five principal faults that collectively have formed a well-developed, pull-apart basin with a deep, rhombus-shaped depocenter area developed by dextral-oblique faulting (Slemmons et al., 2008). Faults in the lake basin include the range-bounding normal SNFF on the west and the dextral-oblique southern Inyo Mountains fault (SIMF) on the east, plus the active dextral-oblique OVF along the axis of the valley and lake basin (Fig. 3). The southern section of the OVF extends along the entire western margin of the lake basin. During the AD 1872 earthquake, normal-oblique displacements produced subsidence in the depocenter area of Owens Lake that created a seismic seiche, raised the western shoreline, and shifted the position of the eastern shoreline of the lake several hundred meters to the west (Smoot et al., 2000). Other faults that accommodate slip within the pull-apart basin are the normal Owens River-Centennial Flat fault (OR-CFF) and normal Keeler fault (KF) (Fig. 3).

Deformation of shorelines in Owens Lake basin is commonly expressed as fault offsets, short lengths of monoclinal warping, and broad warping or uniform tilting (Carver, 1970). Two of the oldest and highest shorelines in Owens Valley are primarily erosional but include a few preserved constructional features that show progressive deformation. Elevations of the two shorelines referred to as the 1160 and 1180 m asl shorelines have dates of 40.0 ± 5.8 ka and 160 ± 32 ka that are both lower on the east side of the lake basin at ~1155 and 1180 m asl and higher on the west side at ~1165 and 1200 m asl, respectively (Jayko and Bacon, 2008; Bacon et al., in review).

3. Materials and methods

Studies that construct lake-level curves use a variety approaches with a range of uncertainties, but all involve plotting the age of landforms and/or deposits with respect to altitude to constrain the position of water levels from either specific stratigraphic facies and fossils (e.g., Stine, 1990; Oviatt, 1997; Bacon et al., 2006; Adams, 2007; Bartov et al., 2007; Reheis et al., 2014) or carbonate (tufa) deposits (e.g., Benson et al., 2013; Hudson et al., 2017).

3.1. Radiocarbon dating

We integrated 47 new and previously published radiocarbon (^{14}C) ages from Owens Lake to refine prior reconstructions of water levels for the lake over the last 50 ka. Thirteen previously unpublished accelerator mass spectrometry (AMS) ages from samples of aquatic and semi-aquatic bivalve and gastropod shells, ostracode valves, lithiod tufa (carbonate), and charcoal from Owens Lake basin and its overflow channel are from this study and Black and Veatch (2013), whereas 34 previously published AMS and conventional ages from similar material, plus carbonized wood and organic sediment (bulk organic carbon) from around the basin were collectively used in our study to reconstruct a refined lake-level curve of Owens Lake (Beanland and Clark, 1994; Koehler, 1995; Bacon et al., 2006, 2018; Bacon and Pezzopane, 2007; Orme and Orme, 2008) (Table 1).

3.1.1. Radiocarbon reservoir effects

Previous studies have demonstrated the potential uncertainty in using ^{14}C ages from tufa and shell to define the age of shoreline features and deposits because these types of carbonate materials can be contaminated by either younger, post-depositional carbon from either meteoric water and pedogenic processes or by syndepositional older carbon in ground-water fed spring and lake waters (e.g., Lubetkin and Clark, 1988; Benson, 1993; Bischoff et al., 1993; Brennan and Quade, 1997; Pigati et al., 2004; Rosenthal et al., 2017). Some species of semi-aquatic gastropods that live in springs, rivers, and lakes are more suitable for radiocarbon dating because their shells are relatively less susceptible to contamination with older carbon compared to fully aquatic mollusks (e.g., Brennan and Quade, 1997; Pigati et al., 2004; Rosenthal et al., 2017).

A detailed analysis on the paleoenvironmental conditions and suitability of aquatic and semi-aquatic mollusks for ^{14}C dating was performed on samples from China Lake basin and Salt Wells Valley by Rosenthal et al. (2017; Fig. 1). Their study provides important paleoenvironmental information and insight on the potential reservoir correction required to account for the hard water effects from ambient ^{14}C-depleted carbon for the overall paleo-Owens River system. The study of Rosenthal et al. (2017) concluded that ^{14}C determinations from tufa and aquatic and semi-aquatic mollusk shells may be as much as 140–350 years older than the true age of the samples. The magnitude of reservoir effects for China Lake basin and Salt Wells Valley tufa and shell is similar to the reservoir correction of 330 years for tufa at the highstand shoreline in nearby Searles Lake basin based on comparisons between ^{14}C and ^{230}Th/^{234}U ages

(Peng et al., 1978; Lin et al., 1998) (Fig. 1). In addition to tufa and shell requiring a reservoir correction, bulk samples of carbonate-rich lacustrine mud (marl) ^{14}C dated in several Owens Lake sediment cores (OL-84B and OL-97) had a reservoir effect of 600–1000 yr (Benson et al., 1998a; Smoot et al., 2000; Benson et al., 2002; Benson, 2004). A reservoir effect of 1000 yr was later confirmed by temporal correspondence between the age of lake expansion inferred from lake cores and the Late Holocene shoreline chronology of Owens Lake that was determined by ^{14}C ages from charcoal and luminescence ages from sands in beach ridge deposits (Bacon et al., 2018).

In contrast to previously published lake-level curves for Owens Lake (e.g., Bacon et al., 2006; Reheis et al., 2014), Searles Lake (Smith, 2009; Knott et al., 2019), and Panamint Lake (Jayko et al., 2008) that did not incorporate a reservoir correction to ^{14}C ages because of the uncertainty and lack of confident reservoir corrections for each lake basin, we accept the reservoir corrections of Lin et al. (1998) and Rosenthal et al. (2017) as reasonable estimates for the magnitude of reservoir effects in the paleo-Owens River system. A reservoir correction, however, was used in the development of the lake-level curve of China Lake (Rosenthal et al., 2017). As a result, a uniform reservoir correction of 300 years was applied prior to calibrating ^{14}C ages from aquatic and semi-aquatic mollusk shells, ostracod valves, tufa, oolitic sand, and marl samples used in our study to refine the lake-level curve of Owens Lake. Conventional ^{14}C ages are reported in radiocarbon years before present (^{14}C yr BP) and have been calibrated to calendar years before present (cal yr BP) using the CALIB7.1 program (Stuiver and Reimer, 1993; Stuiver et al., 2017) with the IntCal13 data set (Reimer et al., 2013) (Table 1).

3.2. Luminescence analysis

Luminescence dating determines the last process of sediment reworking and therefore enables the direct age determination of the depositional age of sediment (Rhodes, 2011). Two methods of luminescence dating were used in this study including: post-infrared infrared stimulated luminescence (post-IR-IRSL) and optically stimulated luminescence (OSL) that require sand-sized mineral grains of feldspar and quartz, respectively. We also used previously published post-IR-IRSL dates from several shorelines that are Late Holocene in age (Bacon et al., 2018) and Late Pleistocene in age (~40 ka) (Bacon et al., in review).

3.2.1. Post-infrared infrared stimulated luminescence dating

We used post-IR-IRSL analysis to directly date sediments of a previously undated suite of five prominent beach ridges at Centennial Flat (Table 2). The crests of the sampled beach ridges are at elevations of ~1114, 1120, 1127, 1129, 1131 m asl. A total of 10 samples were collected in light-resistant plastic tubes driven horizontally into sand-rich horizons in cleaned, natural exposures along shallow channels cut across each beach ridge. Duplicate samples were taken from the ~1114, 1120, 1127, and 1129 m beach ridges, whereas a single sample could only be recovered from the ~1131 m beach ridge due to hard consistency of sediment, in addition to an additional sample from the ~1127 m beach ridge. Samples were prepared and processed at the University of California, Los Angeles (UCLA) Luminescence Laboratory. Dating was based on the post-$IRSL_{225}$ single-grain luminescence dating method (Rhodes, 2015). This method has been used recently in Owens Lake basin to date aeolian and shoreline deposits lacking suitable quartz (e.g., Bacon et al., 2018; Bacon et al., in review) and enables accurate dating of feldspar grains with a precision equal in many cases to radiocarbon analysis of detrital charcoal for Holocene deposits – thereby allowing the dating of previously undateable strata and landforms. Rhodes (2015) and Supplement 2 provide descriptions of the post-$IRSL_{225}$ technique and analysis.

3.2.2. Optically stimulated luminescence dating

OSL analysis of sediment sampled during a geotechnical investigation in the northern end of the Owens Lake overflow channel (Black and Veatch, 2013), and prepared and processed at the Luminescence Dating Laboratory at the University of Cincinnati, are used to define the age of potential overflow episodes. The samples were collected from fluvial-deltaic (channel fill) sedimentary facies of undisturbed cores from a deep borehole drilled within the overflow channel (Samples HD 1, 2, and 3), as well as alluvial/colluvial sedimentary facies in steel tubes driven horizontally into sand-rich horizons in cleaned, deep excavations on colluvial slopes along the eastern margin of the overflow channel (Samples HD 6, 7-1, 7-2, and 9) (Table 3). Dating was based on the single-aliquot regenerative-dose (SAR) OSL dating method (e.g., Murray and Wintle, 2000, 2003). Supplement 3 provides detailed descriptions of the OSL technique and analysis.

3.3. Paleolake water-level reconstruction

Sedimentologic and geomorphic indicators of former lake levels can be accurately measured across broad areas and preserved for millennia, thus allowing reconstruction of long paleoclimate records provided tectonic effects and/or isostatic rebound can either be assessed or corrected (Reheis et al., 2014). Most geomorphic and geologic studies focused on reconstructing lake levels are either limited to periods with relative highstands because of a lack of preserved landforms and outcrop evidence for lower water levels (e.g., Adams, 2007; Bartov et al., 2007) or rely on inferences from stratigraphy exposed in lower parts of lake basins without shoreline data (e.g., Negrini et al., 2006). Lacustrine sediment cores are also useful in identifying changes in relative lake levels from proxy evidence (e.g., sediment size, geochemistry, biology) (e.g., Benson, 2004), but there is large uncertainty in use of proxy evidence to infer corresponding water depths and associated water levels (e.g., Smith, 1997; Reheis et al., 2014). As a result, we applied the methods of Bacon et al. (2018) to estimate lake levels in the absence of shoreline evidence by integrating new shoreline data and previously published shoreline and lake core data sets from Owens Lake with threshold lake-water depth estimates from wind-wave and sediment entrainment modeling of lake core sedimentology. This integrated approach was previously shown to be suitable in producing a continuous ~4000-yr lake-level record of Owens Lake during the Late Holocene that agreed well with proxy evidence of wet and dry periods from tree-ring and glacial records within the watershed, as well as showed the timing, duration, and magnitude of hydroclimate variability.

3.3.1. Geomorphic shoreline and sedimentary datasets

Documentation of shoreline features in Owens Lake basin and channel fill and alluvium at the overflow channel were based on field observations and mapping of the lacustrine and alluvial geomorphology and bedrock geology at each site. The aerial extent and identification of landforms and related features (e.g., wave-formed scarps, beach ridge crests), as well as subsurface stratigraphy were confirmed from georeferenced satellite imagery in a geographic information systems (GIS) platform, from numerous natural exposures, several exploratory trenches, and several deep geotechnical borings. Lacustrine landforms were classified following the categorization schemes of Peterson (1981) and Otvos (2000). We made field descriptions of deposits from cleaned, natural exposures to establish lacustrine and alluvial sequence stratigraphy and sedimentological characteristics. Lithofacies and facies associations were classified in the field according to grain size, sedimentary structure, and as lateral and vertical stratigraphic position (e.g., Einsele, 2000).

Elevation control at new and previously published shoreline sites in Owens Lake basin (Table 2) was determined in our study with a Trimble GPS Pathfinder® ProXRT receiver with differential correction services. Measurements of elevation during surveying had a vertical accuracy of ±80 cm. Landforms reported in previous studies were resurveyed to keep elevation data within the same georeferenced frame and to minimize the error associated with different surveying methods. Previous studies had elevation control based on either total-station surveys (Orme and Orme, 2008; Slemmons et al., 2008) or hand-held GPS units cross-checked with 1:24,000 topographic quadrangle maps and 10-m-digital elevation models (DEMs) (Bacon et al., 2006; Jayko and Bacon, 2008; Reheis et al., 2014). Elevation control of exploratory trenches and geotechnical borings at the overflow channel site was made by a licensed surveyor (Black and Veatch, 2013). All reported elevations are relative to mean sea level.

Previously published sedimentologic descriptions and interpretations of depositional environments commonly reported with numerical ages and elevations were used to reconstruct water levels (e.g., Table 1). These sedimentologic descriptions were made from both natural exposures (e.g., Bacon et al., 2006; Orme and Orme, 2008) and exploratory pits and trenches excavated on key landforms (e.g., Bacon and Pezzopane, 2007).

3.3.2. Lake sediment core datasets

Sediment cored from beneath the playa surface of Owens Lake includes up to a ~370 m record of climate change over the past 800 ka (Smith and Bischoff, 1997). Sedimentologic characteristics were used in combination with a simple method for calculating deterministic wind-wave characteristics for deep water sediment entrainment (USACE, 1984; 2002) to estimate threshold lake-water depth, which in turn was used to reconstruct lake level (e.g., Bacon et al., 2018). We used stratigraphic and geochemical proxy information from sediment cores in the depocenter of the lake basin including the ~320-m-long core OL-92, ~28-m-long core OL-90, and ~9-m-long core OL-84B from of Owens Lake basin (Benson et al., 1996, 1997, 1998; Smith and Bischoff, 1997) (Fig. 3).

A range of geochronological techniques have been used to date sediment cores from Owens Lake including dating methods consisting of radiocarbon and uranium-series, plus correlation methods involving tephrochronology, paleomagnetic analysis, and pollen assemblages (e.g., Benson et al., 1996; Smith and Bischoff, 1997; Bischoff and Cummins, 2001; Phillips, 2008). At shallow depths, sediment cores from Owens Lake (~2–30 m) yielded ^{14}C ages from wood, disseminated carbon (i.e., humate), carbonate, and shell that range from ~4 to 50 ka (Benson et al., 1996, 1997, 1998, 2002; Smith and Bischoff, 1997). A revised age-depth model was developed for the last 230 ka of core OL-92 that is based on the correlation between palynostratigraphies defined by U-Th ages from salt layers in Searles Lake core LDW-6 and similar pollen assemblages identified in Owens Lake sediments (Litwin et al., 1999). In our study we use the revised age-depth model of Litwin et al. (1999) for age control of the lithologic log of core OL-92 in Smith and Bischoff (1997).

3.3.3. Tectonic ground deformation

Understanding the rates and style of tectonic deformation within seismically active lake basins provides information to correlate shoreline features, as well as to accurately reconstruct past lake levels. Shoreline features and associated lacustrine deposits can be correlated within lake basins based on their elevation and characteristics if the geomorphic and geologic processes that created them are understood, and if ground deformation is considered (Oviatt, 2000; Reheis et al., 2014). Previously published water-level reconstructions of Owens Lake or other lakes in the paleo-Owens River system did not include corrections for tectonic ground deformation (e.g., Bacon et al., 2006; Jayko et al., 2008; Phillips, 2008; Smith, 2009; Rosenthal et al., 2017). The approach we used to reconstruct the depositional position of terrestrial and lacustrine features and deposits is after a simple method of Bacon et al. (in review) that was used to reconstruct deformed shorelines in Owens Lake basin to absolute elevations based on a differential fault-block model. In contrast to other regional tectonic lake basins in the western U.S. (e.g., Lahonton and Bonneville basins), where slip and vertical ground deformation are principally accommodated solely by single fault systems, plus isostatic crustal flexure and rebound of relatively thin crust (e.g., Adams et al., 1999; Hampel and Hetzel, 2006), the approach of Bacon et al. (in review) is applicable for tectonically complex and seismically active lake basins where isostatic rebound from loading of lakes is negligible, but vertical ground deformation is accommodated by distributed slip on two or more primary normal and dextral-oblique faults (Fig. 2).

We used previously published information on the locations, style of faulting, and vertical slip rates for primary faults in Owens Lake basin to correct the elevations of geomorphic and outcrop study sites, lake-core sites, and spillways for tectonic ground deformation (Table 4; Fig. 2). The location and sense of motion for primary faults in Owens Lake basin are from geologic and fault maps, plus the Quaternary fault and fold database (Slemmons et al., 2008; Jayko, 2009; USGS, 2016). Vertical slip rates on faults in Owens Lake basin are from studies on the tectonic geomorphology of the Sierra Nevada frontal fault (SNFF; Le et al., 2007), paleoseismology on the southern Owens Valley fault (OVF; Bacon and Pezzopane, 2007) and Sage Flat fault (SFF; Amos et al., 2013), as well as tectonic-geomorphology of other faults in the lake basin including the Keeler fault and Owens River-Centennial Flat fault (KF and OR-CFF; Bacon et al., in review) (Table 4 and Figs. 2 and 3).

3.4. Wind-wave and lake bottom sediment entrainment modeling

Application of wind-wave and sediment entrainment models are commonly used to estimate erosion potential within intertidal to open water coastal environments for coastal protection and habitat rehabilitation (e.g., USACE, 1984, 2002; Teeter et al., 2001; Rohweder et al., 2008; Fagherazzi and Wiberg, 2009). These types of models have also been used in lacustrine environments to estimate the distribution of sediment texture at the lake bottom (e.g., Håkanson, 1977), as well as to quantify potential impacts to water quality and clarity from resuspension of sediment, plus nutrients, heavy metals, and other toxic substances for water resource management (e.g., Reardon et al., 2016; Ji, 2017). In this study, we apply a similar approach to model the wind-wave characteristics and threshold lake-water depths required for the sedimentology described in sediment cores. The approach we use is based on Bacon et al. (2018) that was previously calibrated and verified by modeling the sedimentology described in the historical section in core OL-97 (Li et al., 2000; Smoot et al., 2000) with limnological conditions for the period AD 1872–1878 when Owens Lake was at its historical maximum water level.

Wind-driven sediment entrainment occurs when water depth is shallow enough to effectively transfer the momentum of wind-waves from the water surface to the sediment-water interface (Håkanson and Jansson, 2002; Reardon et al., 2016). Wind waves and the fluid shear stresses they produce within the water column are the main mechanism responsible for sediment erosion and resuspension when the critical shear stress of bottom sediment is exceeded (e.g., Fagherazzi and Wiberg, 2009). The wind-wave model we used is based on linear wave theory and consists of a series of analytical solutions for estimating deep-water wave characteristics, including: significant wave height, wave length, spectral peak wave period, maximum orbital wave velocity, and critical shear stress (USACE, 1984, 2002; Rohweder et al., 2008).

An initial step in the modeling procedure is to determine the wave characteristics of wave height, period, and length in deep water. The shape of wind waves is predominately controlled by the intensity and duration of wind shear across open water surfaces, therefore wind velocity and fetch are the principal variables used to determine wave characteristics that control the magnitude of the boundary velocity below the wave crest at a specified depth. Modeling of intermediate to shallow wind-waves (e.g., USACE, 2002; Le Roux, 2010) was not performed in this study because sediment cores were extracted from the depocenter area.

3.4.1. Wind

Wind direction is strongly controlled by the orientation and topography of its surrounding mountain ranges, e.g., Owens Lake basin has a wind regime with two primary directional sectors of N-NNW and S-SSE (Lancaster et al., 2015) (Fig. 1). We used the classification of wind potential to produce dust raising events from a study in Owens Lake basin to characterize wind in the wind-wave model. Data from three continuous meteorological stations around Owens Lake playa operating from AD 1988 to 1991 show that high and extreme-high wind events in the lake basin have hourly average wind speeds of ≥7 and ≥18 m/s, respectively, with extreme-high wind events occurring only a few times per year having wind gusts in excess of 22 m/s mostly from the N-NNW (Zhong et al., 2008). Furthermore, measured wind speeds of 15–17 m/s for fetch-limited water bodies have previously been used in wind-wave models because these magnitudes generate waves causing sediment erosion and resuspension (e.g., Rohweder et al., 2008; Fagherazzi and Wiberg, 2009).

3.4.2. Fetch

Fetch is the unobstructed distance traveled by wind or waves across open water (e.g., Fagherazzi and Wiberg, 2009). Limited fetch conditions existed at Owens Lake even at highstand water levels because of its relatively small and linear lake size with fetches of up to ~70 km. Fetch was determined by using the distance between study sites (shoreline, outcrop, lake cores) and corresponding elevation from either N-NNW or S-SSE directed winds. The measured fetch is a minimum estimate because there is an unknown height of water above the sites (i.e., depth), which is the purpose of the threshold lake-water depth modeling procedure to calculate. A minimum fetch input variable in the model also produces lower lake-water depth relations because relatively smaller waves are simulated, therefore it is considered a conservative approximation.

3.4.3. Critical shear stress

Critical shear stress represents the threshold for the initiation of potential particle motion when the drag force of flowing water against a particle exceeds the gravitational force holding it in place. The routine used to calculate the critical shear stress is based on the methods described in USACE (2002), which accounts for laminar flow along a flat lake bottom surface, as well as particle size and density in water with a specific density and viscosity. Salinity of large lakes along the eastern Sierra Nevada between ~1876 and 1886 AD ranged from ~0.07 g/l at Lake Tahoe (freshwater), ~3 g/l at Walker Lake (slightly saline), to ~50–70 g/l at Mono and Owens Lakes (brine) (Russel, 1885; Winkle and Eaton, 1910; Fig. 1). We used a salinity of 2 g/l to simulate slightly saline lake conditions, which is a typical value commonly associated with living and fossil molluscan and microcrustacean (ostracode) assemblages identified in the paleo-Owens River system during the late Pleistocene to Early Holocene (e.g., Sharpe and Forester, 2008; Rosenthal et al., 2017). This value was used to calculate a water density of 1000.5 kg/m^3 and kinematic viscosity of 1.1414 x 10^{-6} m^2/s at an elevation of 1096 m asl (Owens Lake historical shoreline) and temperature of 15°C based on MATLAB code of the MIT seawater thermophysical properties library (Sharqawy et al., 2010; Nayar et al., 2016). General sediment characteristics were assumed to have a density of quartz (2.65 g/cm^3), well sorted, and rounded with particle diameters of clay (2 μm), coarse silt (31 μm), coarse sand (2 mm), and up to coarse pebble (32 mm) that coincide with the boundaries between the size classes of the Wentworth (1922) scale.

4. Results

4.1. Owens Lake basin study sites

4.1.1. Post-IR-IRSL dating of Centennial Flat beach ridges

The best preserved and most complete geomorphic record of historical to late Pleistocene shorelines in Owens Valley is located in the southeastern sector of the lake basin along the northwestern flank of the Coso Range near Centennial Flat wash (Jayko and Bacon, 2008; Orme and Orme, 2008; Jayko, 2009; Fig. 3). The Centennial Flat site consists of a well-preserved and isolated beach plain comprised of a suite of ten well-developed, tectonically undeformed beach ridges and shoreline scarps at elevations between ~1096 and 1131 m asl, and a tectonically deformed beach ridge, locally at ~1165 m asl (Orme and Orme, 2008; Bacon et al., in review) (Fig. 4). The second highest shoreline in Owens Lake basin is vertically deformed up to 9.8 ± 1.8 m with a maximum elevation of ~1166 m asl that has a post-IR-IRSL date of 40.0 ± 5.8 ka from beach ridge deposits (Bacon et al., in review; Fig. 4). Sediment and erosional features of the highest shoreline preserved in the valley are nearby at elevations of ~1174–1180 m asl and are 160 ± 32 ka from a ^{36}Cl age from a lithoid tufa mound (Jayko and Bacon, 2008).

We performed the first post-IR-IRSL analysis to estimate direct ages on sediment from Centennial Flat beach ridges at elevations of ~1114, 1120, 1127, 1129, 1131 m asl (Table 2; Fig. 4). Freshly cleaned surfaces were made in natural exposures along active channels that were locally filled with windblown sand. Deposits at sample sites consisted of well-rounded, spherical to disk-shaped, sandy to gravelly beach ridge facies with either basinward, horizontal or landward dipping tabular beds that formed based on their position within the beach ridge (i.e., foresets, topsets or backsets, respectively; e.g., Adams and Wesnousky, 1998). The soil-geomorphic characteristics of all the beach ridges indicate that they are relatively younger and not recessional shorelines associated with the higher late Pleistocene (~40 ka) highstand beach ridge at the site because the lower beach ridges lack well-developed soil indices typical of late Pleistocene landforms in Owens Valley (e.g., Zehfuss et al., 2001) (Fig. 3). The lower beach ridges are sparsely covered by shrubs with coppice dunes and gravel-sized ventifacts from active eolian sand transport across the area (Orme and Orme, 2008). The surfaces of the beach ridges have moderately developed desert pavement with weakly developed desert varnish and subsurface rubification (i.e., reddening) coatings on gravel clasts, a thin vesicular A (Av) horizon (e.g., McFadden et al., 1998), and a ~20- to 40-cm thick, weakly developed soil with carbonate (k) and Avk/Bwk/Ck profile lacking soil structure, plus very few and patchy carbonate coatings on bottom of gravel clasts (e.g., Birkeland, 1999). These soil characteristics are similar to descriptions made on gravelly Holocene alluvial fans in the southwestern U.S. (e.g., McDonald et al., 2003), and slightly better developed compared to nearby late Holocene beach ridges below elevations of ~1108 m asl in Owens Valley (Bacon et al., 2018).

The post-IR-IRSL samples were taken from depths between 0.4 and 1.55 m within stratified sandy layers that lacked evidence of bioturbation. A single sample from the 1131 m beach ridge at a depth of 1.14 m from a hard, silty sand bed within topsets yielded an age of 8.4 ± 0.6 ka. Two samples from the 1129 m beach ridge were taken in a vertical profile at depths of 0.8 and 1.55 m from loose, sandy beds within topsets that were separated by a clear and horizontal boundary defined by a hard and thin, sandy silt layer overlain by a concentration of disk-shaped gravel (Fig. 4). Samples from the 1129 m beach ridge returned ages in stratigraphic order of 12.8 ± 1.1 and 8.1 ± 0.6 ka (Table 2). A total of three samples were recovered from the 1127 m beach ridge. Two closely spaced samples from near the crest of the beach ridge at depths of 0.4 and 0.6 m within the same loose, sandy backset yielded ages of 6.0 ± 0.5 and 6.7 ± 0.5 ka that are within their uncertainties, having a mean age of 6.4 ± 0.7 ka (Table 2). The third sample was taken ~15 m basinward of the crest at a depth of 0.5 m from a loose, sandy bed within foresets that returned an age of 7.6 ± 0.6 ka (Table 2; Fig. 4). The ~1120 m asl shoreline at the Centennial Flat site consists of two closely spaced beach ridges with GPS crest elevations of 1120.9 and 1121.2 m asl for the inner (basinward) and outer (landward) ridges, respectively (Fig. 4). Two closely spaced samples from below the crest of the inner ridge at depths of 0.9 and 1.0 m within the same loose, sandy foreset returned ages of 5.9 ± 0.5 and 6.5 ± 0.5 ka that are within their uncertainties, having a mean age of 6.2 ± 0.6 ka.

The lowest sample site was of the ~1114 m beach ridge. Here, two samples below the crest of the ridge at similar depths of 1.15 m and separated by ~0.6 m yielded ages of 5.8 ± 0.4 and 8.8 ± 0.6 ka from different loose, sandy backsets underlain by a massive, hard silty sand in the bottom of the exposure (Table 2; Fig. 4). These post-IR-IRSL ages are not within their uncertainties and not in stratigraphic order given that the younger sample was situated basinward and stratigraphically below the forests of the older sample (Fig. 4). This relation is confirmed by how backsets are formed by a process called barrier rollover. Barrier rollover occurs when storm waves wash sand and gravel from the beach face over the crest of a barrier (i.e., ridge) and onto the backside depositing younger backsets over older ones (e.g., Adams and Wesnousky, 1998; Reheis et al., 2014). Evidence of possible reworking of older sediment at the site is from the presence of detrital shells found within deposits of the ~1114 m beach ridge and the active wash that dissects it. The sediment of the beach ridge contained less than 5% mollusk shell fragments of up to ~2 cm long from an aquatic mussel (*Anodonta californiensis*) concentrated within the coarser fraction along the tabular beds of backsets. Similar shells of *Anodanta* sp. from deposits of the same ~1114 m beach ridge, but in a different wash ~250 m to the southwest, have a ^{14}C age of ~14,600 cal yr BP (Orme and Orme, 2008), as well as from articulated shells from sites along the northeast sector of the lake basin at Keeler with ^{14}C ages of ~24,000 to 25,000 cal yr BP (Bacon et al., 2006) (Table 1; Fig. 3). There were also detrital shell fragments of *Anodanta* sp. in deposits of the inner beach ridge at ~1120 m sampled for post-IR-IRSL analysis. In addition, a nearby exposure of a concentration of shells of a semi-aquatic snail (*Helisoma* (*Carinifex*) *newberryi*) at an elevation of ~1130 m asl has a ^{14}C age of ~38,700 cal yr BP (Table 1; Fig. 4). The range in age of sediment associated with the ~1114 m beach ridge, and presence of older shell fragments in deposits indicates possible reworking of older deposits from later water-level fluctuations, where the lowest elevations of past water levels appear to have all stabilized near an elevation of ~1111–1113 m asl.

4.1.2. Swansea shoreline stratigraphic site

New shoreline and stratigraphic investigations were performed at additional sites in the lake basin to refine the lake-level record of Owens Lake. These new investigations included GPS surveys and ^{14}C dating of tufa and mollusk shells at sites near Swansea in the northeastern sector of the lake basin (Fig. 3). The Swansea site includes a well-developed beach ridge complex composed of stratified sand and gravel with common mollusk-rich beds that formed at the base of steep bedrock cliffs within the Swansea embayment (Orme and Orme, 2000, 2008; Fig. 3). There are three well-developed beach ridges at the site with crest elevations of ~1119, 1123, and ~1128–1129 m asl that yielded latest Pleistocene ages from ^{14}C ages on mollusk shells from deeper sections (Orme and Orme, 2000, 2008; Bacon et al., 2006; Table 1). We performed a GPS survey to confirm beach ridge elevations at the site. Our new survey identified that the previously surveyed beach ridge at ~1119 m (e.g., Orme and Orme, 2008) is not a single ridge across the embayment, but occurs primarily as a pair of closely spaced ridges. The crests have GPS elevations of 1120.4 and 1120.7 m asl for the inner and outer ridges, respectively, which are at similar elevations to the paired beach ridges at the Centennial Flat site (e.g., Fig. 4).

The Swansea site also has a lower beach ridge and shoreline scarps at ~1108 m asl that truncate the beach plain with higher beach ridges, which is at a similar elevation of the shoreline scarp at the Centennial Flat site (e.g., Fig. 4). The soil-geomorphic characteristics of the ~1108 m beach ridge deposit indicate a Late Holocene age, which is supported by duplicate post-IR-IRSL samples that returned a mean age of 3.6 ± 0.4 ka (Bacon et al., 2018). The continuity in shoreline elevations between the Swansea and Centennial Flat sites indicates there has been negligible vertical tectonic ground deformation between the sites in the eastern sectors of the basin during the latest Quaternary (Bacon et al., in review).

In addition to evaluating the shoreline geomorphology at the site, tufa and mollusk shells were sampled to define lower water levels in the basin. The northwestern margin of the Swansea embayment has a cliff headland with several wave-formed notches on bedrock. Surfaces of the lowest notch, as well as on an accumulation of clast supported 0.5–1.5 m boulders have thick coatings of dense tufa at an elevation of 1108.1 m. The morphology and depositional environment of the tufa coatings is similar to encrusting tufa described at Pyramid Lake, Nevada (e.g., Benson, 1994). A tufa sample from a bedrock surface returned an age of 10,280 ± 40 ^{14}C yr BP (11,620–11,260 cal yr BP) with a median probability age of 11,400 cal yr BP (Table 1). A nearby site of shoreline sediment exposed in a road cut at an elevation of ~1109 m asl was also investigated at the base of the cliff headland at the Swansea embayment. The exposure consisted of a thin cover of alluvial sediment and windblown sand that was underlain by a ~1.0–1.5 m thick sequence of well stratified and interbedded sands and gravels with a concentration of mollusk shells within foreset beds. The shell-rich shoreline deposits were underlain by a lag of clast-supported, rounded cobbles and boulders cemented with beach rock on an abrasion platform developed on bedrock. The shell-rich bed contained a mixed mollusk assemblage composed mostly of disarticulated bivalves consisting of the mussel *Anodonta* sp. and the clam *Pisidium* sp., as well as snails *Hiliosoma newberryi* and *Parapholyx gesteri*. Of this assemblage, a snail shell of *Hiliosoma newberryi* with preserved pigment was sampled and yielded an age of 14,460 ± 45 ^{14}C yr BP (17,450–17,060 cal yr BP) with a median probability age of 17,200 cal yr BP (Table 1). The shell-rich deposit is typical of a relatively high-energy beach face depositional environment. The mixed mollusk assemblage includes species that live below the shoreline within different lacustrine environments ranging from relatively deep to shallow water (e.g., Koehler, 1995). As a result we interpret the mixed mollusk assemblage as likely reworked from older deposits sourced nearby. Nonetheless, the ^{14}C age provides a maximum determination, as well as is likely close to the depositional age of the shoreline deposit given similar shell ages from sediment nearby.

4.1.3. Dirty Socks and OVF shoreline stratigraphic sites

New shoreline and stratigraphic investigations were performed at sites in the lake basin to refine the lake-level record of Owens Lake. These investigations included ^{14}C dating of tufa and mollusk shells at sites near Dirty Socks and the Owens Valley fault in the southeastern sector of the lake basin (Fig. 3). The Dirty Socks and OVF sites are located in areas of the lake basin that previously lacked stratigraphic investigations to define lake levels. The Dirty Socks site is located near Dirty Socks hot spring ~2 km northeast of the trace of the OVF between the elevations of ~1103 and ~1107 m asl, whereas the OVF site is located within the fault zone between ~1105 and 1122 m asl (Fig. 3). A total of ten mollusk shells from shoreline deposits were collected for ^{14}C dating, four at the OVF site and six at the Dirty Socks site (Table 1). Sample sites were from natural exposures in active channels cut across a broad beach plain with shoreline scarps that is locally overlain by recent alluvium and windblown sand (Jayko, 2009). The shoreline geomorphology of the Dirty Socks and OVF stratigraphic sites is not straightforward because of active faulting and related ground deformation on the OVF in the form of distributive faulting and localized anticlinal growth structures (Slemmons et al., 2008). The five historical to late Holocene shorelines between ~1096 and ~1108 m asl identified in other parts of the lake basin are present in the area of the Dirty Socks and OVF sites. The number and elevations of several higher shoreline scarps between ~1109 and 1160 m asl, however, do not match with dated shorelines identified in other areas of the lake basin, therefore are interpreted to be tectonically deformed. The beach plain in the area shows geomorphic evidence for mostly erosional shoreline processes along the mapped trace of the OVF, with the latest period of surface modification up to an elevation of ~1131 m asl associated with the Latest Pleistocene-Early Holocene water levels that constructed the Centennial Flat beach ridges, as well as the lower Late Holocene lake-level fluctuations at and below ~1108 m asl (e.g., Fig. 4).

4.1.4. Dirty Socks site

The Dirty Socks stratigraphic site included sampling in two ~1–1.5-m-deep active channels separated ~25 m from each other. One channel exposed a sequence of faulted shore to nearshore sedimentary facies composed of stratified and interbedded silty to sandy deposits with mollusk-rich beds, where the other channel exposed similar stratigraphy without faults. The channel with faults included deposits juxtaposed against dissimilar beds on either side of a single vertical fault, typical of strike-slip faulting (e.g., McCalpin, 1996). Mollusk shells were sampled for ^{14}C dating at two sites along the channel. Two bivalve shells were sampled on both sides of a fault at different depths below an elevation of ~1103 m asl. An articulated mussel sample of *Anodonta* sp. at a depth of ~0.3 m from a silty sand bed returned an age of 34,700 ± 320 ^{14}C yr BP (39,700–38,300 cal yr BP) with a median probability age of 38,900 cal yr BP (Table 1). In addition, an articulated clam sample of *Sphaerium striatinum* at a depth of ~1.0 m from a silty sand bed mixed with shells of articulated *Anodonta* sp. returned an age of 35,160 ± 340 ^{14}C yr BP (40,150–38,640 cal yr BP) with a median probability age of 39,400 cal kyr BP (Table 1). The other site in the same channel consisted of a sequence of mostly shore stratigraphic facies. Single samples of bivalve and gastropod shells were sampled on both sides of a fault at different depths below an elevation of ~1104 m asl. A disarticulated clam sample of *Sphaerium* sp. at a depth of ~0.4 m from a cross-bedded sandy layer returned an age of 42,560 ± 840 ^{14}C yr BP (47,270–44,040 cal yr BP) with a median probability age of 45,600 cal yr BP (Table 1). In addition, a snail sample at a depth of ~1.0 m from a sandy bed returned an age of 31,730 ± 230 ^{14}C yr BP (35,850–34,800 cal yr BP) with a median probability age of 35,300 cal yr BP (Table 1). The apparent ages and corresponding depths of samples from the ~1104 m site are not in stratigraphic order because sample sites are separated by several fault strands in exposures, thereby are tectonically deformed.

Sites in the channel without faults were sampled at higher elevations of ~1106 and 1108 m asl. An articulated mussel of *Anodonta* sp. at a depth of ~1 m from a mollusk-rich sandy layer returned an age of 36,910 ± 420 ^{14}C yr BP (41,920–40,340 cal yr BP) with a median probability age of 41,200 cal yr BP (Table 1). The articulated shells of *Anodonta* sp. in the mollusk-rich bed were commonly filled with smaller clams of *Sphaerium* sp. and *Pisidium* sp., plus small gastropods. In addition, the higher site consisted of stratified sands and gravels in the upper section of shoreline sediment associated with ~3.5 ka beach ridge deposits. The Late Holocene gravelly deposits were underlain by a depositional boundary composed of a layer of tufa over a sandy layer with articulated *Anodonta* sp. shells. The tufa at the site resembles palmate tufa, which commonly forms in nearshore environments where thermal springs discharge (e.g., Benson, 1994). A sample of *Anodonta* sp. from a depth of ~1 m from the mollusk-rich sandy layer returned an age of 10,345 ± 30 ^{14}C yr BP (11,750–11,300 cal yr BP) with a median probability age of 11,500 cal yr BP (Table 1).

4.1.5. OVF site

The OVF stratigraphic site included sampling in ~1–1.5-m-deep active channels across a gravelly beach plain. All four sample sites consisted of a 0.5–1-m-thick gravelly beach plain deposit underlain by shore to nearshore sedimentary facies composed of stratified, shell-rich silts and sands. The lowest elevation site at ~1106 m asl included an exposure of gravelly deposits underlain by gastropod-rich sandy sediment. A snail sample from a depth of ~1 m returned an age of 24,200 ± 130 ^{14}C yr BP (28,270–27,690 cal yr BP) with a median probability age of 27,900 cal yr BP (Table 1). At a higher elevation of ~1108 m asl, an abrasion surface underlain by a sandy layer with articulated *Anodonta* sp. shells were sampled at a depth of ~0.5 m. The articulated *Anodonta* sp. yielded an age of 11,630 ± 35 ^{14}C yr BP (13,270–13,090 cal yr BP) with a median probability age of 13,200 cal yr BP (Table 1). The other two samples sites were at higher elevations of ~1116 and 1123 m asl. The sample site at ~1116 m included a surface locally covered by densely packed palmate tufa underlain by a sequence of thinly interbedded silts and sands. An ostracode sample from a ostracode-rich lens interbedded with silt layers at a depth of ~1.3 m returned an age of 16,900 ± 50 ^{14}C yr BP (20,200–19,830 cal yr BP) with a median probability age of 20,000 cal yr BP (Table 1). The site at ~1123 m included an exposure of gravelly beach plain deposits underlain by thick mollusk-rich sandy sediment. An articulated *Anodonta* sp. sample from a depth of ~1 m returned an age of 11,435 ± 35 ^{14}C yr BP (13,100–12,900 cal yr BP) with a median probability age of 13,000 cal yr BP (Table 1). The articulated shells of *Anodonta* sp. in the mollusk-rich bed were partly filled with sand and smaller clams of *Sphaerium* sp. and *Pisidium* sp., plus small gastropods and ostracodes. The ^{14}C ages from tufa and mollusk shells from the stratigraphic sites in the eastern and southern sectors of Owens Lake basin provide new shoreline ages to revise the latest Pleistocene (~13 ka) and define the late Pleistocene (~45 to 16 ka) part of the lake-level record of Owens Lake.

4.1.6. Previously published data from Owens Lake basin

Owens Lake has been the focus of numerous paleohydrologic studies because of a robust record of climate change is preserved in lacustrine sediments and shoreline geomorphic features. Most of these studies have focused on resolving the late Pleistocene history of pluvial Owens Lake through analyses of sediment cores with records going back ~800 ka (e.g., Smith and Pratt, 1957; Newton, 1991; Lund et al., 1993; Benson et al., 1996, 1997, 2004; Smith et al., 1997 and references therein; Mensing, 2001) and shoreline features as old as ~140 ka (Carver, 1970; Beanland and Clark, 1994; Bacon et al., 2006; 2018; in review; Bacon and Pezzopane, 2007; Jayko and Bacon, 2008; Orme and Orme, 2008). The previously developed lake-level record of Owens Lake was constructed from a total of 42 ^{14}C ages on tufa, mollusk shell, charcoal, and organic-rich sediment over the last 27 ka (Bacon et al., 2006; Reheis et al., 2014). The stratigraphic context and elevation of ^{14}C ages that were sampled from different sedimentary facies ranging from terrestrial, delta plain to lacustrine (shore, nearshore), plus proxy information from sediment cores were collectively used to define the position of water levels. In our study, we refine the previous lake-level curve for Owens Lake and extend the record to 50 ka by including the previously unpublished data presented in sections 4.1.1.–4.1.5. with the previously published shoreline and outcrop stratigraphic sites used in Bacon et al. (2006) (Table 1).

The majority of the data previously used to develop the lake-level record came from paleoseismic trench sites (AGPS and QPS) on the OVF north of Lone Pine (Beanland and Clark, 1994; Bacon and Pezzopane, 2007), as well as stratigraphic sites along bluffs of the Owens River (ORB) in northern Owens Lake basin, plus additional sites along the northeastern sector of the basin at Swansea and Keeler (Bacon et al., 2006) (Fig. 3). All these sites were used to collectively define Latest Pleistocene to Early Holocene lake levels based on integrating sequence stratigraphy of interbedded nearshore, shore, delta, and delta plain depositional environments from numerous natural and trench exposures and ^{14}C ages from charcoal, organic sediment, tufa, and mollusk shells. In addition, the latest Pleistocene ages of mollusk shells in beach ridge deposits used to define maximum oscillations in lake level were from detailed stratigraphic studies previously performed at the Swansea and Centennial Flat sites (Orme and

Orme, 2000; 2008). Furthermore, other investigations at the Owens River delta site characterized a mixed assemblage of bivalves and gastropods that yielded ^{14}C ages from mollusk shells in areas at the mouth of the Owens River to define relatively low lake levels during the latest Pleistocene (Koehler, 1995; Orme and Orme, 2008; Fig. 3). Maximum lake-levels were also estimated from the age and elevation of soluble pack rat middens preserved at the base of the Inyo Mountains at the Haystack site (Koehler and Anderson, 1994; Table 1; Fig. 3).

4.2. Owens Lake overflow channel and sill

The overflow channel (i.e., spillway) of Owens Lake is a prominent, north-south axial channel that has incised across distal piedmont slopes of the Sierra Nevada and Coso Range in the southern end of the lake basin (Figs. 3 and 5). The overflow channel crosses dissected late Pliocene to Pleistocene alluvium that is underlain by gently dipping, interbedded lacustrine sandstone and siltstone with volcanic tuff and flow rocks of the ~3–6 Ma Coso Formation (Jayko, 2009). The channel is bounded on the west by the east-dipping normal SNFF and on the northeast by the east-dipping dextral-oblique OVF. The normal SFF locally forms a graben in the northern reach of the overflow channel (Fig. 5). The modern sill has formed at an elevation of ~1145 m asl associated with recent alluvial fan aggradation in the central confined reaches of the overflow channel at the confluence of two of the larger streams draining the Sierra Nevada and Coso Range (Fig. 5). The lowest elevations within the overflow channel near the drainage divide have been submerged since AD 1913 by construction of Haiwee Reservoir. The reservoir is part of the Los Angeles Aqueduct system and consists of two dams (North and South Haiwee Dams) that impound water on both sides of the drainage divide (Fig. 5). As a result, there has been a lack of detailed studies of the sill area since construction of the reservoir.

Prior to our study, the sill was considered to be relatively stable at ~1145 m asl, therefore the age of either shorelines identified below this elevation or proxies for closed basin conditions from sediment lake cores were interpreted to be associated with no overflow conditions at or below this level (Smith and Street-Perrot, 1983; Smith and Bischoff, 1997; Bacon et al., 2006). Conversely, Orme and Orme (2008) speculated that an earlier spillway of Owens Lake was ~1 km west of its current position at unknown elevations from ground deformation from either faulting or volcanism. We present previously published and unpublished subsurface geologic evidence and chronologic ages of sediment from geotechnical investigations of the Haiwee

Reservior area to characterize the morphometry of the entire overflow channel and directly date the latest episodes of overflow, thereby resolving the apparent asynchrony between the latest Pleistocene overflow records of Owens Lake (Bacon et al., 2006; Orme and Orme, 2008; Reheis et al., 2014) and China-Searles Lake (Phillips, 2008; Rosenthal et al., 2016).

4.2.1. Geomorphology and geology of the overflow channel

Pre-construction topographic surveys of the overflow channel and geological observations of foundation materials of the South Haiwee Dam site were used to characterize the geomorphology of the entire overflow channel, as well as the thickness of channel fill and depth to bedrock in the southern reach of the channel (Los Angeles Board of Public Service Commissioners, 1916). A longitudinal profile along the axis of the overflow channel from digitized contours of the georeferenced map of pre-construction topography shows the transverse profiles of four coalescing alluvial fans that have formed within the confined reaches of the channel, where the highest alluvial fan controls the position of the modern sill at an elevation of ~1145 m asl (A–A'; Figs. 5 and 6). In the vicinity of the South Haiwee dam site, three deep test wells along with a deep trench were excavated to depths of up to 36 m into bedrock across a constriction in the overflow channel prior to and during construction in AD 1911. The excavations were logged and a survey-controlled geologic cross section of the proposed dam site was produced by the City of Los Angeles engineers. The cross section and geologic descriptions demonstrate that channel fill is composed of up to 33.5-m-thick sequence of poorly consolidated and poorly sorted, sandy to bouldery alluvial fan deposits sourced from nearby granitic bedrock of the Sierra Nevada and basalt from either the Coso Formation or Coso Range. The channel fill is underlain by a sharp depositional contact developed on indurated bedrock of the Coso Formation that is composed of gently tilted siltstone across most of the bottom of the channel and volcanic flow rocks on the eastern margin of the channel, whereas hard, cemented sandy to gravelly alluvial fan sediment also underlain by Coso Formation bedrock is on the upper western margin of the channel (Los Angeles Board of Public Service Commissioners, 1916). The depositional contact over the width of the bottom of the channel has planar topography with an elevation as low as 1097.3 m asl that we interpret to be a strath terrace (A–A'; Fig. 6).

A geotechnical investigation of foundation materials at the toe of the North Haiwee Dam site was also used to characterize the stratigraphy and thickness of channel fill, depth to bedrock, and age of sediment from OSL dating in the northern reach of the channel (Black and Veatch, 2013). A transect of 10 exploratory sonic boreholes, 31 cone penetration testing probes, and seismic reflection surveys across the overflow channel (B–B') show channel fill is composed of up to ~35-m-thick sequence of poorly consolidated and moderately sorted, interbedded silty sand to sandy silt with lesser gravel alluvial-type deposits sourced mostly from nearby granitic bedrock of the Sierra Nevada. The base of the channel fill consists of a ~1.5-m-thick moderately-sorted, subrounded to rounded, elliptical- to disk-shaped basal gravel deposit that is underlain by a sharp depositional contact on indurated interbeds of siltstone and sandstone of the Coso Formation. The depositional contact over the width of the bottom of the channel has planar to wavy topography with a mean elevation of 1112.8 ± 2.7 m asl that we interpret to be a strath terrace. The upper margins of the channel are composed of sandy to gravelly alluvial fan deposits with varying degrees of pedogenic carbonate that also overly a higher strath terrace formed on Coso Formation bedrock (Black and Veatch, 2013) (B–B'; Figs. 5 and 6).

4.2.2. Age of channel fill and colluvial slope deposits

The northern reach of the overflow channel in the vicinity of North Haiwee Dam is relatively wide and consists of a pair of prominent terraces between the elevations of ~1162 and 1165 m asl that are inset with older alluvial fan deposits along upper channel margins (Beanland and Clark, 1994). The pair of terraces become narrow in width and grade to a channel constriction ~2 km south of North Haiwee Dam. The elevation and geomorphology of the terraces suggest that they are likely beach plains formed near the outlet of the lake based on the presence of spit-like features and shoreline scarps at similar elevations of the ~40 ka shoreline at ~1165 m asl (e.g., Jayko, 2009; Bacon et al., in review) (Fig. 5). The upper alluvial fan deposits along the channel margins are estimated to be Pleistocene in age based on soil-geomorphologic characteristics and geologic mapping (Jayko, 2009). Exposures of alluvial fan deposits on the eastern margin of the channel show pedogenic carbonate stage IV development and other soil indices within soil profiles (e.g., Birkeland, 1999) indicating a likely age of ~100 ka, whereas lower sections with buried soils, in addition to alluvial fan deposits on the western margin of the channel collectively have better developed soil indices, suggest relatively older ages of greater than 100 ka (Black and Veatch, 2013) (B–B'; Fig 6). Modification of alluvial fan surfaces and development of the beach terrace within the upper overflow channel near the outlet of the lake provide minimum ages for the alluvial fan deposits to older than ~40 ka, thereby supporting the inferred ages of ≥100 ka (Fig. 6).

Geochronologic dating included ^{14}C and OSL analyses to determine the age of sediment exposed in exploratory trenches and encountered in deep boreholes in the northern reach of the overflow channel (Black and Veatch, 2013). An ~85-m-long and up to 4.6-m-deep trench was excavated along the B-B' transect between boring SB-12-09 and North Haiwee Dam to characterize the upper section of channel fill (Fig. 6). The trench exposed a continuous section of horizontally stratified alluvial sediment consisting of poorly-sorted, angular to subangular sandy silt to silty sand with gravel. Detrital charcoal sampled from near the base of the trench at an elevation of 1135.5 m asl returned an age of 5060 ± 30 ^{14}C yr BP (5900–5740 cal yr BP) with a median probability age of 5800 cal yr BP (Black and Veatch, 2013) (Table 1; Fig. 6). Sediment from a deeper section of channel fill was also sampled for dating from a ~21-m-deep sonic boring. Three OSL samples were taken from boring SB-12-09 at depths of 9.4, 13.4, and 16.4 m below an elevation of 1136.9 m asl in an area ~330 m north of North Haiwee Dam near the eastern channel margin. The samples consisted of well-sorted, fine- to medium-grained sand that lacked angular to subangular gravel typical of alluvium encountered in the upper ~5 m of sediment at the borehole site and nearby trench exposures. The OSL samples yielded ages in stratigraphic order of 6.9 ± 1.1, 7.6 ± 1.3, and 11.6 ± 1.8 ka (Black and Veatch, 2013; Table 3; Fig. 6). The luminescence signals for samples from the channel fill (HD 1, 2, and 3) were well behaved having tightly clustered distributions of equivalent doses, thereby providing confidence in the ages (see Supplement 3).

The colluvial slopes along the eastern channel margin were also sampled for OSL dating by Black and Veatch (2013) at sites ~0.7 km south of North Haiwee Dam. Colluvial slopes in this area are derived from weathered late Pliocene to early Pleistocene alluvial sediment that locally fringe the overflow channel and cap an erosion surface developed on Coso Formation bedrock (Jayko, 2009). Three ~4–5 m deep trenches spaced up to ~45 m from each other were excavated across the transition between the footslope and midslope of the eastern channel wall where it steepens between the elevations of ~1150 and 1166 m asl (e.g., B–B'; Fig. 6). Trenches exposed colluvial deposits consisting of loose, massive and poorly sorted, angular to subangular silty sand with gravel to cobbles. The colluvial deposits have an unconformable depositional contact over slightly hard to very hard, moderately stratified and poorly-sorted, angular to subangular sandy silt to silty sand with gravel and cobbles alluvial fan deposits of likely late Pliocene to early Pleistocene age based on geologic mapping in the area (Jayko, 2009), morpho-stratigraphic position with nearby alluvial surfaces, and soil-geomorphologic characteristics of deposits.

The OSL samples were taken from depths between 0.6 and 2.1 m within gently dipping, matrix supported sandy deposits typical of colluvial wedge stratigraphy. Sample sites are from depths that also show evidence of pedogenic processes and bioturbation. Three OSL samples taken from colluvium in a trench at depths of 1.4 and 2.1 m returned ages of 22.8 ± 8.4 ka for a single sample and 29.1 ± 8.0 and 21.4 ± 9.5 ka for duplicates samples, respectively. Samples at shallower depths of 0.6 and 0.8 in colluvium from different trenches yielded ages of 7.7 ± 1.5 and 35.9 ± 13.7 ka, respectively (Black and Veatch, 2013) (Table 3). The luminescence signal for the youngest sample (HD 8) was well behaved with a tightly clustered distribution of equivalent doses, thereby providing confidence in the age. The other signals, however, had poorly clustered distributions of equivalent does and the confidence level for these samples is low (see Supplement 3). The poor behavior of the samples (HD 6, 7-1, 7-2, and 9) might be the consequence of significant volcanic quartz within samples derived from ash flow tuff units in the Coso Formation. This would produce a high residual level and decay pattern for the OSL signal that is sluggish, and not characteristic of the normal shine down curve for quartz (Black and Veatch, 2013). As a result, samples from deeper depths with ages of ~21 to 29 ka (HD 6, 7-1, and 7-2) are considered to be generally reasonable, but likely underestimate the age of the deposits, therefore are interpreted to be minimum ages. The oldest sample with an age of ~36 ka derived from near surface colluvium (HD 9) is considered problematic because of its older age and shallow depth (Black and Veatch, 2013). Therefore the age of sampled HD 9 is uncertain and considered unreliable rather than a minimum age and not used in our study.

4.2.3. Spillway of Owens Lake basin

Previous studies that addressed the location and character of sills in Owens Lake basin were either somewhat limited in scope (Bacon et al., 2006; Jayko and Bacon, 2008) or did not include site-specific data to support proposed overflow models (Orme and Orme, 2008). Two of the highest documented shorelines in Owens Valley are tectonically deformed at elevations of ~1155–1165 m asl from a ~40 ka lake level (Bacon et al., in review) and ~1180–1200 m asl from a ~160 ka lake level (Jayko and Bacon, 2008). The bottom of the overflow channel of Owens Lake is characterized as a stable, "hard" sill at ~1113 m asl below North Haiwee Dam that would control spill when there is a lack of channel fill. At elevations above ~1113 m asl the sill of Owens Lake is controlled by the level of unconsolidated sediment confined in the narrow reach of the channel, thereby forming an unstable and erodible "soft" sill. We performed an assessment of potential areas within the overflow channel that may have controlled the latest highstand water levels of Owens Lake that formed the ~40 and 160 ka shorelines.

Several transverse topographic profiles across the entire length of the overflow channel from a 10-m-resolution DEM were used to identify landforms that coincide with the range of elevations of the deformed ~40 and 160 ka shorelines in Owens Lake basin. Two of the profiles at the outlet of the overflow channel along transects C–C' and D–D' provided the best evidence for landforms related to the highstand shorelines (Fig. 5A). The upstream transect crosses dissected alluvial fans with a suite of terraces down to the channel bottom on the western margin and a large landslide feature developed on pervasively jointed and moderately dipping volcanic flow rock of the Coso Formation on the eastern margin of the channel (C–C'; Figs. 5 and 7). Given the uncertainties with the 10-m-resolution DEMs, the geomorphic profile shows sharp breaks-in-slope, benches, and channel features between the elevations of ~1172 and 1180 m asl, as well as another set of breaks-in-slope and a bench between ~1156 and 1165 m asl that coincide with the elevations of the ~160 and ~40 ka shorelines, respectively (C–C'; Fig. 7). The downstream transect crosses dissected alluvial fans on the western margin of the channel similar to transect C–C', but also crosses a steeper and narrower active channel within volcanic flow rock of the Coso Formation (D–D'; Figs. 5 and 7). There is no obvious evidence of landforms associated with ~160 ka shoreline at elevations near ~1180 m asl along the D–D' profile. The profile does, however, show sharp breaks-in-slope, benches, and a channel feature at elevations between ~1140 and 1165 m asl that may be associated with down-cutting from spill at the ~40 ka water level (D–D'; Fig. 7).

The fluvial geomorphology of the outlet indicates that the spillway of the ~40 and ~160 ka shorelines may have been located in the southern reaches of the overflow channel, whereas the more recent outlet during the latest Pleistocene and Early Holocene was likely in the northern reach. Prior to ~160 ka, it is possible that the position of a paleo-spillway channel was where the large landslide mass is today (Figs. 7 and 8). This implies there has been several subsequent episodes of cut-and-fills since the lake was impounded at this time. A model of channel filling with alluvial fan sedimentation during inter-pluvials (i.e., inter-glaciations) followed by contemporaneous alluvial sedimentation during highstand water levels at ~40 and 160 ka likely influenced the height of the sill during these times. The sills during the highstands were likely soft similar to the modern configuration, but reaching greater thickness and height, and would have had minor spillway channels along channel margins, such as the inset terraces and elevated channel features developed on more stable older alluvial fans, the large landslide feature, and bedrock. The area of the outlet that is currently devoid of sediment was likely plugged with sediment during the highstands at ~40 and 160 ka. This plug would be reflected downstream of the spillway outlet as an alluvial fan in Rose Valley with an alluival fan apex graded to areas of transects C–C' and D–D' (Figs. 5 and 7). Remnants of this alluvial fan appear to be preserved on the western margin of the outlet in the form of a broad and well-developed inset terrace with a bouldery surface along the toe of dissected older alluvial fans (Figs. 5 and 8). A reconnaissance-level investigation of the degree of surface boulder weathering and subsurface soil-geomorphic characteristics of the broad inset terrace indicates an age older than ~20–25 ka when compared to similar alluvial fans in Owens Valley (e.g., Zehfuss et al., 2001).

4.3. Lake-Level Reconstruction

4.3.1. Elevation of shoreline features and lacustrine deposits

The differential fault-block model we use to reconstruct water levels for Owens Lake is applicable for tectonically complex and seismically active lake basins where vertical ground deformation is accommodated by distributed slip on two or more normal and strike-slip fault systems. We account for vertical deformation by identifying the absolute elevations of landforms and deposits on individual fault blocks because differential motion occurs on closely spaced faults with different vertical slip rates (e.g., Bacon et al., in review). Calculating a net vertical slip rate across the lake basin and overflow area (sill) that are bounded by two or more faults produces more accurate estimates of the absolute magnitude of vertical deformation of individual study sites. A net vertical slip rate is calculated by either using a single mean slip rate if the study site is on a fault block adjacent to a single fault or using the sum of two or more mean slip rates if the study site is situated on a fault block bounded by two or more parallel faults. The location of study sites relative to individual faults determines if vertical slip rates are either positive values representing footwall deformation (i.e., uplift rates) or negative values for hanging-wall deformation (i.e., subsidence rates) for both normal and dextral-oblique faults. The approach used to estimate tectonic ground deformation was to multiply the net vertical slip rate of the fault block containing landforms and deposits with their age to solve for the magnitude and direction of vertical deformation. If the sign is negative then the value of vertical deformation is then added to the observed field elevation, whereas if the sign is positive then the value is subtracted from the observed field elevation to correct the elevation of study sites to pre-deformed positions (Bacon et al., in review).

Owens Lake basin contains five subparallel faults, including the primary SNFF and OVF systems, as well as the less active normal Keeler fault (KF), normal Owens River-Centennial Flat fault (OR-CFF), and the dextral-oblique southern Inyo Mountains fault (SIMF) (Fig. 3). Spatiotemporal changes in the distribution of slip in the lake basin are defined by the ~40 ka highstand beach ridge that is vertically deformed ~10 m and undeformed suite of ~11–16 ka beach ridge deposits at elevation of ~1114–1129 m asl. Integration of paleoseismic records in Owens Valley with the tectonic geomorphic record of deformed beach ridges and alluvial fans indicates that both normal and strike-slip faulting occurred between ~11–16 and 40 ka across all faults in the lake basin, whereas strike-slip faulting on the OVF and SIMF has been the predominant style of slip since ~16 ka (Bacon et al., in review). In general, the apparent slip distributed in the lake basin is accommodated by two structural domains, a western domain including fault blocks between the SNFF, OVF and OR-CFF and an eastern domain consisting of fault blocks between the OR-CFF, KF, and SIMF (Fig. 3).

Study sites in the western structural domain (AGPS, ORB, QPS, Owens River delta, Haystack, Dirty Socks, and OVF) required accounting for vertical deformation on the SNFF and OVF (Fig. 3). The majority of sample locations at these sites are located on the hanging walls of the OVF and SNFF, therefore sample sites were corrected to higher elevations based on a net subsidence rate of 0.37 m/ka from the summation of mean rates for the OVF and SNFF of –0.12 and –0.25 m/ka, respectively (Table 4). In contrast, all sample locations at the OVF study site, as well as a single sample location at the QPS study site are located on the footwall of the OVF and hanging wall of the SNFF. As a result, sample sites were corrected to higher elevations based on a net subsidence rate of 0.13 m/ka from the summation of mean rates for the OVF and SNFF of 0.12 and –0.25 m/ka, respectively (Table 4). Study sites in the eastern structural domain

(Swansea, Keeler, and Centennial Flat) are situated within a sector of the lake basin that requires accounting for net subsidence. The sample locations at these sites are located in an area where 9–10 m of ground deformation resulted from the cumulative effects of faulting, uniform tilting, and basin-wide subsidence since ~40 ka (Bacon et al., in review). As a result, sample sites in the eastern sector of the lake basin were corrected to higher elevations using a uniform, mean net subsidence rate of 0.24 m/ka (Table 4). The corrected elevations of previously reported sample sites with ^{14}C ages and new ^{14}C, post-IR-IRSL, and OSL ages of our study are shown in Tables 1–3.

4.3.2. Lake bottom elevation

The absolute elevation of the lake bottom during the time of deposition is required when performing a threshold lake-water depth analysis of sediment in lake cores. Estimating the absolute elevations of sediment layers at lake-core sites involves accounting for settlement from consolidation and subsidence from active faulting (e.g., Bacon et al., 2018). Sediment in lacustrine settings consolidates with burial, requiring normalization of sediment thickness based on dry density or water content to allow direct comparison of recent and ancient sedimentation rates (e.g., Martin and Rice, 1981; Davidson et al., 2004). To reconstruct the lake bottoms to depositional elevations by accounting for consolidation, we used the water contents of ~62.7–44.0 wt.% at depths of 1–70.8 m for silty clay layers reported in Owens Lake core OL-92 (Friedman et al., 1997). We modeled down to a depth of ~71 m in sediment cores because this depth corresponded to ages older than 50 ka. A natural logarithm function was developed from water content and depth data in core OL-92. The normalized water content versus depth data was fitted by a logarithmic trend line ($r^2 = 0.95$), similar to the presentation of compression test data of soil, where the void ratio of a soil decreases linearly with the logarithm of pressure (e.g., Handy and Spangler, 2007). Normalized water content (W_w) was calculated as:

$$W_w = -0.062\ln(d) + 0.998 \quad (1)$$

where the bottom of sediment layer depth (d) in meters is the variable. Settlement due to consolidation (δ_c) of sediment layers in lake cores was estimated as:

$$\delta_c = t - (t * W_w) \quad (2)$$

where thickness of each layer (*t*) in meters is the variable.

Estimating rates of subsidence from active faulting at core sites was done similar to the approach used to vertically correct the elevations of shoreline features and deposits for tectonic ground deformation. The reconstruction of ground deformation at the core OL-92 site was based on a maximum net subsidence rate of 0.46 m/ka from combining the maximum vertical slip rates for the SNFF of –0.30 m/ka and for the OVF of –0.16 m/ka, given that the core site is located on the hanging wall of both faults (Table 4; Fig. 3). We used a maximum subsidence rate because this value was used in the calibration of the threshold lake-water depth analysis with historical shoreline and sediment core data from core OL-97 (Bacon et al., 2018). The absolute elevations of sediment layers in lake cores were calculated by multiplying the subsidence rate with the duration of time between individual sediment layers to derive values of tectonic subsidence, which was followed by adding this value to the magnitude of consolidation of each sediment layer. The cumulative value of the total consolidation and tectonic subsidence for each sediment layer since ~ 50 ka was then added to its corresponding field elevation. The magnitude of correction for consolidation and subsidence at a depth of ~28 m in core OL-92 are ~4 and 18 m, respectively.

4.3.3. Threshold lake-water depth analysis

The erosion potential of lake bottom sediments was assessed by modeling the threshold lake-water depths required to best match sedimentology described in core OL-92. The wind wave-generated bottom shear stress at the water-sediment boundary and critical shear stress for bottom erosion were calculated after the methods of USACE (1984, 2002). The hourly average wind speeds of 7 and 18 m/s for strong breeze and whole gale conditions, respectively, along with fetch lengths up to 70 km were used in the model to simulate two wind event scenarios that would potentially define the effective wave base at core sites (Fig. 9). The wave characteristic calculated by the wind-wave model include significant wave height (H_s), spectral peak wave period (T_p), and wave length (L). The wave characteristics driven by wind speeds of 7 and 18 m/s over a fetch of up to 70 km have values ranging from (H_s=1.1 m; T_p=4.6 s; L=32.6 m) to (H_s=2.9 m; T_p=6.3 s; L=62.3 m), respectively. The critical bottom shear stresses at fetches between 0 and 70 km were calculated to entrain four particle sizes ranging from clay (2 μm) to coarse pebble (32 mm).

The threshold lake-water depth to initiate sediment entrainment was determined by iterating water depth until the ratio between the bottom shear stress below the wave crest and the critical bottom shear stress to entrain a given particle size exceeded 1. Potential sediment entrainment for a range of particles sizes described in the sediment core were modeled. The modeling shows that the threshold lake-water depth of the finer sediment with clay-sized particles (2 μm) can potentially be entrained at depths of ~20 and 44 m under waves driven by wind events of 7 and 18 m/s over a fetch of up to 70 km, respectively (Fig. 9). The modeling also shows that coarser sediment of pebble-sized particles up to 32 mm under the same two wind events and fetch can potentially be entrained at depths of ~2.7 and 8.6 m, respectively (Fig. 9). The threshold lake-water depth analysis was used in conjunction with sedimentology described in the lake core to estimate minimum potential water levels in the absence of shoreline positions.

4.3.4. Spillway elevations

Spillways and sills composed of alluvium in seismically active lake basins are especially dynamic because they are relatively more erodible compared to bedrock and can occupy different positions through time. Changing sill positions are mostly controlled by channel down-cutting—influenced by the combination of fluctuating rates of base-level changes, headward erosion, and tectonic or isostatic ground deformation. Understanding the types of ground deformation in sill areas affords an assessment of potential processes and accurate reconstruction of overflow levels similar to the approach taken for shorelines. We reconstructed spillway elevations by accounting for differential fault-block vertical deformation in sill areas similar to the approach used to correct the elevations of shoreline features and deposits, and lake core sites. Given the uncertainty of the absolute position of alluvial-filled spillways without information, we reconstructed the elevations of bedrock sills at 1 ka time steps to provide minimum estimates of the absolute elevations of periods with overflow conditions since 50 ka.

The northern half of the spillway channel of Owens Lake is bounded by the normal SNFF and dextral-oblique OVF, as well as situated within a graben of the normal SFF (Figs. 3 and 5). Total vertical deformation in the area of the overflow channel and sill was estimated by accounting for distributed slip between normal and dextral-oblique faulting. Paleoseismic investigations on the SFF indicate the most recent event on the fault occurred at ~28 ka (Amos et al., 2013). Furthermore, dextral-oblique faulting on the OVF has also been the primary source of deformation in Owens Valley over the last ~16 ka, which was preceded by a period that included both normal and dextral-oblique faulting from all faults in the basin between ~16 and 40 ka (Bacon et al., in review). As a result, we accounted for spatiotemporal patterns of the distribution of slip at the overflow channel by reconstructing the elevation of the lowest strath terrace in the channel at an elevation of ~1113 m asl with two net vertical slip rates (B–B'; Fig. 6). Ground deformation at the spillway during the most recent period between 0 and 28 ka was estimated by accounting for only footwall deformation on the OVF, which required a mean uplift rate of 0.12 m/kyr. (Table 4). The uplift rate of the OVF yielded as much as ~3.4 m of correction to lower elevations in the last 28 ka. The period from 28 to 50 ka, however, required a mean net subsidence rate of 0.22 m/ka from the summation of mean vertical rates for hanging wall deformation on the SNFF and SFF, and footwall deformation on the OVF of –0.25, –0.09, and 0.12 m/ka, respectively (Table 4). The net subsidence rate resulted in as much as ~4.8 m of correction to higher elevations during the earlier 22 ka period. The reconstruction shows the bottom of the northern reach of the spillway channel has been relatively stable with a net ~1.4 m of mean subsidence in the last 50 ka when accounting for net vertical deformation, as well as earthquake cycles and distributed slip on bounding faults.

4.4. Lake-level Indicators

Reconstructing accurate lake-level curves requires detailed knowledge of how the lake surface has fluctuated through time. Lake-level curves are typically constructed from the ages and elevations of samples that were deposited above, at or near, or below lake level (Reheis et al., 2014, and references therein). The lake-level curve in this study was constructed from shoreline elevations and ages of a variety of indicators for depositional environments, but also included threshold lake-water depth modeling of lake-core sedimentology to produce continuous estimates of water-level variations in the absence of shoreline information (Bacon et al., 2018). The curve also includes reconstructions of lake bottom and spillway elevations to produce a fully integrated model of lake-level variations that are corrected for vertical ground deformation (Fig. 10). The elevation of lake levels shown on the curve was developed from the type of depositional environment indictor and assigned water depths based on conservative estimates to minimize errors in modeled lake size.

4.4.1. Beach ridges and depositional carbonate

Beach ridges are the most precise indictor for the location of water level at the time of deposition, and as a result, the position of lake level shown on the curve corresponds to the reported elevation of ridge crests. A variety of calcium carbonate materials have also been used in lake-level reconstructions (e.g., Benson et al., 2013; Hudson et al., 2017, but there are large uncertainties in the absolute water depth at the time of deposition if the material is either depositional (i.e., tufa, marl, oolites) or faunal (i.e., gastropod, bivalve, ostracode). Studies in Pyramid Lake subbasin and Lahontan basin, Nevada identified several conditions or processes to explain the occurrence and uneven spatial distribution of tufa deposits, beginning with the most important process as follows: (1) stable lake level; (2) proximity to a source of calcium; (3) existence of a hydrologically closed system; (4) presence of a stable substrate; and (5) elevated water temperature (Benson, 1994). In general, the morphology of tufa accumulations can indicate lake-level dynamics during the time of deposition. Large accumulations commonly occur at elevations that coincide with lake levels stabilized by either relative changes in bathymetry of the lake basin or spill levels into adjoining basin or sub-basins, whereas relatively thinner sheet-like tufa deposits form during fluctuating lake levels in response to climate change (Benson, 1994).

The uncertainty of water depth for tufa ages in Owens Lake basin was accounted for by assigning a depth of 3 m. Other carbonate deposits including oolitic sand and marl (mud) were also used to define water levels in this study. These types of lacustrine sediment form in shallow (i.e., high-energy) and deep (i.e., low-energy) depositional environments, respectively (Ehlers and Blatt, 1982). Field observations of modern lacustrine oolitic sand deposits are commonly restricted to a depth of 0 to 5 m (e.g., Davaud and Girardclos, 2001). Therefore, a typical water depth of 2 m was assigned to oolitic sand samples to define water levels. Sample sites of marl, however, were assigned variable water depths from the threshold lake-water depth analysis using a study site's fetch and a range of particle sizes of coarse silt to clay for muddy sediment.

4.4.2. Fossil mollusk and crustacean shells

Additional carbonate materials including shells from mollusks were used to define water levels of Owens Lake. Deposits with either articulated bivalve shells or well-preserved gastropod shells have the highest confidence in representing the substrate utilized by mollusk species while living, whereas deposits with either disarticulated bivalve shells or a mixed assemblage of species is evidence of post-mortem transport and reworking. A variety of mollusk taxa associated with different aquatic habitats have been identified and dated in the paleo-Owens River system (Miller, 1989; Koehler, 1995; Smith, 2009; Rosenthal et al., 2017). We only used mollusk species from lacustrine deposits as lake-level indicators in an effort to not include species typically associated with terrestrial environments disconnected from a large water body, such as springs and ponds. Up to four species of bivalve have been documented in Owens Lake lacustrine sediment (Miller, 1989; Koehler, 1995), however, only two species (*Sphaerium striatinum* and *Anodonta californiensis*) have been dated from samples collected from shore to nearshore depositional environments (Table 1). In general, living *Sphaerium* sp. throughout North America and Northern California are found mostly in clean permanent lakes at depths of several cm to ~20 m and prefers sandy to gravelly substrates. Living *Anodonta* sp. in the western U.S. also predominantly live in large perennial lakes, but require a specific host fish during its larval stage and prefers sandy to muddy substrates (e.g., Koehler, 1995). A water depth of 4 m was assigned to bivalve lake-level indicators in this study given the wide range of water depths associated with living *Sphaerium* sp. and *Anodonta* sp., in conjunction with sample sites consisting mostly of silty sand to gravelly sand sediment that are deposited in relatively shallow water.

Many more gastropod species have been identified and dated in the paleo-Owens River system with up to twenty-two species of aquatic and semi-aquatic gastropod identified in deposits associated with either terrestrial or lacustrine depositional environments (Miller, 1989; Koehler, 1995; Smith, 2009; Rosenthal et al., 2017). Only two species have been dated from samples collected from deposits in Owens Lake basin interpreted to be from shore to nearshore depositional environments (Table 1). One of the gastropods *Amnicola*is a gilled species and the other *Helisoma* is a pulmonate. Interpreting the depositional environment of pulmonate species is complicated because many of them are found in both terrestrial (i.e., spring, delta plain) and lacustrine (i.e., back-barrier lagoon, wetlands) environments. We reduce this uncertainty by using gastropods that are sampled from both deltaic and lacustrine deposits, as well as from elevations with other supporting stratigraphic and geomorphic lake-level indictors. In general, the gastropods including *Helisoma newberryi* live in large perennial lakes and streams. This species prefers muddy substrate with or without vegetation (e.g., Koehler, 1995). The other dated gastropod including *Amnicola palustris* is commonly found in waters with a wide range of water qualities and temperatures and can tolerate seasonal fluctuations in water level within wetlands, small streams, and ponds. These species commonly prefer densely vegetated shallow water environments (e.g., Koehler, 1995). A uniform water depth of 2 m was assigned to the gastropod lake-level proxy in this study given that most shells were sampled from deposits interpreted to be from wetlands to shoreline depositional environments.

In addition to mollusk species, ostracod valves were also identified in lacustrine deposits of Owens Lake. We use ostracods to define lake levels by assigning variable water depths to the elevation of sample locations from the threshold lake-water depth analysis using a fetch for the lake core site and a range of particle sizes of coarse silt to clay for muddy sediment.

4.4.3. Terrestrial landforms and deposits

Landforms and deposits associated with terrestrial depositional environments were also used to define maximum lake level. Most of the materials dated were sampled from deposits associated with environments adjacent to or distant to the water's edge, including delta and alluvial plains, wetlands, and springs. The materials include organic sediment, plant material, peat, carbonized wood, charcoal, and soluble pack rat middens (Table 1). Sandy deposits from colluvial slopes in the Owens Lake overflow channel were also dated by OSL and used to define maximum lake levels (Table 3). The elevation of sample sites associated with terrestrial environments were used to limit the position of water levels shown on curves to below their respective elevations.

4.4.4. Sediment core proxy records

Proxy evidence in lake cores from Owens Lake including variations of total organic carbon (TOC), total inorganic carbon (TIC) and $\delta^{18}O$ values (Benson et al., 1996; 1997; 1998) and presence of thick oolitic sand deposits (Smith and Bischoff, 1997) were collectively used as proxy indicators of relative evaporation in the lake system to represent either drops in lake level or hypersaline lake conditions. Reconstructed depths of proxy data in lake cores were also used in this study to constrain the direction of lake-level oscillations in the absence of shoreline data (e.g. Bacon et al., 2006).

5. Discussion

5.1. Revised Owens Lake water-level record

We revised the Owens Lake water-level record with new ages and estimates of the timing and elevation of lake levels without shoreline data from threshold lake-water depth modeling of sedimentology in core OL-92. We also provide new direct ages for episodes of spill of Owens Lake based on geotechnical investigations and reconstructions of sill elevations within the overflow channel. Integration of these new data offers a comprehensive and continuous characterization of the lake-level history of Owens Lake that, in turn, allows refinement and extension of the lake-level curve to 50 ka (Fig. 10). The following discussion includes descriptions of modeled water-level variations of Owens Lake and periods of potential overflow in relation to periods of rapid climate change and general comparisons with Owens Lake sediment core records and lake-level records of downstream China and Searles Lakes basins.

5.1.1. Overflow record (50 to 6.4 ka)

Many basins in the western U.S. were hydrologically integrated by streams or coalescing lakes during pluvial periods (Smith and Street-Perrott, 1983; Jannik et al., 1991; Reheis, 1999; Phillips, 2008). In general, sills and associated overflow channels controlled the absolute water level of hydrologically open lakes, which could either be characterized as stable (i.e., hard) or unstable (i.e., soft) in terms of erodibility (e.g., Pengelly et al., 1997). Sill areas in seismically active lake basins in the Basin and Range are commonly affected by either uniform tilt related to isostatic rebound or faulting from single fault system (e.g., Mifflin and Wheat, 1979; Adams et al., 1999) or vertical ground deformation related to distributed normal and oblique faulting in lake basins that are within the southern WLB, such as in Owens Valley (Fig. 2). Accounting for distributed slip at the Owens Lake overflow channel and sill in our study afforded reconstruction of overflow levels, as well as provided limiting elevations to constrain the timing of potential overflow episodes. The majority of contemporary annual streamflow in the Owen River watershed is from rain and snowmelt runoff from ~20% of the drainage area on the eastern slopes of Sierra Nevada (Hollet et al., 1991). Discharge from the Owens River watershed is required to support downstream lakes in China and Searles basins, even during pluvial periods, because of high rates of evaporation from valleys bottoms and low runoff from surrounding mountains due to rain shadow positions and a lack of high elevations in both watersheds (e.g., Smith and Street-Perrott, 1983; Jannik et al., 1991; Phillips, 2008).

New geotechnical investigations of the sill area of Owens Lake presented in this study provided stratigraphy and ages to link water levels between the overflow channel and shoreline features in the lake basin, providing the timing of the most recent episodes of overflow. Data from the overflow channel indicated that the sill of the basin is dynamic and has ranged in elevation from ~1113 to 1165 m during the late Pleistocene to Early Holocene, thereby suggesting far more recent hydrologic connections between Owens Lake and downstream lake basins than previously understood. The characterization of the overflow channel in combination with accounting for vertical ground deformation has produced reconstruction of sill elevations that define the minimum elevations of potential overflow levels (Fig. 10).

The well sorted and rounded sandy sedimentology described in the overflow channel with OSL ages of ~11.6, 7.6, and 6.9 ka suggests that the channel fill was deposited as the fluvial-deltaic sedimentary facies of an overflowing lake. Accounting for tectonic ground deformation at the borehole site results in corrected elevations between ~1119 and 1127 m asl for water levels associated with the fluvial-deltaic sediment (Table 3; Fig. 10). The range of elevations and OSL ages of the fluvial-deltaic sediment are similar to the higher beach ridges at the Centennial Flat site that developed at elevations between ~1127.9 and 1131.3 m at 12.8 to ~6.2 ka (Tables 2 and 3; Fig. 10). The new OSL ages from the overflow channel provide direct evidence of latest Pleistocene spill as recently as 11.6 ± 1.8 ka. The data also indicates that Owens Lake last overflowed between ~8.4 and 6.4 ka, which is ~4–5 ka later than previously inferred (Fig. 10). A change to alluvial deposition above ~1134.8 m asl in the overflow channel beginning at ~5800 cal yr BP from a ^{14}C age on wood in trenches is the same age as the youngest and lowest beach ridge at the Centennial Flat site, as well as the beginning of oolitic sand deposition and shallow conditions at Owens Lake indicating a change to dryer hydroclimatic conditions by this time (Fig. 10).

The stratigraphic and geochronologic data showed the spillway of Owens Lake basin is dynamic and currently composed of up to ~40 m of unconsolidated fluvial-deltaic and alluvial sediment, rather than a stable and perhaps shallow bedrock sill, as previously interpreted (e.g., Smith and Street-Perrott, 1983; Bacon et al., 2006). The position of the strath terrace in the northern reach of the overflow channel provides minimum elevations for potential overflowing water levels of Owens Lake at 1112.8 ± 2.7 m. Reconstruction of the strath terrace at this elevation using variable vertical slip rates based on spatiotemporal patterns of distributed fault slip in the area shows that a net subsidence of ~1.5 m has occurred in the channel since 50 ka (Fig. 10). This implies that the sill has been relatively stable during this period. Presence of prominent shorelines features at ~1114 m asl and evidence of both in situ and reworked shoreline deposits, plus mollusk-rich deposits from many sites encompassing the lake basin at ~1111–1113 m asl have reconstructed elevations that corroborate sill-controlled and mostly overflowing water levels at relatively low elevations from ~46 to 13 ka (Table 1; Fig. 10). The revised overflow record of Owens Lake confirms previous inferences that Searles Lake was predominantly the terminal lake in the paleo-Owens River system based on thick sequences of lacustrine mud and interbedded evaporate layers in sediment cores of Pliocene to late Pleistocene age (e.g., Smith, 1979; Phillips, 2008), coupled with no stratigraphic evidence of hypersaline lake conditions or complete desiccation of Owens Lake between ~50 and 6 ka (Benson et al., 1996; Smith and Bischoff, 1997).

5.1.2. Lake-level record (50 to 12.8 ka)

The new mollusk and ostracod ages from the Dirty Socks, OVF, and Swansea sites of our study and previously published lake-level ages from other sites that encompass the lake basin were used to revise the lake-level record of Owens Lake from 50 to 12.8 ka (Table 1; Fig. 10). Relatively low reconstructed elevations of nine mollusk and ostracod data show good elevation correspondence with reconstructed sill elevations for periods of overflow. The majority of the mollusk used are bivalves, and in particular *Anadonta* sp., which is an indicator taxa for a “fresh” aquatic environment and open lake system (i.e., overflowing) because it relies on fish for its reproductive cycle, whereas palmonate gastropods indicate relatively less open and likely a more saline aquatic environment (Firby et al., 2008; Table 1; Fig. 10). Without performing the elevation reconstruction of sample sites with aquatic mollusks it would have been difficult to reconcile their field elevations, because all sites are located well below the hard sill level, thereby suggesting a closed lake system. The good elevation correspondence between the reconstructed positions of mollusk species requiring overflowing lake conditions at or near sill levels validates the approach developed in this study to reconstruct elevations by accounting for distributive faulting across individual fault blocks in the lake basin and in the overflow channel area (Fig. 10).

Moderate to high water levels above the hard sill were also identified from mollusk and tufa ages of this study and previously reported luminescence ages for highstand lake levels. A major transgression of Owens Lake up to an elevation of ~1165 m asl was previously dated by post-IR-IRSL analysis. Duplicate samples from sandy beach ridge deposits at an elevation of ~1156 m returned a mean age of 40.8 ± 4.9 ka and a single sample from ~1163 m asl yielded an age of 40.1 ± 3.0 ka (Bacon et al., in review). The mean ages and elevations show that the second highest shoreline in the lake basin was constructed by a major transgression that was relatively short lived (~700 yr) prior to falling to low, but overflowing lake levels near the hard sill (Fig. 10). Maximum overflow defined from OSL ages of colluvial slope deposits along the overflow channel and soluble packrat middens near Lone Pine support the age of the ~1165 m highstand shoreline (Fig. 10). Bounding ages from mollusks near the hard sill level suggest the ~40.5 ka lake-level oscillation and major transgression was controlled by high rates of alluvial fan deposition in the overflow channel to out compete down-cutting from discharge of the lake during this time.

The timing of seven lake-level oscillations between 37.0 and 28.6 ka inferred from TOC proxy data in lake core OL-90 combined with threshold lake-water depth analysis were also used to estimate episodes with little to no overflow during this time (Fig. 10). Moderate oscillations in lake level centered at ~26–23, 20.0–19.3, 17.5, 15.6, 14.6, and 13.8 ka reached elevations up to ~5–20 m above the hard sill from mollusk and tufa indictors (Fig. 10). The timing of the four later transgressions centered at ~17.5, 15.6, 14.6, and 13.8 ka have good offset temporal correspondence with the ages of lake-level fluctuations to lower levels at 16.9, 15.1, 14.2, and 13.2 ka inferred from $\delta^{18}O$ proxy data in lake core OL-84B that collectively define the magnitude of complete lake-level cycles above and below the hard sill during this period (Table 1; Figs. 10).

5.1.3. Lake-level record (12.8 to 5.8 ka)

The stratigraphy and new post-IR-IRSL ages of beach ridges of our study at the Centennial Flat site provide evidence for at least two lake-level cycles between the elevations of

~1114 and 1133 m asl from ~12.8 to 5.8 ka that had not been previously recognized at such high temporal and elevational resolutions in Owens Lake basin (Fig. 10). Sediment dated within the deeper section of the ~1129 m beach ridge below a clear depositional boundary indicates the first transgression reached an elevation up to ~1131 m asl by ~12.8 ka (Table 2; Figs. 4 and 10). Additional sediment of latest Pleistocene age was not dated in other beach ridges at the site, because sediment was either reworked into younger deposits by subsequent alluvial and lacustrine processes or is present at deeper depths than sampled. Tufa and mollusks from several other sites (Dirty Socks, OVF, Swansea) at similar elevations to the Centennial Flat site support a transgression at ~13 ka, and two lower transgressions up to ~1119 and 1121 m asl that were centered at ~11.6 and ~10.6 ka, respectively (Table 1; Figs. 3 and 10). The two oscillations in lake level between ~13.0 and 11.4 ka are well constrained with post-IR-IRSL and OSL ages from beach ridge in the lake basin and fluvial-deltaic deposits in the overflow channel, as well as many mollusk and tufa ages across the lake basin that show lake levels fluctuated between elevations of ~10–20 m above the hard sill to as low as ~10 below the hard sill.

The timing of three transgressions centered at ~12.8, 11.6, and 10.6 ka also have temporal correspondence with the ages of preceding lake regressions from wood and organic sediment in delta plain deposits at sites north of Lone Pine (AGPS, ORB, QPS), in addition to lake-level fluctuations to lower levels centered at 12.2 and 11.3 ka inferred from $\delta^{18}O$ proxy data in lake core OL-84B (Tables 1 and 2; Figs. 3 and 10). An additional dry period is also indicated by the threshold lake-water depth analysis of silty sediment in core OL-92 that shows low water levels below the sill between ~10.5 and 9.0 ka (Fig. 10). This major drop in lake level also appears to have significantly impacted mollusk population structure because mollusks have not been identified in lacustrine deposits younger than ~10.5 ka, suggesting possible extirpation of aquatic mollusk species in the lake basin during sustained and low lake levels.

The ~1.5 ka period with low lake levels was followed by a major Early Holocene transgression. The Early–Middle Holocene post-IR-IRSL ages from our study from the upper sections of all the beach ridges at the Centennial Flat site are supported by soil-geomorphologic characteristics observed in each beach ridge. The post-IR-IRSL ages define the magnitude and duration of the second and last significant lake-level cycle of Owens Lake. The ~8.8 ka age for sediment from the lowest beach ridge at ~1114 m asl indicates it was subsequently reworked into younger deposits, but that it may also represent the age of older deposits associated with lower water levels at this elevation prior to an Early Holocene transgression. A rise in water level of ~17 m to an elevation of ~1131 m asl is indicated by the construction of the highest beach ridge at ~8.4 ka that was short lived before dropping ~2 m to construct the ~1129 m beach ridge at ~8.1 ka (Figs. 4 and 10). Water level was relatively stable with minor lake-level variations for ~2 ka after the initial transgression. Stable lake levels during this period is from the age of sediment from the lower beach face of the ~1127 m beach ridge that indicates that a water level reached an elevation of up to ~1126 m asl by ~7.6 ka, prior to a subsequent rise in water level that formed the ~1127 m beach ridge at ~6.4 ka (Figs. 4 and 10). A major regression with no overflow after ~6.4 ka is indicated by a large drop in water level of ~7 m that briefly stabilized to form the inner ~1120 m beach ridge at ~6.2 ka, followed by an additional drop in water level of ~6 m which formed the ~1114 m beach ridge at ~5.8 ka (Figs. 4 and 10).

Geomorphic and stratigraphic analysis of paleoseismic trench sites (AGPS, QPS, ORB) north of Lone Pine previously identified an Early Holocene transgression of Owens Lake that reached elevations ranging from 1113 to 1128 m asl, with a maximum estimate of up to 1135 m asl (Bacon et al., 2006; Bacon and Pezzopane, 2007; Fig. 3). The ages of carbonized wood and organic sediment from interbedded delta plain layers with lacustrine deposits exposed in both fault trenches and banks of the Owens River were previously used to define the beginning of the Early Holocene transgression to after ~10.2 ka. Shore and nearshore stratigraphy in fault trenches combined with tufa ages provided the first information on the elevations and timing of the Early Holocene transgression above elevations of ~1122 and 1117 m asl between ~8.4 and 7.5 ka, respectively (Bacon et al., 2006; Bacon and Pezzopane, 2007) (Table 1; Fig. 10). The geomorphology and post-IR-IRSL ages of beach ridges of this study have revised the maximum elevation of the Early Holocene transgression up to ~1133 m asl after accounting for tectonic ground deformation, as well as providing additional lake-level indicators on the timing of the regression to a much later period extending into the Middle Holocene (Figs. 10).

5.1.4. Lake-level record (5.8 ka to 1872 AD)

The Owens Lake water-level record during the beginning of the Middle Holocene warm period reflects extreme hydroclimatic variability in the form of persistent, multi-centennial to multi-millennial scale drought conditions. Shallow and hypersaline lake conditions between ~5.8 and 3.2 ka are shown by many ^{14}C ages from a well-sorted oolitic sand deposit in core OL-92

(Smith and Bischoff, 1997), which is supported by a post-IR-IRSL age of 5.0 ± 0.2 ka on alluvial fan deposits at an elevation as low as 1099 m in the lake basin (Bacon et al., 2018; Fig. 10). The recently revised Late Holocene lake-level history of Owens Lake based on post-IR-IRSL analysis on sandy sediment of four shoreline features above the historical water level (1096.4 m) in AD 1872–1878 provides information to better understand hydroclimate variability in the southern Sierra Nevada during the Late Holocene based on the ages of major transgressions up to elevations of ~1108, 1103, and 1099–1101 m (Bacon et al., 2018). Furthermore, up to eighteen oscillations were estimated from threshold lake-water depth analysis of interbedded muddy and sandy layers in core OL-97, thereby showing Owens Lake had significantly lower water levels not reflected in the geomorphic record from ~3.6 ka to AD 1872–1878 (Fig. 10).

5.2. Spatiotemporal patterns of Owens Lake water-level fluctuations with regional and global climate variability

Past studies in the western U.S. have correlated the age of Holocene lake-level fluctuations to regional climate variability (e.g., Enzel et al., 1989; Stine, 1990; Adams, 2003; Kirby et al., 2014, 2015; Bacon et al., 2018) and late Pleistocene highstands to changes in North Atlantic climatic phases (e.g., Benson et al., 1996, 1997; 1998b, Negrini, 2002; Zic et al., 2002; Munroe and Laabs, 2013; Garcia et al., 2014; Reheis et al., 2015; Knott et al., 2019). The North Atlantic climatic phases were reflected by periods of relatively warm air and sea surface temperature referred to as Dansgaard–Oeschger (D–O) cycles that were followed by relatively cold phases associated with increased melting of the Laurentide Ice Sheet and discharge of icebergs known as Hienrich events or stadials (e.g., Heinrich, 1988; Bond et al., 1992; Dansgaard et al., 1993; Hemming, 2004). Shoreline and speleothem records in the southwestern U.S. and Great Basin demonstrate during the last deglaciation wetter conditions in the region were coincident with cool periods in the North Atlantic, such as Heinrich 1 and Younger Dryas stadials, and drier conditions coincident with warm periods, such as the Bølling and Allerød interstadials (i.e., D–O cycles) (e.g., Asmerom et al., 2010; Munroe and Laabs, 2011; Oster et al., 2015). Furthermore, older shoreline and speleothem records mostly from the southern Great Basin and Mojave Desert in eastern California also demonstrate lake-level fluctuations and cool wet conditions between ~45 and 25 ka coincided with Heinrich stadials 3 and 4 (Garcia et al., 2014; Reheis et al., 2015; Knott et al., 2019; Oster et al., 2014).

Studies of Owens Lake sediment cores have also linked $\delta^{18}O$, TOC, and TIC proxy data of rapid climate change to D–O cycles and Heinrich stadials 4–1 between ~53 and 18 ka, thereby indicating nearly synchronous climate change in the northern Hemisphere (Benson et al., 1996). The synchronous climate change is generally reflected in lacustrine sediment core records in the Great Basin as high lake levels during warm North Atlantic climatic phases (D–O cycles) and low lake levels during cold ones (Heinrich stadials) (e.g., Benson et al., 1996, 1997; 1998b; Negrini, 2002; Zic et al., 2002) in contrast to correlations made using shoreline and speleothem records that show the opposite relations. The apparent discrepancy between the different types of records maybe related to uncertainty in age-depth models used in lake cores (Munroe and Laabs, 2011; Reheis et al., 2015; Franke and Donner, 2019). Potential errors are likely associated with uncertainty in accurate reservoir corrections applied to ^{14}C ages (Benson et al., 1997), as well as a lack of correction for sediment compaction which would also underestimate the age of progressively deeper sediment containing proxy indicators. Although Benson et al. (1996; 1997) acknowledged errors in their age-depth model that prohibit absolute synchroneity between Owens Lake and North Atlantic climate records, they did show a similar number of large and abrupt climate signals in the proxy data to major latest Pleistocene climatic phases in the Northern Hemisphere.

We performed a comparison of the revised lake-level record of Owens Lake from our study with the $\delta^{18}O$ ice core record from the North Greenland Ice Core Project (NGICP; Andersen et al., 2004) to verify correlations between rapid climate change in the Northern Atlantic and the Owens River watershed (Fig. 11). We also compared the $\delta^{18}O$, TOC, and TIC proxy records from Owens Lake cores OL-84B and OL-90 of Benson et al. (1996, 1997) to the water-level record of Owens Lake to understand potential differences or limitations in comparing these types of lacustrine datasets (Fig. 11). We corrected for compaction and reservoir effects in the Owens Lake core proxy records to assess if these corrections increased the temporal correspondence between both the Owens Lake shoreline and North Atlantic ice core records. The reported age-depth models for cores OL-84B and OL-90 were refined by using equation 1 to account for compaction. We also applied a reservoir correction of 1000 yr to the lake core age-depth models, which was an increase from the previously used reservoir correction of 600 yr (Benson et al., 1996; 1997). This reservoir correction was chosen because a comparison between late Holocene shoreline and lake core OL-97 records demonstrate that the carbonate-rich mud in lake cores used for ^{14}C dating had a reservoir effect of ~1000 yr (Smoot et al., 2000; Bacon et al., 2018). In general, the adjusted $\delta^{18}O$, TOC, and TIC proxy records have good temporal correspondence between the Owens Lake shoreline and North Atlantic ice records, where decreases in $\delta^{18}O$ and TIC commonly agree with the age of relative highstands and timing of Heinrich stadials (wet conditions), and increases in TOC (dry conditions) generally coincide with relative lowstands and D–O interstadials, similar to other shoreline and spelothem records in the western U.S. (e.g., Asmerom et al., 2010; Munroe and Laabs, 2011; Oster et al., 2014, 2015; Reheis et al., 2015; Fig. 11).

5.2.1. Owens Lake highstands

There is good temporal correspondence of water-level variations between transgressions of Owens Lake and hydroclimate variability during the late Pleistocene and Holocene. The major transgressions of Owens Lake at ~41–40 ka and smaller transgression at ~38.7 ka, plus corresponding variations in the geochemical proxy records of core OL-90 coincide with Heinrich stadial 4 (HS4; Fig. 11). Supporting stratigraphic evidence for moderate to deep lakes and high sedimentation rates in the overflow channel of Owens Lake during HS4 is from additional core proxy data, plus alluvial and glacial stratigraphy in the Sierra Nevada. Core OL-92 shows the highest weight percent of clay deposition since ~130 ka occurred at ~39.5–43 ka indicating a deep lake during this time (Smith and Bischoff, 1997; Litwin et al., 1999). In addition, the rock flour record of composite core OL-90/92 shows evidence of two glacier advances at 49.0–45.1 and 42.8–39.0 ka, with the latter advance coinciding with the ~40 ka transgression of Owens Lake (Bischoff and Cummins, 2001). Geomorphic evidence of increased runoff in the watershed at 32–44 ka from surface exposure dating of wide-spread alluvial fan deposits in Owens Valley near Line Pone indicates an increase in runoff to the lake during a broadly defined period encompassing HS4 (Benn et al., 2006). The two major oscillations in lake level during HS4 reached elevations of ~45 and 20 m above the hard sill prior to major glacial advances in the Sierra Nevada during the Tioga glaciation (MIS 2) from 30.5 to 15.0 ka that encompassed HS3–HS1 (Clark and Gillespie, 1997; Bischoff and Cummins, 2001; Phillips et al., 2009; Gillespie and Clark, 2011; Rood et al., 2011; Moore and Moring, 2013; Fig. 11).

Given the geomorphic and numerical age uncertainties of lake-level indicators used in our study, six later transgressions that reached 10–20 m above the hard sill at ~26–23, 19.3, 17.5, 15.6, 13.8, and 12.8 ka coincided with periods of global-scale climate change (Fig. 11). The age of highstands at ~26–23, 19.3, and 15.6 ka are within the range of ages for Tioga glacial fluctuations and deglaciation in the Owens River watershed (Phillips et al., 1996, 2009; Gillespie and Clark, 2011; Rood et al., 2011). There is good temporal correspondence between the ~26–23 ka and ~17.5 and 15.6 ka transgressions of Owens Lake and HS2 and HS1, respectively, whereas the period of HS3 is reflected by little to no overflow (Fig. 11). The major transgression at ~19.3 ka, however, did not occur during a Hienrich event, but instead coincided with the age of last glacial maximum retreat in the Sierra Nevada at 18.8 ± 1.9 ka (Rood et al., 2011). Corresponding variations in the $\delta^{18}O$, TIC, and TOC proxy records of core OL-90 indicate mostly overflowing conditions during the Tioga glaciation (Benson et al., 1996). The core proxy records generally show good temporal correspondence with lake-level fluctuations, where the $\delta^{18}O$ record exhibits the greatest correspondence during the Tioga glaciation (Fig. 11). Furthermore, the broad transgression of Owens Lake with overflowing water levels ending by ~15.6 ka during HS1 coincided with the age of high lake levels of China-Searles Lake (Rosenthal et al., 2017) and the highstand of Lake Lahontan in northern Nevada at ~15.7 ka (Adams and Wesnousky, 1999).

The post-glacial highstands of Owens Lake at ~13.8 and 12.8 ka also occurred during periods of climate change in the Sierra Nevada coinciding with the Recess Peak glaciation from 14.1–13.1 ka during the Older Dryas stadial (Clark and Gillespie, 1997; Phillips et al., 2009) and the beginning of cold and wet climate during the Younger Dryas stadial from lake core proxy indicators at Owens Lake and high elevations lakes (Mensing, 2001; MacDonald et al., 2008; Fig. 11). The transgressions of Owens Lake between ~13.8 and 12.8 ka also have good temporal correspondence with high lake-level oscillations of a coalesced China-Searles Lake (Rosenthal et al., 2017), as well as variations in water levels of Pyramid Lake on the east side of the northern Sierra Nevada (Adams and Rhodes, 2019b; Fig. 1). The last two transgressions with overflowing lake conditions during the latest Pleistocene occurred at ~11.6 and 10.7 ka that coincided with the end of the Younger Dryas stadial and beginning of the Holocene during relatively wet and brief periods inferred from pollen and algal proxy data in core OL-84B (Mensing, 2001). Changes in hydroclimate variability at the Pleistocene-Holocene transition (~14.6–8 ka) in the southwestern U.S. has been linked to semi-permanent El Niňo-like conditions in the Tropical Pacific, which enhanced the frequency of winter frontal storms and increased penetration of tropical cyclones that influenced alluvial fan aggradation in most of the region (Antinao and

McDonald, 2013). The magnitude of post-glacial highstands of Owens Lake were likely controlled, in part, by variations in alluvial fan aggradation in the overflow channel that created soft sills that impounded Owens Lake during this period.

An Early-Middle Holocene transgression of Owens Lake attained high and stable water levels between 8.8 and 5.8 ka. Owens Lake spilled during this transgression at elevations ranging from ~1132–1129 m asl between ~8.4 and 6.4 ka, which likely had low-energy surface flows based on stratigraphy and paleoenvironmental conditions in Rose Valley during this time (e.g., Rosenthal et al., 2017; Fig. 1). The Early Holocene highstand documented by geomorphic data in the lake basin is also supported by δ^{18}O and TIC values in sediment cores that indicate relatively wet conditions at 10–8 ka (Benson et al., 2002; Fig. 11). The Early Holocene highstand of Owens Lake attained its highest level at ~8.4 ka coincident with an Early Holocene cooling event at ~8.4–8.0 ka identified in Greenland ice-core proxies (e.g., Alley et al., 1997) and towards the end of a period with enhanced winter sub-Tropical moisture flux across the southwestern U.S., commonly referred as atmospheric rivers (e.g., Enzel et al., 1989; Antinao and McDonald, 2013; Kirby et al., 2015; Steponaitis et al., 2015). The timing of the Early-Middle Holocene transgression of Owens Lake with two distinct oscillations and associated highstands at ~9.2–7.6 and ~7.6–5.8 ka is also similar to the lake-level records of nearby Mono and Tulare Lakes. The watersheds of Mono and Tulare Lakes share common drainage divides with the Owens River watershed (Fig. 1). Mono Lake on the north had two early Holocene lake-level oscillations and associated highstands at ~9.4–7.2 and ~7.2–5.5 ka (Stine, 1990). Tulare Lake on the west side of the southern Sierra Nevada in the San Joaquin Valley is directly west of Owens Lake and also had two early Holocene highstands and evidence of deep lakes at ~9.5–8.0 and ~6.9–5.8 ka (Negrini et al., 2005; Blunt and Negrini, 2015).

Owens Lake had mostly shallow to near desiccation water levels since ~6.4 ka that were punctuated with transgressions of up to ~11–25 m. Post-IR-IRSL ages of major transgressions at elevations of ~1108, 1103, and 1099–1101 m asl coincided with wetter and cooler climate during the Neopluvial (~3.6 ka), Medieval Pluvial (~0.8 cal kyr BP), and Little Ice Age (~0.35 ka), respectively (Fig. 11). The Late Holocene ages of lake-level oscillations shown on the lake-level curve of Owens Lake have good temporal correspondence with proxy indicators of wet and dry conditions from shifts in δ^{18}O values and stabilizing of TIC and magnetic susceptibility in sediments of core OL-84B (Benson et al., 2002; Fig. 11). These lake-level oscillations where likely driven by renewed hydroclimatic variability and increased runoff in the Owens River watershed from enhanced winter sub-Tropical moisture in the region (e.g., Kirby et al., 2014).

The age of Late Holocene water-level variations of Owens Lake also have good temporal correspondence to the Late Holocene lake-level records of nearby Mono Lake (Stine, 1990) and Walker Lake (Adams and Rhodes, 2019a) on the east side of the central Sierra Nevada (Fig. 1). Comparison of shoreline records of large lakes on the west and east sides of the Sierra Nevada shows good temporal correspondence during the latest Pleistocene and Holocene indicating that even with inherited geologic uncertainties and dating methods in the different studies, all records show that each lake basin responded in a similar manner to hydroclimatic forcing coinciding with periods of global-scale climate change during the Holocene (e.g., Mayewski et al., 2004) (Fig. 11).

5.2.2. Owens Lake lowstands

The lake-level and sill reconstructions of Owens Lake show several periods of low lake levels during little to no overflow conditions that also correspond to regional and global hydroclimate variability. The timing of episodes with little to no overflow have good temporal correspondence with periods of major lake-level oscillations in downstream lakes. Seven of the earlier episodes are inferred from a lack of shoreline data at and above sill levels combined with TOC proxy data from core OL-90 for the age of changes in Owens Lake levels between ~37 and 28.5 ka (Figs. 10 and 11). Major lake-level oscillations at Searles Lake from U-Th and ^{14}C ages of salt layers and bounding muddy sediment in lake core X-52 collectively show playa lake environments to near desiccation at ~36.9, 33.8, 32.3, 30.3 and 28.5 ka (Lin et al., 1998; Phillips, 2008). The ages of salt deposition at Searles Lake have good temporal correspondence with the TOC proxy data from Owens Lake supporting little to no overflow during these times (Benson et al., 1996). The ages of little to no overflow of Owens Lake and shallow conditions at Searles Lake occurred primarily during warm phases in the North Atlantic during numerous D–O cycles between HS4 and HS2 (Fig. 11). Episodes of little to no overflow of Owens Lake also occurred between ~18 and 11 ka that are indicated by both proxy data in lake cores and shoreline indicators (Figs. 10 and 11). Two of the episodes had water levels ~10–12 m below sill levels at ~17.8 ka based on threshold lake-water depth analysis of a thin sandy layer in core OL-92 (Smith and Bischoff, 1997) and at ~13.1 ka from several mollusk ages from sites near the mouth of the

Owens River. Little to no overflow at these times were likely brief because lake-level reconstructions show a return to overflowing conditions shortly after the lowstands were reached (Figs. 10). The lowstand at ~17.8 ka coincided with a dry episode during the early Mystery Interval in the Great Basin centered at ~17.5 ka prior to HS1 (e.g., Broecker et al., 2009) (Fig. 11). The other lowstand at ~13.1 ka from mollusk ages is supported by geochemical, as well as pollen and algal proxy data in core OL-84B that indicate low lake levels and drought conditions at ~13.0 ka (Benson et al., 1997; Mensing, 2001). The major oscillation to low lake levels at ~13.0 ka occurred near the transition between the Bølling interstadial and Younger Drays stadial (Fig. 11). Furthermore, a regression of Owens Lake from $\delta^{18}O$ proxy data and shoreline indicators also occurred at ~15.5–14.9 ka that is reflected as a major oscillation to sill levels near the transition between HS1 and the Allerød interstadial (Figs. 10 and 11). The timing of this oscillation coincided with the end of Tioga deglaciation in the Owens River watershed by 15.0–14.5 ka (e.g., Clark and Gillespie, 1997; Phillips et al., 2009) and the last major D–O cycle in the North Atlantic region (Fig. 11).

A steady decrease in spill from Owens Lake and dryer and more variable hydroclimatic conditions at the Pleistocene-Holocene transition is indicated by the progressive age of desiccation of downstream lakes. The downstream lakes desiccated between ~0.6 and 1.1 ka of each other with Panamint Lake first desiccating at ~12.8 ka followed by Searles Lake at 11.7 ka and then China Lake by 11.1 ka (Jayko et al., 2008; Phillips, 2008; Hoffman, 2009; Smith, 2009; Rosenthal et al., 2017). Owens Lake attained fluctuating, but overflowing levels between ~12.8 and 10.5 ka with discharge insufficient to support perennial lakes, but great enough to provide a source of low-energy surface flow to support extensive perennial wetland habitats downstream in Rose Valley and the delta plain area of China Lake through inundation and local groundwater recharge from the paleo-Owens River in contrast to deeper mountain block recharge as previously inferred (e.g., Rosenthal et al., 2017). Owens Lake followed the trend of progressive desiccation by dropping below sill levels for ~1–2 ka beginning at 10.5 ka that is also reflected in the $\delta^{18}O$ and TOC proxy records (Fig. 11). The onset of low lake levels corresponds to a period of maximum solar insolation between 11 and 10 ka that appears to have resulted in a warm and dry climate, as indicated by pollen evidence in core OL-84B of a modern vegetation assemblage in Owens Valley at this time (Mensing, 2001), as well as lake core proxy evidence in the Mojave

Desert (Kirby et al., 2015), and speleothem records in the Great Basin (e.g., Lachniet et al., 2014; Steponaitis et al., 2015).

Owens Lake had mostly shallow to near desiccation water levels since the Early-Middle Holocene highstand ending at ~6.4 ka. This highstand was followed by near desiccation of Owens Lake between ~5.8 and 4.2 ka during the global-scale Mid-Holocene warm period (e.g., Bartlein et al., 2011). The frequency and duration of Owens Lake lowstands after ~4.2 ka are also in general agreement with periods of severe multidecadal to multicentennial droughts (i.e., megadroughts) documented in the western Great Basin and south-central Sierra Nevada during the early part of the late Holocene and the Medieval Climatic Anomaly centered at ~0.89 and 0.67 ka (e.g., Stine, 1994; Benson et al., 2002; Mensing et al., 2008, 2013; Cook et al., 2010; Bacon et al., 2018).

6. Conclusions

We refined the lake-level history of Owens Lake for the past 50 ka by applying a method to construct a continuous lake-level curve. New studies of several sites in the lake basin and subsurface geotechnical investigations within the overflow channel yielded stratigraphic and geochronologic information to define the timing of potential episodes of overflow. New post-IR-IRSL ages of beach ridges and previously unpublished OSL ages from fluvial-deltaic and alluvial sediment filling the overflow channel established the first spatiotemporal connections between Early-Middle Holocene and latest Pleistocene shorelines and overflow levels of Owens Lake, thereby resolving the apparent asynchrony between late Pleistocene overflow records of Owens Lake (Bacon et al., 2006; Reheis et al., 2014) and downstream lake basins (Orme and Orme, 2008; Phillips, 2008; Smith, 2009; Rosenthal et al., 2017). Geotechnical data and lake-level data demonstrated that the overflow area is a dynamic and deeply entrenched channel with soft sill elevations that ranged from the ~40 ka highstand at ~1165 m asl to the hard sill at ~1113 m asl from variable infilling of fluvial-deltaic and alluvial sediment. The lake-level curve shows temporal correspondence in the frequency of oscillating water levels that is controlled by spill of Owens Lake. The record indicates Owens Lake spilled most of the time at or near minimum sill levels that supported moderately sized water levels of Searles Lake between 50 and ~11.5 ka (e.g., Phillips, 2008; Smith, 2009).

Given the range of numerical dating methods used to define water levels, the lake-level curve and reconstruction of sill/spillway levels show the entire system of lakes between Owens and Searles basins were hydrologically connected most of the time with major transgressions of Owens Lake corresponding to sediment aggradation in the overflow channel that coincided with documented periods of glaciations in the Sierra Nevada and global-scale hydroclimate variability associated with abrupt cold/warm oscillations in the North Atlantic region. A steady decrease in spill from Owens Lake at the Pleistocene-Holocene transition influenced progressive desiccation of downstream lakes over ~0.6 to 1.1 ka period with China Lake the last to desiccate by 11.1 ka (e.g., Rosenthal et al., 2017). Owens Lake last spilled from ~8.4 to 6.4 ka during an Early-Middle Holocene transgression that was during a time when other lakes in the southern Sierra Nevada watershed (i.e., Mono and Tulare Lakes) and on the east side of the northern Sierra Nevada (i.e., Pyramid Lake) also expanded.

The good temporal correspondence between the reconstruction of shoreline indictors and spillway and lake bottom positions from this analysis provides confidence in the approach developed in this study to produce an integrated lake-level curve to accurately identify overflow episodes, as well as to estimate the timing, duration, and magnitude of regional climate change. Our integrated approach to generate a continuous lake-level record of Owens Lake with well-defined oscillating water levels is the first step in performing accurate hydrologic water-balance modeling of the paleo-Owens River system and quantify the pattern of hydroclimate variability along south-central Sierra Nevada overt the past 50 ka.

Acknowledgements

Funding for this work was partially provided by U.S. Government Contract #N68936–09–D–0040, National Science Foundation EAR #1252225, and Vice President for Research Office of the Desert Research Institute to S. Bacon. Many discussions with Thomas Bullard throughout the study is gratefully appreciated. The authors acknowledge Ken Adams for field discussions and assistance with luminescence sampling at the Centennial Flat site. The authors thank John Umek for discussions on mollusk aquatic ecology. We also thank the Los Angeles Department of Water and Power (LADWP) for providing access to the Black and Veatch (2013) report and all the geologists from LADWP, Black and Veatch, URS, and Lettis Consultants International, Inc. who worked on the comprehensive assessment of local faulting in the Haiwee Reservoir area.

Appendix A. Supplementary data

References

Adams, K.D., 2003. Age and paleoclimatic significance of late Holocene lakes in the Carson Sink, NV, USA. Quaternary Research 60, 294–306.

Adams, K.D., 2007. Late Holocene sedimentary environments and lake-level fluctuations at Walker Lake, Nevada, USA. Geological Society of America Bulletin 119, 126–139.

Adams, K.D., and Wesnousky, S.G., 1998. Shoreline processes and the age of the Lake Lahontan highstand in the Jessup embayment, Nevada. Geological Society of America Bulletin 110, 1318–1332.

Adams, K.D., and Rhodes, E.J., 2019a. Late Holocene paleohydrology of Walker Lake and the Carson Sink in the western Great Basin, Nevada, USA. Quaternary Research 92, 165–182.

Adams, K.D., and Rhodes, E.J., 2019b. Late Pleistocene to present lake-level fluctuations at Pyramid and Winnemucca Lakes, Nevada, USA. Quaternary Research 92, 146–164.

Adams, K.D., Wesnousky, S.G., and Bills, B.G., 1999. Isostatic rebound, active faulting, and potential geomorphic effects in the Lake Lahontan basin, Nevada and California. Geological Society of America Bulletin, 111, 1739–1756.

Alley, R.B., Mayewski, P.A., Sowers, T., Stuiver, M., Taylor, K.C., Clark, P.U., 1997. Holocene climatic instability: a prominent, widespread event 8200 yr ago. Geology 25, 483–486.

Amos, C.B., Lutz, A.T., Jayko, A.S., Mahan, S.A., Burch Fisher, G., and Unruh, J.R., 2013a, Refining the southern extent of the 1872 Owens Valley earthquake rupture through paleoseismic investigations in the Haiwee Area, southeastern California. Bulletin of the Seismological Society of America 103, 1022–1037.

Antinao, J.J., and McDonald, E., 2013. An enhanced role for the Tropical Pacific on the humid Pleistocene-Holocene transition in southwestern North America. Quaternary Science Reviews 78, p. 319–341.

Argus, D.F., and Gordon, R.G., 1991. Current Sierra Nevada-North America motion from very long baseline interferometry: Implications for the kinematics of the western United States. Geology19, 1085–1088.

Asmerom, Y., Polyak, V.J., Burns, S.J. 2010. Variable winter moisture in the southwestern United States linked to rapid glacial climate shifts. Nature Geoscience 3, 114–117.

Bacon, S.N., and Pezzopane, S.K., 2007. A 25,000-year record of earthquakes on the Owens Valley fault near Lone Pine, California: Implications for recurrence intervals, slip rates, and segmentation models. Geological Society of America Bulletin 119, 823–847.

Bacon, S.N., Jayko, A.S., and McGeehin, J.P., 2005. Holocene and latest Pleistocene oblique dextral faulting on the southern Inyo Mountains fault, Owens Lake basin, California. Bulletin Seismological Society of America 95, 2472–2485.

Bacon, S.N., Lancaster, N., Stine, S., Rhodes, E.J., and McCarley Holder, G.A., 2018. A continuous 4000-year lake-level record of Owens Lake, south-central Sierra Nevada, California, USA. Quaternary Research 90, 276–302.

Bacon, S.N., Bullard, T.F., Keen-Zebert, A.K., Jayko, A.S., and Decker, D.L., in review. Spatiotemporal patterns of distributed slip in southern Owens Valley indicated by deformation of late Pleistocene shorelines, eastern California. Geological Society of America Bulletin.

Bartlein, P.J., and 18 others, 2011. Pollen-based continental climate reconstructions at 6 and 21 ka: a global synthesis. Climate Dynamics 37, 775–802.

Bartov, Y., Enzel, Y., Porat, N., Stein, M., 2007. Evolution of the late Pleistocene-Holocene Dead Sea Basin from sequence stratigraphy of fan deltas and lake-level reconstruction. Journal of Sedimentary Research 77, 680–692.

Beanland, S., and Clark, M.M., 1994. The Owens Valley fault zone, eastern California, and surface rupture associated with the 1872 earthquake. U.S. Geological Survey Bulletin 1982, 29 p.

Benn, D.I., Owens, L.A., Finkel, R.C., and Clemmens, S., 2006. Pleistocene lake outburst floods and fan formation along the eastern Sierra Nevada, California: implications for the interpretation of intermontane lacustrine records. Quaternary Science Reviews 25, 2729–2748.

Benson, L.V., 1993. Factors affecting 14C ages of lacustrine carbonates: timing and duration of the last highstand lake in the Lahontan basin. Quaternary Research 39, 163–174.

Benson, L.V., 1994. Carbonate deposition, Pyramid Lake Subbasin, Nevada: 1. Sequence of formation and elevational distribution of carbonate deposits (Tufas). Palaeogeography, Palaeoclimatology, Palaeoecology 109, 55–87.
Benson, L., 2004. Western Lakes. In: Gillespie, A.R., Porter, S.C., Atwater, B.F. (Eds.), The Quaternary Period in the United States. Elsevier, New York, pp. 185–204.
Benson, L.V., Currey, D.R., Dorn, R.I., Lajoie, K.R., Oviatt, C.G., Robinson, S.W., Smith, G.I., and Stine, S., 1990. Chronology of expansion and contraction of four Great Basin lake systems during the past 35,000 years. Palaeogeography, Palaeoclimatology, Palaeoecology 78, 241–286.
Benson, L., Kashgarian, M., Rubin, M., 1995. Carbonate deposition, Pyramid Lake subbasin, Nevada: 2. Lake levels and polar jet stream positions reconstructed from radiocarbon ages and elevations of carbonates (tufas) deposited in the Lahontan basin. Palaeogeography, Palaeoclimatology, Palaeoecology 117, 1–30.
Benson, L.V., Burdett, J.W., Kashgarian, M., Lund, S.P., Phillips, F.M., Rye, R.O., 1996. Climatic and hydrologic oscillations in the Owens Lake basin and the adjacent Sierra Nevada, California. Science 274, 746–749.
Benson, L., Burdett, J., Lund, S., Kashgarian, M., Mensing, S., 1997. Nearly synchronous climate change in the Northern Hemisphere during the last glacial termination. Nature 388, 263–265.
Benson, L.V., May, H.M., Antweiler, R.C., Brinton, T.I., Kashgarian, M., Smoot, J.P., and Lund, S.P., 1998a. Continuous lake-sediment records of glaciation in the Sierra Nevada between 52,600 and 12,500 ^{14}C yr B.P. Quaternary Research 50, 113–127.
Benson, L.V., Lund, S.P., Burdett, J.W., Kashgarian, M., Rose, T.P., Smoot, J.P., Schwartz, M., 1998b. Correlation of Late-Pleistocene lake-level oscillations in Mono Lake, California, with North Atlantic climate events. Quaternary Research 49, 1–10.
Benson, L., Kashgarian, M., Rye, R., Lund, S., Paillet, F., Smoot, J., Kester, C., Mensing, S., Meko, D., Lindstrom, S., 2002. Holocene multidecadal and multicentennial droughts affecting northern California and Nevada. Quaternary Science Reviews 21, 659–682.
Benson, L.V., Smoot, J.P., Lund, S.P., Mensing, S.A., Foit Jr., F.F., Rye, R.O., 2013. Insights from a synthesis of old and new climate-proxy data from the Pyramid and Winnemucca lake basins for the period 48 to 11.5 cal ka. Quaternary International 310, 62–82.
Birkeland, P.W., 1999. Soils and Geomorphology, 3rd ed., Oxford Univ. Press, New York, p. 372 p.
Bischoff, J.L., Rosenbauer, R.H., and Smith, G.I., 1985. Uranium-series dating of sediments from Searles Lake: differences between continental and marine climate records. Science 227, 1222–1224.
Bischoff, J.L., and Cummins, K., 2001. Wisconsin glaciation of the Sierra Nevada (79,000-15,000 yr B.P.) as recorded by rock flour in sediments of Owens Lake, California. Quaternary Research 55, 14–24.
Black and Veatch, 2013. Local fault considerations for proposed North Haiwee Dam Number 2, Inyo County, California. Project No. 169501 report prepared by Black & Veatch, URS, and Lettis Consultants International for Los Angeles Department of Water and Power, September 24, 2013, 95 p. plus appendices.
Blunt, A.B., and Negrini, R.M., 2015. Lake levels for the past 19,000 years from the TL05-4 cores, Tulare Lake, California, USA: Geophysical and geochemical proxies. Quaternary International 387, 122–130.
Bond G.C., Heinrich H., Broecker W.S., et al. 1992. Evidence for massive discharges of icebergs into the North Atlantic Ocean during the last glacial period. Nature 360, 245–249.
Bowerman, N.D., and Clark, D.H., 2011. Holocene glaciation of the central Sierra Nevada, California. Quaternary Science Reviews 30, 1067–1085.
Brennan, R., Quade, J., 1997. Reliable late-Pleistocene stratigraphic ages and shorter groundwater travel times from ^{14}C fossil snails from the southern Great Basin. Quaternary Research 47, 329–336.
Broecker, W.S., McGee, D., Adams, K.D., Cheng, H., Lawrence Edwards, R., Oviatt, C.G., and Quade, J., 2009. A Great Basin-wide dry episode during the first half of the Mystery Interval? Quaternary Science Reviews 28, 2557–2563.
Clark, D.H., and Gillespie, A.R., 1997. Timing and significance of late-glacial and Holocene cirque glaciation in the Sierra Nevada, California. Quaternary International 38/39, 21–38.
Cohen, A.S., 2003. Paleolimnology: The History and Evolution of Lake Systems. Oxford University Press, New York, NY 500 p.
Cook, E.R., Seager, R., Heim, R.R. Jr., Vose, R.S., Herweijer, C., Woodhouse, C., 2010. Megadrought in North America: placing the IPCC projections of hydroclimate change in a long-term paleoclimate context. Journal of Quaternary Science 25, 48–61.
Dansgaard, W., Johnsen, S.J., Clausen, H.B., Dahl-Jensen, D., Gunderstrup, N.S., Hammer, C.U., Steffensen, J.P., Svein-björnsdottir, A., Jouzel, J., and Bond, G., 1993. Evidence for general instability of past climate from a 250-kyr ice-core record. Nature 364, 218–220.

Davaud, E., and Girardclos, S., 2001. Recent freshwater ooids and oncoids from western Lake Geneva (Switzerland): Indications of a common organically mediated origin. Journal of Sedimentary Research 71, 423–429.

Davidson, G.R., Carnley, M., Lange, T., Galicki, S.J., Douglas, A., 2004. Changes in sediment accumulation rate in oxbow lake following late 9th century clearing of land for agricultural use: A 210Pb, 137Ce, and 14C study in Mississippi, USA. Radiocarbon 46, 755–764.

Dettinger, M.D., Cayan, D.R., Diaz, H.F., Meko, D.M., 1998. North-south precipitation patterns in western North America on interannual-to-decadal timescales. Journal of Climate 11, 3095–3111.

Dokka, R.K., and Travis, C.J., 1990. The role of the Eastern California shear zone in accommodating Pacific-North American plate motion. Geophysical Research Letters 17, 1323–1326.

Ehlers, E.G., and Blatt, H., 1982. Petrology: Igneous, Sedimentary, and Metamorphic. W.H Freeman and Company, New York, 732 p.

Einsele, G., 2000. Sedimentary Basins: Evolution, Facies, and Sediment Budget, second ed. Springer, New York, NY 804 p.

Enzel, Y., Cayan, D.R., Anderson, R.Y., Wells, S.G., 1989. Atmospheric circulation during Holocene lake stands in the Mojave Desert: evidence of regional climate change. Nature 341, 44–48.

Enzel, Y., Wells, S.G., Lancaster, N., 2003. Late Pleistocene lakes along the Mojave River, southeast California. In: Enzel, Y., Wells, S.G., Lancaster, N. (Eds.), Paleoenvironments and Paleohydrology of the Mojave and Southern Great Basin Deserts, Geological Society of America Special Paper 368, pp. 61–77.

Fagherazzi, S., Wiberg, P.L., 2009. Importance of wind conditions, fetch, and water levels on wave-generated shear stresses in shallow intertidal basins. Journal of Geophysical Research 114, F03022. http://dx.doi.org/10.1029/2008JF001139.

Firby, J.R., Sharpe, S.E., Whelan, J.F., Smith, G.R., and Spaulding, W.G., 1997. Paleobiotic and isotopic analysis of mollusks, fish, and plants from core OL-92: Indicators for an open or close lake system. In: Smith, G.I., and Bischoff, J.L., eds., An 800,000-year paleoclimatic record from core OL-92, Owens Lake, southeast California. Geological Society of America Special Paper 317, p. 127–142.

Forester, R.M., Lowenstein, T.K., and Spencer, R.J., 2005. An ostracode based paleolimnologic and paleohydrologic history of Death Valley: 200 to 0 ka. Geological Society of America Bulletin 117, 1379–1386.

Franke, J.G., and Donner, R.V., 2019. Correlating paleoclimate time series: Sources of uncertainty and potential pitfalls. Quaternary Science Reviews 212, 69–79.

Friedman, I., Bischoff, J.L., Johnson, A., Tyler, S.W., Fitts, J.P., 1997. Movement and diffusion of pore fluids in Owens Lake sediment: An 800-k.y. record of saline/fresh cycles in core OL-92. In: Smith, G.I., Bischoff, J.L. (Eds.), An 800,000-year Paleoclimatic Record from Core OL-92, Owens Lake, Southeast California. Geological Society of America Special Paper 317, pp. 49–66.

Gale, H.S., 1914. Salines in the Owens, Searles, and Panamint basins, southeastern California. U.S. Geology Survey Bulletin 580-L, 251-323.

Garcia, A.L., Knott, J.R., Mahan, S.A., Bright, J., 2014. Geochronology and paleoenvironment of pluvial Harper Lake, Mojave Desert, California, USA. Quaternary Research 81, 305–317.

Gillespie, A.R., and Clark, D., 2011. Glaciations in the Sierra Nevada, California, USA. Developments in Quaternary Science 15, 447–462.

Haddon, E.K., Amos, C.B., Zielke, O., Jayko, A.S., Bürgmann, R., 2016. Surface slip during large Owens Valley earthquakes. Geochemical, Geophysical, Geosystems 17, 2239–2269.

Håkanson, L., 1977. The influence of wind, fetch, and water depth on the distribution of sediments in Lake Väern, Sweden. Canadian Journal of Earth Sciences 14, 397–412.

Håkanson, L., Jansson, M., 2002. Principles of Lake Sedimentology. The Blackburn Press, New Jersey.

Hampel, A., and Hetzel, R., 2006. Response of normal faults to glacial-interglacial fluctuations of ice and water masses on Earth's surface. Journal of Geophysical Research 111, B06406.

Handy, R.L., and Spangler, M.G., 2007. Geotechnical Engineering: soil and foundation principles and practice, 5th ed. McGraw-Hill, New York, NY, 904 p.

Hatchett, B.J., Boyle, D.P., Putnam, A.E., Bassett, S.D., 2015. Placing the 2012–2015 California-Nevada drought into a paleoclimatic context: Insights from Walker Lake, California-Nevada, USA. Geophysical Research Letters 42, doi:10.1002/2015GL065841.

Hatchett, B.J., Boyle, D.P., Garner, C.B., Kaplan, M.L., Bassett, S.D., Putnam, A.E., 2019. Sensitivity of a western Great Basin terminal lake to winter northeast Pacific storm track activity and moisture transport. In

Starratt, S.W., and Rosen, M.R., (Eds.), From Saline to Freshwater: The Diversity of Western Lakes in Space and Time: Geological Society of America Special Paper 536, doi.org/10.1130/2018.2536(05).

Heinrich H., 1988. Origin and consequences of cyclic ice rafting in the northeast Atlantic Ocean during the past 130,000 years. Quaternary Research 29, 142–152.

Hemming S.R., 2004. Heinrich events; massive late Pleistocene detritus layers of the North Atlantic and their global climate imprint. Reviews of Geophysics 42: RG1005.1–RG1005.43.

Hoffman, W.R., 2009. Late Pleistocene slip rate along the Panamint Valley fault zone, eastern California. Unpublished M.Sc. Thesis, The Pennsylvania State University, 81 p.

Hollett, K.J., Danskin, W.R., McCafferey, W.F., Walti, C.L., 1991. Geology and water resources of Owens Valley, California. U.S. Geological Survey Water-Supply Paper 2370-B, 77 p.

Hough, S.E., and K. Hutton, 2008. Revisiting the 1872 Owens Valley, California, earthquake. Bulletin Seismological Society of America 98, 931–949.

Hudson, A.M., Quade, J., Ali, G., Boyle, D., Bassett, S., Huntington, K.W., De los Santos, M.G., Cohen, A.S., Lin, K., Wang, X., 2017. Stable C, O and clumped isotope systematics and 14C geochronology of carbonates from the Quaternary Chewaucan closed-basin lake system, Great Basin, USA: Implications for paleoenvironmental reconstructions using carbonates. Geochim. Cosmochim. Acta. 212, 274–302.

Jannik, N.O., Phillips, F.M., Smith, G.I., Elmore, D., 1991. A ^{36}Cl chronology of lacustrine sedimentation in the Pleistocene Owens River system. Geological Society of America Bulletin 103, 1146–1159.

Jayko, A.S., 2009, Surficial geologic map of the Darwin Hills 30' x 60' quadrangle, Inyo County, California: U.S. Geological Survey Scientific Investigations Map 3040, 20 p. pamphlet, 2 plates, scale 1:100,000.

Jayko, A.S., Bacon, S.N., 2008. Late Quaternary MIS 6-8 shoreline features of pluvial Owens Lake, Owens Valley, eastern California. In: Reheis, M.C., Hershler, R., Miller, D.M. (Eds.), Late Cenozoic drainage history of the southwestern Great Basin and lower Colorado River Region: geologic and biotic perspectives, Geol. Soc. Amer. Spec. Paper 439, pp. 185–206.

Jayko, A.S., Forester, R.M., Kaufman, D.S., Phillips, F.M., Yount, J.C., McGeehin, J., Mahan, S.A., 2008. Late Pleistocene lakes and wetlands, Panamint Valley, Inyo County, California. In: Reheis, M.C., Hershler, R., Miller, D.M. (Eds.), Late Cenozoic Drainage History of the Southwestern Great Basin and Lower Colorado River Region: Geologic and biotic perspectives, Geol. Soc. Amer. Spec. Paper 439, pp. 151–184.

Ji, Z.G., 2017. Hydrodynamics and Water Quality: Modeling Rivers, Lakes, and Estuaries. John Wiley & Sons Inc., New Jersey.

Kirby, M.E., Feakins, S.J., Hiner, C.A., Fantozzi, J., Zimmerman, S.R.H., Dingemans, T., Mensing, S.A., 2014. Tropical Pacific forcing of Late-Holocene hydrologic variability in the coastal southwest United States. Quaternary Science Reviews 102, 27–38.

Kirby, M.E., Knell, E.J., Anderson, W.T., Lachniet, M.S., Silveira, E., Palermo, J.,Hiner, C.A., Eeg, H., Arevalo, A., Lucero, R., Murrieta, R., 2015. Evidence for Insolation and Pacific Forcing of Late Glacial through Holocene Climate in the Central Mojave Desert (Silver Lake, CA), Quaternary Research 84, 174–186.

Knott, J.R., Liddicoat, J.C., Coe, R.S., and Negrini, R.M., 2019, Radiocarbon and paleomagnetic chronology of the Searles Lake Formation, San Bernardino County, California, USA. In Starratt, S.W., and Rosen, M.R., eds., From Saline to Freshwater: The Diversity of Western Lakes in Space and Time: Geological Society of America Special Paper 536, doi.org/10.1130/2018.2536(06).

Koehler, P.A., 1995. Late Pleistocene mollusks from the Dolomite site, Owens Lake playa, California. The Veliger 38, 312–318.

Koehler, P.A., and Anderson, R.S., 1994. Full-glacial shoreline vegetation during the maximum highstand at Owens Lake, California. Great Basin Naturalist 54, 142–149.

Lancaster, N., Baker, S., Bacon, S., McCarley-Holder, G., 2015. Owens Lake dune fields: Composition, sources of sand, and transport pathways. Catena 134, 41–49.

Lachniet, M.S., Denniston, R.F., Asmerom, Y., Polyak, V.J., 2014. Orbital control of western North America atmospheric circulation and climate over two glacial cycles. Nat. Commun. 5, 3805.

Le, K., Lee, J., Owen, L.A., and Finkel, R., 2007, Late Quaternary slip rates along the Sierra Nevada frontal fault zone, California: Evidence for slip partitioning across the western margin of the Eastern California shear zone/Basin and Range Province: Geological Society of America Bulletin, v. 119, p. 240–256.

Lee, C.H., 1915. Report on hydrology of Owens Lake basin and the natural soda industry as affected by the Los Angeles Aqueduct diversion. Hydraulic Engineer, Los Angeles, California.

Lee, J., Stockli, D.F., Owen, L.A., Finkel, R.C., and Kislitsyn, R., 2009, Exhumation of the Inyo Mountains, California: Implications for the timing of extension along the western boundary of the Basin and Range

Province and distribution of dextral fault slip rates across the eastern California shear zone: Tectonics, v. 28, TC1001, doi:10.1029/2008TC002295.
Le Roux, J.P., 2010. Sediment entrainment under fully developed waves as a function of water depth, boundary layer thickness, bottom slope and roughness. Sedimentary Geology 223, 143–149.
Litwin, R.J., Smoot, J.P., Durika, N.J., and Smith, G.I., 1999. Calibrating Late Quaternary terrestrial climate signals: radiometrically dated pollen evidence from the southern Sierra Nevada, USA. Quaternary Science Reviews 18, 1151–1171.
Lin, J.C., Broecker, W.S., Hemming, S.R., Hajdas, I., Anderson, R.F., Smith, G.I., Kelley, M., Bonani, G., 1998. A reassessment of U-Th and 14C ages for late-glacial high-frequency hydrological events at Searles Lake, California. Quaternary Research 49, 11–23.
Los Angeles Board of Public Service Commissioners, 1916. Complete report on the construction of the Los Angeles Aqueduct. California Department of Public Service, city of Los Angeles, 331 p.
Lubetkin, L.K.C., and Clark, M.M., 1988, Late Quaternary activity along the Lone Pine fault, eastern California: Geological Society of America Bulletin, v. 100, p. 755–766.
Lund, S.P., Newton, M.S., Hammond, D.E., Davis, O.K., Bradbury, J.P., 1993. Late Quaternary stratigraphy of Owens Lake, California. In: Benson, L.V., (Ed.), Proceedings on the Workshop "Ongoing Paleoclimatic Studies in the Northern Great Basin. U.S. Geological Survey Circular 1119, p. 47–52.
Lyle, M., Heusser, L., Ravelo, C., Yamamoto, M., Barron, J., Diffenbaugh, N.S., Herbert, T., and Andreasen, D., 2012. Out of the tropics: The Pacific, Breat Basin lakes, and late Pleistocene water cycle in the western United States. Science 337, 1629–1633.
MacDonald, G.M., Moser, K.A., Bloom, A.M., Porinchu, D.F., Potito, A.P., Wolfe, B.B., Edwards, A.P., Orme, A.R., and Orme, A.J., 2008. Evidence of temperature depression and hydrological variations in the eastern Sierra Nevada during the Younger Dryas state. Quaternary Research 70, 131–140.
Martin, E.A., and Rice, C.A., 1981. Sampling and analyzing sediment cores for 210Pb geochronology. U.S. Geological Survey Open-File Report 81–983.
Mayewski, P.A., and 15 others, 2004. Holocene climate variability. Quaternary Research 62, 243–255.
McDonald, E.V., McFadden, L.D., Wells, S.G., 2003. Regional response of alluvial fans to the Pleistocene-Holocene climatic transition, Mojave Desert, California: In Enzel, Y., Wells, S.G., Lancaster, N., (Eds.), Paleoenvironments and paleohydrology of the Mojave and southern Great Basin Deserts. Geological Society of America Special Paper 368, p. 189–205.
McFadden, L.D., McDonald, E.V., Wells, S.G., Anderson, K., Quade, J., Forman, S.L., 1998. The vesicular layer and carbonate collars of desert soils and pavements: formation, age and relation to climate change. Geomorphology 24, 101–145.
McGee, D., Moreno-Chamarro, E., Wetlandsall, J., Galbraith, E.D., 2018. Western U.S. lake expansions during Heinrich stadials linked to Pacific Hadley circulation. Science Advances 4, eaav0118, DOI: 10.1126/sciadv.aav0118.
Menking, K.M., 1995. Paleoclimate reconstructions from Owens Lake core OL-92, southeastern California. Unpublished Ph.D. Thesis, University of California Santa Cruz, 169 pp.
Mensing, S.A., 2001. Late-glacial and early Holocene vegetation and climate change near Owens Lake, eastern California. Quaternary Research 55, 57–65.
Mensing, S.A., Sharpe, S.E., Tunno, I., Sada, D.W., Thomas, J.M., Starratt, S., Smith, J., 2013. The Lake Holocene Dry Period: multiproxy evidence for an extended drought between 2800 and 1850 cal yr BP across the central Great Basin, USA. Quaternary Science Reviews 78, 266–282.
Mensing, S.A., Smith, J., Norman, K.B., Allen, M., 2008. Extended drought in the Great Basin of western North America in the last two millennia reconstructed from pollen records. Quaternary International 188, 79–89.
Mifflin, M.D., and Wheat, M.M., 1979. Pluvial lakes and estimated pluvial climates of Nevada: Nevada Bureau of Mines and Geology Bulletin 94, p. 57.
Miller, W., 1989. Pleistocene freshwater mollusks on the floor of Owens Lake playa, eastern California. Tulane Studies in Geology and Paleontology 22, 47–54.
Moore, J.G., and Moring B.C., 2013. Range wide glaciation in the Sierra Nevada, California. Geosphere 9, 1804–1818.
Munroe, J.S., Laabs, B.J.C., 2013. Temporal correspondence between pluvial lake highstands in the southwestern US and Heinrich Event 1. Journal of Quaternary Sciences 28, 49–58.
Murray, A.S. and Wintle, A.G., 2000. Luminescence dating of quartz using an improved single-aliquot regenerative-dose protocol. Radiation Measurements 32, 57–73.

Murray, A.S. and Wintle, A.G., 2003. The single aliquot regenerative dose protocol: potential for improvements in reliability. Radiation Measurements 37, 377–381.

Nayar, K.G., Sharqawy, M.H., Banchik, L.D., Lienhard V., J.H., 2016. Thermophysical properties of seawater: A review and new correlations that include pressure dependence. Desalination 390, 1– 24.

Negrini, R.M., 2002. Pluvial lake sizes in the northwestern Great Basin throughout the Quaternary period. In: Hershler, R., Madsen, D.B., Currey, D. (Eds.), Great Basin Aquatic Systems History: Smithsonian Contributions to the Earth Sciences, vol. 33. Smithsonian Institution Press, Washington, D.C, pp. 11e52.

Negrini, R.M., Wigand, P.E., Draucker, S., Gobalet, K., Gardner, J.K., Sutton, M.Q., Yohe, R.M., 2006. The Rambla highstand shoreline and the Holocene lake-level history of Tulare Lake, California, USA. Quaternary Science Reviews 25, 1599–1618.

Neponset Geophysical Company and Aquila Geosciences, Inc., 1997, Final Report Phase 3 and Phase 4 seismic program, Owens Lake, Inyo County, California. Unpublished report prepared for the Great Basin Unified Air Pollution Control District, Bishop, California, 55 p.

Newton, M.S., 1991. Holocene stratigraphy and magnetostratigraphy of Owens and Mono Lakes, eastern California. Unpublished Ph.D. Thesis, University of Southern California, Los Angeles, 330 pp.

Orme, A.R., and Orme, A.J., 1993. Late Pleistocene oscillations of Lake Owens, eastern California. Geological Society of America Abstracts with Programs 25, 129–130.

Orme, A.R., and Orme, A.J., 2008. Late Pleistocene shorelines of Owens Lake California, and their hydroclimatic and tectonic implications, in Reheis, M.C., Hershler, R., and Miller, D.M., eds., Late Cenozoic Drainage History of the Southwestern Great Basin and Lower Colorado River Region: Geologic and Biotic Perspectives: Geological Society of America Special Paper 439, p. 207–226.

Oster, J.L., Montanez, I.P., Mertz-Kraus, R., Sharp, W.D., Stock, G.M., Spero, H.J., Tinsley, J., Zachos, J.C., 2014. Millennial-scale variations in western Sierra Nevada precipitation during the last glacial cycle MIS 4/3 transition. Quaternary Research 82, 236–248.

Oster, J.L., Ibarra, D.E., Winnick, M.J., and Maher, K., 2015. Steering of westerly storms over western North America at the Last Glacial Maximum. Nature Geoscience 8, 201–205.

Oster, J.L., Montaňez, I.P., Santare, L.R., Sharp, W.D., Wong, C., Cooper, K.M., 2015. Stalagmite records of hydroclimate in central California during termination 1. Quaternary Science Reviews 127, 199–214.

Otvos, E.G., 2000. Beach ridges – definitions and significance. Geomorphology 32, 83–108.

Oviatt, C.G., 1997. Lake Bonneville fluctuations and global climate change. Geology 25, 155–158.

Oviatt, C.G., 2000. Lacustrine features and global climate change, in Noller, J.S., Sowers, J.M., and Lettis, W.R., eds., Quaternary Geochronology: Methods and Applications: AGU Reference Shelf Volume 4: Washington D.C., American Geophysical Union, p. 470–478.

Pakiser, L.C., Kane, M.F., and Jackson, W.H., 1964, Structural geology and volcanism of Owens Valley region, California—a geophysical study: U.S. Geological Survey Professional Paper 438, 65 p.

Peng, T.H., Goddard, J.G., and Broecker, W.S., 1978. A direct comparison of 14C and 230^{Th} ages at Searles Lake, California. Quaternary Research 9, 319–329.

Pengelly, J.W., Tinkler, K.J., Parkins, W.G., and McCarthy, F.M., 1997. 12,600 years of lake level changes, changing sills, ephemeral lakes and Niagara Gorge erosion in the Niagara Peninsula and Eastern Lake Erie basin. Journal of Paleolimnology, 17, 377–402.

Peterson, F.F., 1981. Landforms of the Basin and Range province: defined for soil surveys: Nevada agriculture experiment station, University of Nevada, Reno, Technical Bulletin 28, 52 p.

Phillips, F.M., 2008. Geological and hydrological history of the paleo-Owens River drainage since the late Miocene, in Reheis, M.C., Hershler, R., and Miller, D.M., eds., Late Cenozoic Drainage History of the Southwestern Great Basin and Lower Colorado River Region: Geologic and Biotic Perspectives: Geological Society of America Special Paper 439, p. 115–150.

Phillips, F.M., Zreda, M.G., Benson, L.V. Benson, Plummer, M.A., Elmore, D., and Sharma, P., 1996. Chronology for fluctuations in late Pleistocene Sierra Nevada glaciers and lakes. Science 274, 749–751.

Phillips, F.M., Zreda, M., Plummer, M.A., Elmore, D., and Clark, D.H., 2009. Glacial geology and chronology of Bishop Creek and vicinity, eastern Sierra Nevada, California. Geological Society of America Bulletin 121, 1013–1033.

Pigati, J.S., Quade, J., Shahanan, T.M., Haynes Jr., C.V., 2004. Radiocarbon dating of minute gastropods and new constraints on the timing of late Quaternary spring-discharge deposits in southern Arizona, USA. Palaeogeography, Palaeoclimatology, Palaeoecology 204, 33–45.

Reardon, K.E., Moreno-Casas, P.A., Bombardelli, F.A., Schladow, S.G., 2016. Seasonal nearshore sediment resuspension and water clarity at Lake Tahoe. Lake and Reservoir Management 32, 132–145.

Redmond, K.T., Koch, R.W., 1991. Surface climate and streamflow variability in the western United States and their relationship to large scale circulation indices. Water Resources Research 27, 2381–2399.
Reheis, M.C., 1999. Highest pluvial-lake shorelines and Pleistocene climate of the western Great Basin. Quaternary Research 52, 196–205.
Reheis, M.C., Adams, K.D., Oviatt, C.G., Bacon, S.N., 2014. Pluvial lakes in the Great Basin of the western United States – A view from the outcrop. Quaternary Science Reviews 97, 33–57.
Reheis, M.C., Miller, D.M., McGeehin, J.P., Redwine, J.R., Oviatt, C.G., Bright, J., 2015. Directly dated MIS 3 lake-level record from Lake Manix, Mojave Desert, California, USA. Quaternary Research 83, 187–203.
Rhodes, E.J., 2011. Optically stimulated luminescence dating of sediments over the past 200,000 years. Annual Review of Earth and Planetary Sciences 39, 461–488.
Rhodes, E.J., 2015. Dating sediments using potassium feldspar single-grain IRSL: Initial methodological considerations. Quaternary International 362, 14–22.
Rohweder, J., Rogala, J.T., Johnson, B.L., Anderson, D., Clark, S., Chamberlin, F., Runyon, K., 2008. Application of wind fetch and wave models for habitat rehabilitation and enhancement projects. U.S. Geological Survey Open-File Report 2008–1200. United States Government Printing Office, Washington.
Rood, D.H., Burbank, D.W., and Finkel, R.C., 2011. Chronology of glaciations in the Sierra Nevada, California, from ^{10}Be surface exposure dating. Quaternary Science Reviews 30, 646–661.
Russell, I.C., 1885. Geological history of Lake Lahontan, a Quaternary lake of northwestern Nevada. U.S. Geological Survey Monograph 11, 288 p.
Sharqawy, M.H., Lienhard, J.H., Zubair, S.M., 2010. Thermophysical properties of seawater: a review of existing correlations and data. Desalination and Water Treatment 16, 354–380.
Slemmons, D.B., Vittori, E., Jayko, A.S., Carver, G.A., and Bacon, S.N., 2008, Quaternary fault and lineament map of Owens Valley, Inyo County, eastern California: Geological Society of America Map and Chart 96, 25 p.
Smith, G.I., 1979, Subsurface stratigraphy and geochemistry of Late Quaternary evaporates, Searles Lake, California. U.S. Geological Survey Professional Paper 1043, 130 p.
Smith, G.I., 2009, Late Cenozoic geology and lacustrine history of Searles Valley, Inyo and San Bernardino Counties, California. U.S. Geological Survey Professional Paper 1727, 115 p.
Smith, G.I. and Pratt, W.P., 1957. Core logs from Owens, China, Searles, and Panamint Basins, California. US Geological Survey Bulletin 1045-A, 1–62.
Smith, G.I., and Street-Perrott, F.A., 1983. Pluvial lakes of the western United States. In: Porter, S.C. (Ed.), The Late Pleistocene. Univ. Minn. Press, Minneapolis, pp. 190–212.
Smith, G.I., and Bischoff, J.L., eds., 1997. An 800,000-year paleoclimatic record from core OL-92, Owens Lake, southeast California. Geological Society of America Special Paper 317, 165 p.
Smoot, J.P., Litwin, R.J., Bischoff, J.L., and Lund, S.P., 2000, Sedimentary record of the 1872 earthquake and ‘‘Tsunami’’ at Owens Lake, southeast California: Journal of Sedimentary Geology, v. 135, p. 241–254.
Steponaitis, E., Andrews, A., McGee, D., Quade, J., Hseih, Y.-T., Broecker, W.S., Shuman, B.N., Burns, S.J., Cheng, H., 2015. Mid-Holocene drying of the U.S. Great Basin recorded in Nevada speleothems. Quat. Sci. Rev. 127, 174–85.
Stine, S., 1990. Late Holocene fluctuations of Mono Lake, eastern California. Palaeogeograrphy, Palaeoclimatology, Palaeoecology 78, 333–381.
Stine, S., 1994. Extreme and persistent drought in California and Patagonia during Medieval time. Nature 339, 546–549.
Teeter, A.M., Johnson, B.H., Berger, C., Stelling, G., Scheffner, N. W., Garcia, M.H., Parchure, T.M., 2001. Hydrodynamic and sediment transport modeling with emphasis on shallow-water, vegetated areas (lakes, reservoirs, estuaries and lagoons). Hydrobiologia 444, 1–23.
U.S. Army Corps of Engineers (USACE), 1984. Shore Protection Manual, Volume 1. U.S. Army Engineer Waterways Experiment Station, Vicksburg, MS, U.S.A., 502 p.
U.S. Army Corps of Engineers (USACE), 2002. Coastal Engineering Manual. Washington D.C., U.S. Corps of Engineers, Engineer Manual 1110-2-1100, Part II and III.
U.S. Geological Survey (USGS) and California State Geological Survey, 2016. Quaternary fault and fold database for the United States, accessed June, 2016 from USGS web site: https://earthquake.usgs.gov/hazards/qfaults/.
Wentworth, C.K., 1922. A scale of grade and class terms for clastic sediments. *Journal of* Geology 30, 377–392.

Wernicke, B.P., Friedrich, A.M., Niemi, N.A., Bennett, R.A., and Davis, J.L., 2000. Dynamics of plate boundary fault systems from Basin and Range Geodetic Network (BARGEN) and geologic data: GSA Today 10, 1–7.
Wesnousky, S.G., 2005a. Active faulting in the Walker Lane. Tectonics 24, 1–35.
Wesnousky, S.G., 2005b. The San Andreas and Walker Lane fault systems, western North America: transpression, transtension, cumulative slip and the structural evolution of a major transform plate boundary. Journal of Structural Geology 27, 1505–1512.
Winkle, W.V., and Eaton, F.M., 1910. Quality of the surface waters of California. U.S. Geological Survey, Water-Supply Paper 237, 142 p.
Zehfuss, P.H., Bierman, P.R., Gillespie, A.R., Burke, R.M., and Caffe, M.W., 2001, Slip rates on the Fish Springs fault, Owens Valley, California, deduced from cosmogenic 10Be and 26Al and soil development on fans: Geological Society of America Bulletin, v. 113, p. 241–255.
Zhong, S., Li, J., Whiteman, C.D., Bian, X., Yao, W., 2008. Climatology of high wind events in the Owens Valley, California. Monthly Weather Review 136, 3536–3552.
Zic, M., Negrini, R.M., Wigand, P.E., 2002. Evidence of synchronous climate change across the Northern Hemisphere between the Northern Atlantic and the Northwestern Great Basin, United States. Geology 30, 635–638.

Table 1. Radiocarbon ages from carbonized wood, charcoal, organic sediment, mollusk, ostracode, and tufa from sites in Owens Lake basin used in this study.

Table 2. Results of single-grain post-IR-IRSL dating of fine sand in beach ridge deposits at the Centennial Flat study site in Owens Lake basin.

Table 3. Results of single-grain OSL dating of fine quartz sand at the Owens Lake overflow channel.

Table 4. Vertical slip and subsidence rates used to account for tectonic ground deformation in Owens Lake basin.

Figure 1. Major physiographic features along the eastern escarpment of the southern Sierra Nevada, eastern California in relation to modern playas and pluvial Owens Lake, and other lakes of the paleo-Owens River system during the Recess Peak glaciation (Clark and Gillespie, 1997; Bacon et al., 2006; Orme and Orme, 2008; Hoffman, 2009; Rosenthal et al., 2017). Inset is graphical profile of the chain of lakes downstream of Owens Lake showing the elevations of hard and soft sills, plus playa bottoms of each lake basin (modified after Smith and Bischoff, 1997). Watershed boundaries of lake basins are shown for: CL – China Lake; OL – Owens Lake; PL – Panamint Lake; SL – Searles Lake; and SWV – Salt Wells Valley. Mountain ranges are also shown on the map: AR – Argus Range CR – Coso Range; IM – Inyo Mountains; WM –

White Mountains. Other lakes discussed in text include: LT – Lake Tahoe; TL – Tulare Lake; PL – Pyramid Lake; and WL – Walker Lake.

Figure 2. Simplified fault map of the southern Walker Lane belt/Eastern California shear zone showing active and recently active faults in relation to the distribution of present day and Pleistocene lakes of the paleo-Owens River system. Faults: ALF – Airport Lake fault; AHF – Ash Hills fault; FLVF – Fish Lake Valley fault; HMF – Hunter Mountain fault; IMF – Inyo Mountains fault; LLF – Little Lake fault; NDVF – Northern Death Valley fault; OVF – Owens Valley fault; PVF – Panamint Valley fault; SDVF – Southern Death Valley fault; SLF – Stateline fault; SNFF – Sierra Nevada frontal fault; SVF – Searles Valley fault; and WMF – White Mountains fault. Lake basins: OL – Owens Lake; CL – China Lake; SL – Searles Lake; PL – Panamint Lake; LM – Lake Manly. (faults after Lee et al., 2009).

Figure 3. Map of the southern Owens River watershed showing the elevations of prominent beach ridges with Holocene and late Pleistocene post-IR-IRSL (~12.8 ka) and ^{14}C ages for shoreline deposits at similar elevations. Beach ridges with Late Holocene post-IRSL and ^{14}C ages at 1108 m asl (~3.6 ka), 1103 m asl (~0.8 ka), 1099–1101 m asl (~0.35 ka) are not shown (Bacon et al., 2018). The extent of the late Pleistocene highstand shoreline (~1165 m asl) with a post-IR-IRSL age of ~40 ka is also shown (Bacon et al., in review). The modern extent of the playa below an elevation of ~1096 m asl and location of lake-core sites OL-84B, OL-90, and OL-92 are shown with white circles. The name and location of study sites described in text are shown by white boxes and leader lines. Rectangle shows areal extent of map on Figure 5A. Faults shown on map include: KF – Keeler fault; OR-CFF – Owens River-Centennial Flat Fault; OVF – Owens Valley fault; SFF – Sage Flat fault; SIMF – Southern Inyo Mountains fault; SNFF – Sierra Nevada frontal fault. Major physiographic features and towns shown on map include: LP – Lone Pine; RV – Rose Valley.

Figure 4. Views of the ~40 ka highstand beach ridge at ~1165 m asl and location of infrared-stimulated luminescence (IRSL) sampling of five beach ridges between ~1114 and 1131 m asl at the Centennial Flat site (Fig. 3). Stars and numbers of sample sites are shown with associated post-IR-IRSL ages. Below is geomorphic profile across the site showing up to twelve shoreline

features between the highstand beach ridge at ~1165 m asl and lowest shorelines at ~1096 m asl (see Fig. 3 for location of transect). The lower five shoreline features range from historical (AD 1872–1878) beach ridges along the playa margin to Neopluvial (~3.5 ka) beach ridges and shoreline scarps formed up to ~1108 m asl (Bacon et al., 2018). Correlated ages from previously published studies for shoreline features at ~1114 and 1120 m asl are also shown.

Figure 5. Owens Lake overflow channel: (A) hillshade map and elevation contours of the ~40 ka highstand shoreline (~1165 m asl), Early-Middle Holocene beach ridges of the Centennial Flat site (1114–1131 m), and historical (AD 1872–1878) lake level at ~1096 m asl. The location of the north and south dams of Haiwee Reservoir and a large landslide feature in the southern reach of the channel are shown. Nearby faults are also shown including: OVF – Owens Valley fault; SFF – Sage Flat fault; SNFF – Sierra Nevada frontal fault. Location of geomorphic profiles A–A’, B–B’, and C–C’ (Figs. 6 and 7) are shown; and (B) pre-construction topography of the Haiwee Reservoir dam site (Los Angeles Board of Public Service Commissioners, 1916). The location of the modern sill of the lake basin at ~1145 m asl and nearby faults are shown.

Figure 6. Geologic cross sections along longitudinal (A–A’) and transverse (B–B’) transects of the Owens Lake overflow channel showing the morphometery and position of strath surfaces (see Fig. 5A for positions of section lines). The topographic profile shown on A–A’ within the limits of Haiwee Reservoir is from pre-construction topography (Fig. 5B) and shows the transverse profiles of four coalescing alluvial fans that have formed within the confined reaches of the channel. Geology shown on cross section B–B’ is based on a geotechnical investigation that included a transect of 10 exploratory sonic borings, 31 cone penetration testing probes, and seismic reflection surveys across the width of the channel (Black and Veatch, 2013). Geology shown at the southern reach of the channel is from a geologic cross section of foundation materials from exploratory excavations prior to construction of the south dam (Los Angeles Board of Public Service Commissioners, 1916). Age control is from ^{14}C dating of wood in trenches and OSL dating of sands collected in situ from boring SB-12-09 that yielded latest Pleistocene to middle Holocene ages for channel fill. The bottom of the channel at transect B–B’ is a hard sill that provides minimum elevation constraints for potential overflowing water levels of Owens Lake at 1112.8 ± 2.7 m asl.

Figure 7. Geomorphic profiles across the southern reach of the Owens Lake overflow channel at transects C–C' and D–D' (see Fig. 5A for positions of section lines) showing sharp breaks-in-slope, benches, and channel features. These features may be evidence of potential sill areas associated with late Pleistocene highstands of Owens Lake that reached elevations of ~1145 m asl at ~40 ka (Bacon et al., in review) and up to ~1180 m at ~160 ka (Jayko and Bacon, 2008). Profiles were developed from USGS 10-m-resolution DEM.

Figure 8. Views of the outlet of the Owens Lake overflow channel showing: (A) broad inset terrace formed across the toe of older alluvial fans and a knob underlain by resistant volcanic rock of the Coso Formation with a surface elevation of ~1165 m asl, view to the south-southwest into Rose Valley; and (B) large landslide feature, as well as same features described in part A, view to north-northeast. The elevation of the knob coincides with the elevation of the ~40 ka shoreline of Owens Lake. The geomorphology of the outlet terrace appears to be a remnant of the distal portion of an alluvial fan that formed within the overflow channel.

Figure 9. Threshold lake-water depth curves for particle entrainment of coarse pebble, coarse sand, coarse silt, and clay corresponding to fetch at wind speeds of (A) 7 m/s and (B) 18 m/s. The depth and corresponding fetch at which there is no particle entrainment is shown for each particle size.

Figure 10. Refined lake-level curve and reconstructions of sill and lake bottom elevations of Owens Lake since 50 ka. The lake-level curve is a compilation of stratigraphic, geomorphic, and lake core data from new investigations of this study and previously published studies. (see Tables 1–3 and Fig. 3 for ages and study sites, and text for a more complete description of data and methods).

Figure 11. Comparison of shoreline and proxy records since 50 ka including: (A) Owens lake-level curve; (B) $\delta^{18}O$ ice core record from the North Greenland Ice Core Project (NGICP; Andersen et al., 2004); and Owens Lake OL-84B and OL-90 lake core proxies corrected for sediment compaction and reservoir effects showing variations in (C) $\delta^{18}O$; (D) total organic

carbon (TOC); and (E) total organic carbon (TIC) (Benson et al., 1996, 1997). Blue lines represent Owens Lake transgressions. Gray vertical bars are Heinrich stadials (or events) 1–4 (HS1–4) and Younger Dryas (YD) stadial. Green vertical bars are periods of Holocene global climate change (Mayewski et al., 2004). Interstadials related to Dansgaard–Oeschger (D–O) cycles, Allerød (A), and Bølling (B) are shown. Glaciations in the Sierra Nevada are also shown: RPG – Recess Peak glaciation and LIA – Little Ice Age. Relative cool and wet period in the Sierra Nevada referred to as the Neopluvial (NP) is shown.

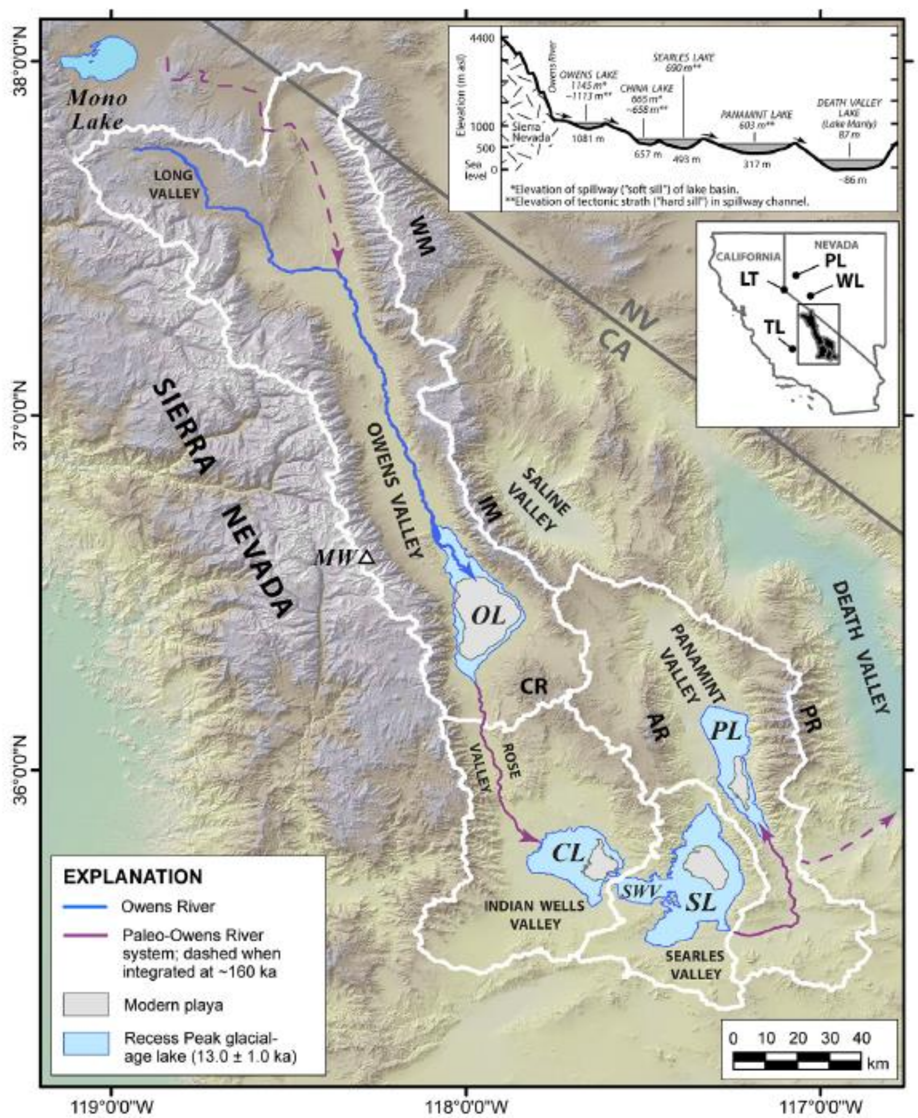

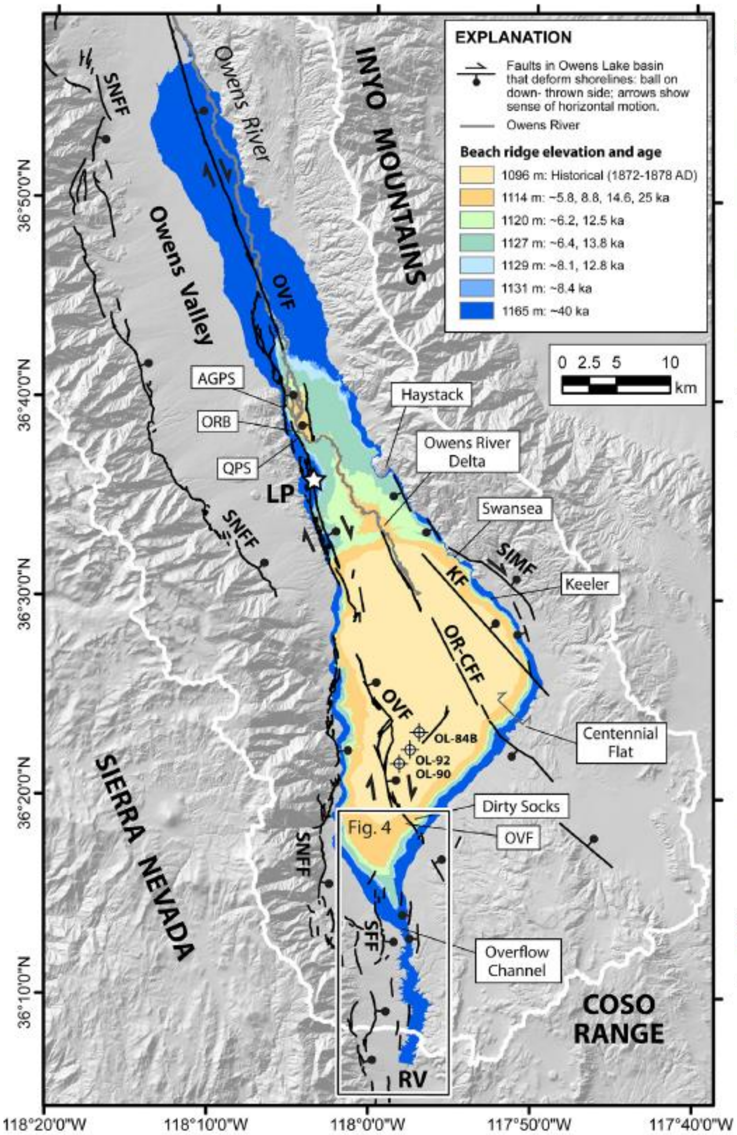

Table 1
Radiocarbon dates from carbonized wood, charcoal, organic sediment, mollusk, ostracode, and tufa from sites in Owens Lake basin used in this study.

Sample Locality	Sample Elevation (meters)	Corrected Elevation[a] (meters)	Material Dated	^{14}C yr BP	$\delta^{13}C/\delta^{12}C$ (‰)	cal yr BP[b] Median Probability[c]	2-σ Range	Lab No.	Ref.
Dirty Socks	1102.8	1117.2	*Anodonta californiensis*	34,700 ± 320	0	38,920	38,300–39,700	USGS-WW8661	1
Dirty Socks	1101.8	1116.3	*Sphaerium striatinum*	35,160 ± 340	0	39,380	38,640–40,150	USGS-WW8662	1
Dirty Socks	1102.4	1119.3	*Sphaerium striatinum*	42,560 ± 840	0	45,580	44,040–47,270	USGS-WW8663	1
Dirty Socks	1103.4	1116.5	gastropod	31,730 ± 230	0	35,310	34,800–35,850	USGS-WW8664	1
Dirty Socks	1104.7	1120.0	*Anodonta californiensis*	36,910 ± 420	0	41,200	40,340–41,920	USGS-WW8665	1
Dirty Socks	1106.9	1111.1	*Anodonta californiensis*	10,345 ± 30	0	11,540	11,300–11,750	USGS-WW8667	1
OVF	1105.0	1108.7	gastropod	24,200 ± 130	−3.0	27,940	27,690–28,270	USGS-WW8693	1
OVF	1107.5	1109.2	*Anodonta californiensis*	11,630 ± 35	−2.6	13,180	13,090–13,270	USGS-WW8695	1
OVF	1114.4	1117.0	ostracode	16,900 ± 50	0	20,030	19,830–20,200	USGS-WW8669	1
OVF	1122.1	1123.8	*Anodonta californiensis*	11,435 ± 35	0	13,030	12,900–13,100	USGS-WW8672	1
Swansea	1109.0	1113.1	*Helisoma newberryi*	14,460 ± 45	−3.2	17,240	17,060–17,450	USGS-WW8697	1
Swansea	1108.1	1110.8	carbonate, tufa	10,280 ± 40	−1.8	11,430	11,260–11,620	Beta-299,115	1
Overflow Ch.	1135.5	1134.8	charcoal	5060 ± 30	−11.2	5820	5740–5900	Beta-335,354	2
Swansea	1118.9	1121.5	*Helisoma newberryi*	9870 ± 90	−2.3	10,920	10,610–11,190	Beta-158,755	3
Swansea	1118.5	1122.3	*Anodonta californiensis*	13,340 ± 40	0	15,630	15,370–15,810	USGS-WW4782	3
Keeler	1124.0	1128.6	carbonate, tufa	16,320 ± 90	+3.5	19,330	19,060–19,580	Beta-166,887	3
Keeler	1111.0	1114.1	carbonate, tufa	11,320 ± 70	+2.2	12,890	12,740–13,040	Beta-166,888	3
Keeler	1111.0	1116.9	*Anodonta californiensis*	20,680 ± 120	−2.8	24,490	24,140–24,960	Beta-166,889	3
Keeler	1111.0	1114.0	carbonate, tufa	10,970 ± 70	+2.2	12,630	12,440–12,730	Beta-166,890	3
Keeler	1111.0	1117.1	*Anodonta californiensis*	21,300 ± 100	0	25,360	25,080–25,610	USGS-WW4044	3
Keeler	1111.0	1115.2	carbonate, tufa	14,810 ± 40	0	17,690	17,520–17,880	USGS-WW4045	3
ORB; OR-2B	1113.0	1117.2	carbonized wood	9990 ± 40	−22.1	11,450	11,270–11,700	Beta-163,551	3
ORB; OR-2A	1113.0	1117.6	organic sediment	10,480 ± 40	−26.1	12,450	12,150–12,570	Beta-163,552	3
ORB; OR-4	1112.5	1116.5	organic sediment	9560 ± 40	−25.4	10,930	10,730–11,090	Beta-163,553	3
AGPS; T2	1121.8	1125.6	carbonized wood	9060 ± 40	−23.9	10,220	10,180–10,260	Beta-163,554	3,4
AGPS; T2	1121.8	1125.6	organic sediment	9030 ± 60	−25.4	10,200	9920–10,290	Beta-163,555	3,4
Sample Locality	Sample Elevation (meters)	Corrected Elevation[a] (meters)	Material Dated	^{14}C yr BP	$\delta^{13}C/\delta^{12}C$ (‰)	cal yr BP[b] Median Probability[c]	2-σ Range	Lab No.	Ref.
QPS; T4	1116.8	1120.6	organic sediment	9160 ± 50	−25.2	10,330	10,230 −10,490	Beta-163,556	3,4
QPS; T4	1116.8	1120.9	organic sediment	9680 ± 50	−25.1	11,110	10,790 −11,220	Beta-163,557	3,4
QPS; T4	1116.8	1121.0	charcoal	9920 ± 50	−24.7	11,330	11,230 −11,600	Beta-163,558	3,4
QPS; T4	1116.8	1120.7	charcoal	9300 ± 60	−25.3	10,490	10,280 −10,660	Beta-163,500	3,4
QPS; T5	1120.5	1121.6	carbonate, tufa	7910 ± 60	−3.2	8410	8330–8540	Beta-163,561	3,4
QPS; P4	1114.5	1117.3	carbonate, tufa	6910 ± 60	−1.2	7500	7430–7580	Beta-168,599	3,4
QPS; P4	1111.5	1117.0	carbonized wood	12,580 ± 60	−27.8	14,920	14,530 −15,180	Beta-168,600	3,4
QPS; P4	1111.5	1117.0	carbonized wood	12,590 ± 60	−28.2	14,940	14,580 −15,200	Beta-168,601	3,4
QPS; P4	1111.5	1117.1	carbonized wood	12,730 ± 60	−28.7	15,170	14,910 −15,360	Beta-168,602	3,4
Swansea	1117.0	1119.5	*Helisoma newberryi*	9580 ± 100	n/r	10,470	10,240 −10,700	Beta-58386	5
Swansea	1118.0	1121.0	*Anodonta californiensis*	10,840 ± 80	n/r	12,490	12,150 −12,690	Beta-82063	5
Swansea	1119.0	1122.0	*Anodonta californiensis*	10,940 ± 70	n/r	12,610	12,430 −12,720	Beta-52398	5
Swansea	1123.0	1126.1	*Anodonta californiensis*	11,450 ± 70	n/r	13,010	12,810 −13,130	Beta-54341	5
Owens River delta	1107.0	1111.9	*Anodonta californiensis*	11,700 ± 110	n/r	13,250	13,070 −13,450	Beta-82061	5
Swansea	1126.0	1129.3	*Anodonta californiensis*	12,210 ± 130	n/r	13,750	13,470 −14,060	Beta-51957	5
Swansea	1114.0	1119.6	*Amnicola paluustris*	19,670 ± 260	n/r	23,330	22,690 −23,960	Beta-61076	5
Centennial Flat	1111.0	1114.5	*Anodonta californiensis*	12,760 ± 80	n/r	14,610	14,210 −15,040	Beta-82062	5
Centennial Flat	1130.0	1139.3	*Helisoma newberryi*	34,540 ± 500	n/r	38,730	37,250 −39,920	Beta-82062	5
AGPS; T3	1122.0	1126.4	charcoal	10,190 ± 70	n/r	11,880	11,410 −12,150	USGS-2339	6
Owens River delta	1097.0	1101.8	*Anodonta californiensis*	11,400 ± 60	n/r	12,960	12,810 −13,080	Beta-67673	7
Haystack	1155	1161–1163	Packrat midden; wood	14,870 ± 130 to 22,900 ± 270	n/r	18,090 to 27,200	17,770 to 27,650	Beta-39274; 39,273	8

Notes: n/r = not reported; Radiocarbon dates determined based on accelerator mass spectrometry (AMS) by Jack McGeehin, US Geological Survey (USGS-WW), Reston, Virginia and Beta Analytical Inc. (Beta), Miami, Florida, USA. References: (1) this study; (2) Black and Veatch (2013); (3) Bacon et al. (2006); (4) Bacon and Pezzopane (2007); (5) Orme and Orme (2008); (6) Beanland and Clark (1994); (7) Koehler (1995); (8) Koehler and Anderson (1994).

[a] Elevation corrected for tectonic deformation based on fault rates and tectonic block model of Bacon et al. (2019a).

[b] A 300-yr reservoir correction is applied to radiocarbon dates from mollusk, ostracodes, and tufa based on study of Lin et al. (1998) in Searles Lake basin; radiocarbon dates are calibrated at ±2σ using CALIB7.1 program (Stuiver and Reimer, 1993) with the IntCal13 data set (Reimer et al., 2013).

[c] Median probability of the calibrated age falling within the reported range as calculated by CALIB7.1 program.

Table 2
Results of single-grain post-IR-IRSL dating of fine sand in beach ridge deposits at the Centennial Flat study site in Owens Lake basin.

Site	Landform	Latitude (°N)	Longitude (°W)	Elevation[a] (m)	Field sample number	Depth (m)	Sample Elevation[b] (m)	Dose rate (Gy/ka)	Mean equivalent dose (Gy)	Age[c] (ka)
Centennial Flat	Beach ridge	36.4018	−117.8518	1131.3	OL814-1	1.14	1132.2	3.91 ± 0.18	32.6 ± 1.7	8.4 ± 0.6
Centennial Flat	Beach ridge	36.4017	−117.8529	1129.4	OL814-2	0.80	1130.6	4.13 ± 0.20	33.6 ± 1.8	8.1 ± 0.6
Centennial Flat	Beach ridge	36.4017	−117.8529	1129.4	OL814-4	1.55	1130.9	3.96 ± 0.18	50.8 ± 3.5	12.8 ± 1.1
Centennial Flat	Beach ridge	36.4021	−117.8531	1127.5	OL814-5	0.40	1128.5	4.59 ± 0.25	27.5 ± 1.7	6.0 ± 0.5
Centennial Flat	Beach ridge	36.4021	−117.8531	1127.5	OL814-6	0.60	1128.5	4.21 ± 0.22	28.2 ± 1.7	6.7 ± 0.5
Centennial Flat	Beach ridge	36.4022	−117.8533	1126.7	OL814-8	0.50	1128.0	4.25 ± 0.22	32.2 ± 1.8	7.6 ± 0.6
Centennial Flat	Beach ridge	36.4033	−117.8555	1120.9	OL814-9	0.90	1121.4	3.67 ± 0.16	21.5 ± 1.3	5.9 ± 0.5
Centennial Flat	Beach ridge	36.4033	−117.8555	1120.9	OL814-10	1.00	1121.5	4.05 ± 0.19	26.4 ± 1.4	6.5 ± 0.5
Centennial Flat	Beach ridge	36.4063	−117.8565	1113.6	OL814-11	1.15	1113.8	4.12 ± 0.20	24.0 ± 1.3	5.8 ± 0.4
Centennial Flat	Beach ridge	36.4063	−117.8565	1113.6	OL814-12	1.15	1114.6	4.10 ± 0.20	36.2 ± 1.8	8.8 ± 0.6

Note: Analysis performed at University of California Los Angeles Luminescence Laboratory, Los Angeles, California. Uncertainty reported at 1σ.

[a] Elevation of surface of sample site. Elevation surveyed with GPS with real-time differential correction with 18–69 cm vertical accuracy.

[b] Elevation of sample is corrected for tectonic ground deformation.

[c] Ages are presented as years before AD 2015.

Table 3
Results of single-grain OSL dating of fine sand at the Owens Lake overflow channel.

Sample site[a]	Sedimentary facies	Latitude (°N)	Longitude (°W)	Field sample number	Elevation[c] (m)	Depth (m)	Sample elevation[d] (m)	Dose rate (Gy/ka)	Mean equivalent dose (Gy)	Age[f] (ka)
Boring SB-12-09	Fluvial-deltaic	36.2331	−117.9649	HD 1	1136.9	9.4	1126.9	4.20 ± 0.21	28.93 ± 4.19	6.9 ± 1.1
Boring SB-12-09	Fluvial-deltaic	36.2331	−117.9649	HD 2	1136.9	13.4	1122.5	3.81 ± 0.21	28.87 ± 4.58	7.6 ± 1.3
Boring SB-12-09	Fluvial-deltaic	36.2331	−117.9649	HD 3	1136.9	16.4	1118.9	4.25 ± 0.25	49.22 ± 7.21	11.6 ± 1.8
Eastern channel	Colluvium	36.2246	−117.9597	HD 6[b]	1166	1.4	1161.9	5.16 ± 0.23	106.33 ± 33.52	22.8 ± 8.4
Eastern channel	Colluvium	36.2246	−117.9597	HD 7-1[b]	1163	2.1	1157.4[e]	4.97 ± 0.23	144.73 ± 86.00	29.1 ± 8.0
Eastern channel	Colluvium	36.2246	−117.9597	HD 7-2[b]	1163	2.1	1157.4[e]	4.97 ± 0.23	12.83 ± 2.01	21.4 ± 9.5
Eastern channel	Colluvium	36.2251	−117.9597	HD 8	1164	0.6	1162.5	5.00 ± 0.23	38.28 ± 7.06	7.7 ± 1.5
Eastern channel	Colluvium	36.2247	−117.9598	HD 9[b]	1170	0.8	1167.6	5.17 ± 0.23	134.07 ± 17.45	35.9 ± 13.7

Note: Analysis performed at University of Cincinnati Luminescence Dating Laboratory, Cincinnati, Ohio.
[a] Samples from sites of geotechnical study at Owens Lake basin overflow area by Black and Veatch (2013) and Goetz et al. (2016).
[b] Sample group does not behave well and their age estimation has large error.
[c] Elevation of surface of sample site. All elevations surveyed by licensed land surveyor.
[d] Elevation of sample is corrected for tectonic ground deformation.
[e] Elevation of sample corrected for tectonic ground deformation based on mean age of 25.3 ka for samples HD 7–1 and 7–2.
[f] Ages are presented as years before AD 2012.

Table 4
Vertical slip and subsidence rates used to account for tectonic ground deformation in Owens Lake basin.

Fault system	Type of fault	Vertical slip rate (m/ka)	Source
Eastern lake basin subsidence	n/a	0.24 ± 0.06	Bacon et al. (2019a)
Southern Owens Valley fault	dextral-oblique	0.12 ± 0.04	Bacon and Pezzopane (2007)
Southern Sierra Nevada frontal fault	normal	0.25 ± 0.05	Le et al. (2007)
Sage Flat fault	normal	0.09 ± 0.01	Amos et al. (2013)

Note: n/a = not applicable.

2217

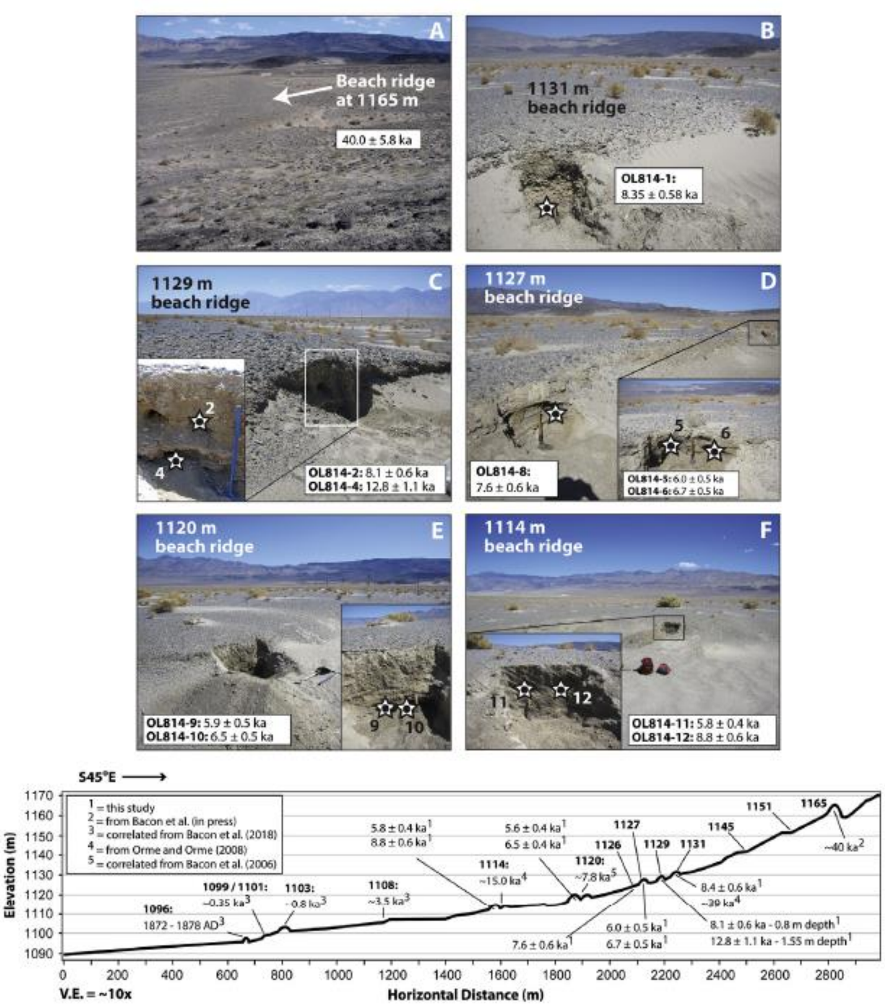

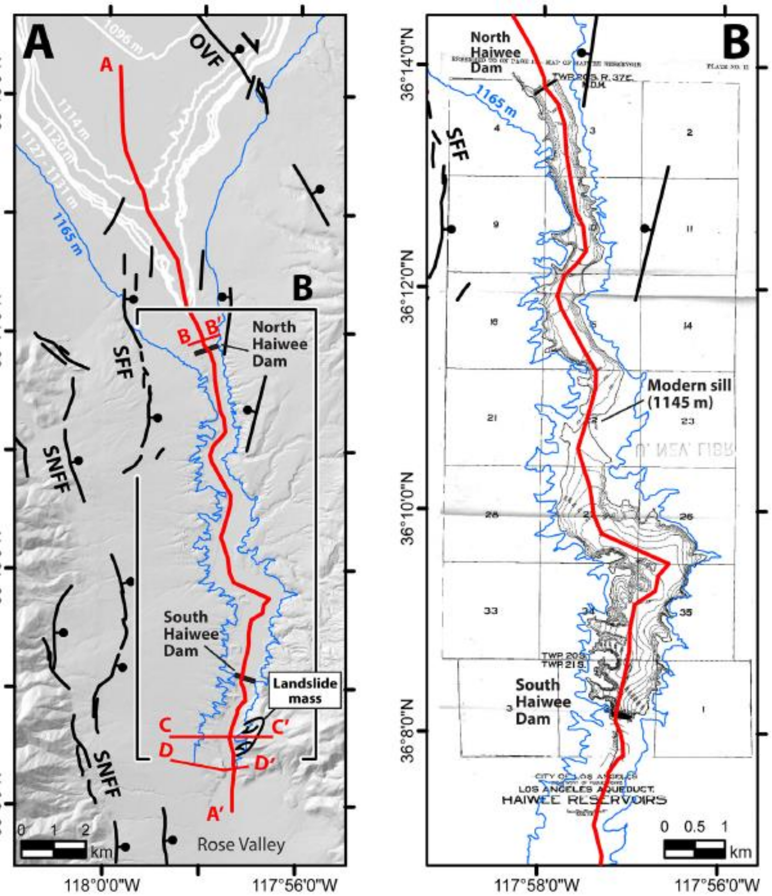

A
B
A
A'
B
B'
C
C'
D
D'
OVF
SFF
SNFF
1165 m
1095 m
1114 m
1120 m
1127 m
1131 m
North Haiwee Dam
South Haiwee Dam
Landslide mass
Rose Valley
Modern sill (1145 m)
LOS ANGELES AQUEDUCT
HAIWEE RESERVOIRS
36°18'0"N
36°14'0"N
36°10'0"N
36°6'0"N
36°12'0"N
36°8'0"N
118°0'0"W
117°56'0"W
117°58'0"W
0 1 2 km
0 0.5 1 km

252

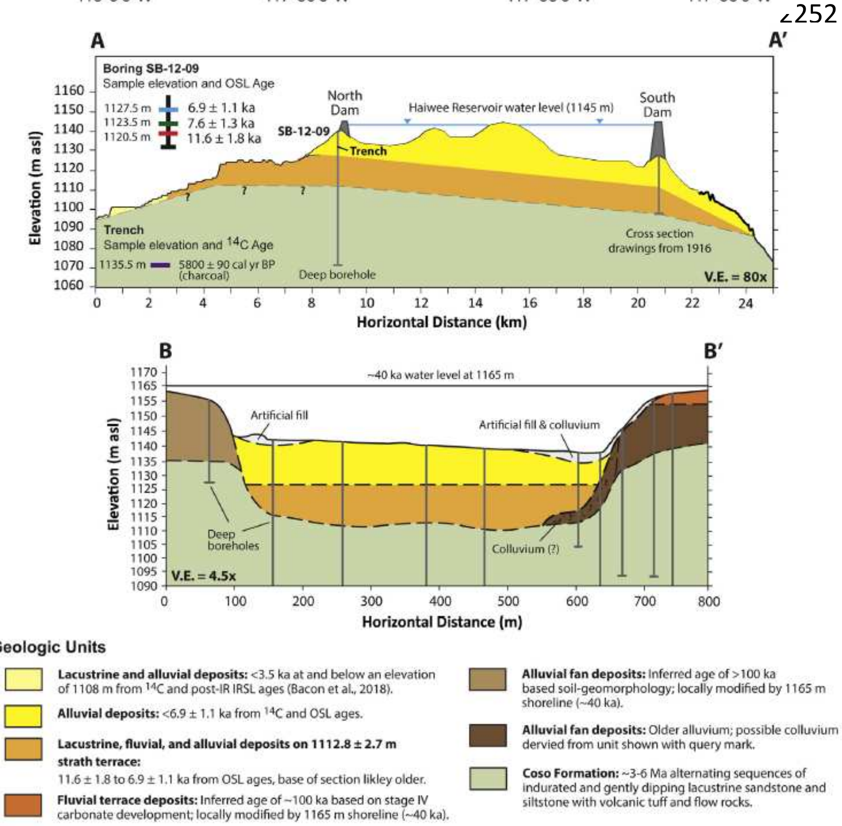

A
A'
Boring SB-12-09
Sample elevation and OSL Age
1127.5 m 6.9 ± 1.1 ka
1123.5 m 7.6 ± 1.3 ka
1120.5 m 11.6 ± 1.8 ka
North Dam
South Dam
Haiwee Reservoir water level (1145 m)
SB-12-09
Trench
Trench
Sample elevation and 14C Age
1135.5 m 5800 ± 90 cal yr BP (charcoal)
Deep borehole
Cross section drawings from 1916
V.E. = 80x
Elevation (m asl)
Horizontal Distance (km)
B
B'
~40 ka water level at 1165 m
Artificial fill
Artificial fill & colluvium
Deep boreholes
Colluvium (?)
V.E. = 4.5x
Elevation (m asl)
Horizontal Distance (m)
Geologic Units
Lacustrine and alluvial deposits: <3.5 ka at and below an elevation of 1108 m from 14C and post-IR IRSL ages (Bacon et al., 2018).
Alluvial deposits: <6.9 ± 1.1 ka from 14C and OSL ages.
Lacustrine, fluvial, and alluvial deposits on 1112.8 ± 2.7 m strath terrace:
11.6 ± 1.8 to 6.9 ± 1.1 ka from OSL ages, base of section likley older.
Fluvial terrace deposits: Inferred age of ~100 ka based on stage IV carbonate development; locally modified by 1165 m shoreline (~40 ka).
Alluvial fan deposits: Inferred age of >100 ka based soil-geomorphology; locally modified by 1165 m shoreline (~40 ka).
Alluvial fan deposits: Older alluvium; possible colluvium dervied from unit shown with query mark.
Coso Formation: ~3-6 Ma alternating sequences of indurated and gently dipping lacustrine sandstone and siltstone with volcanic tuff and flow rocks.

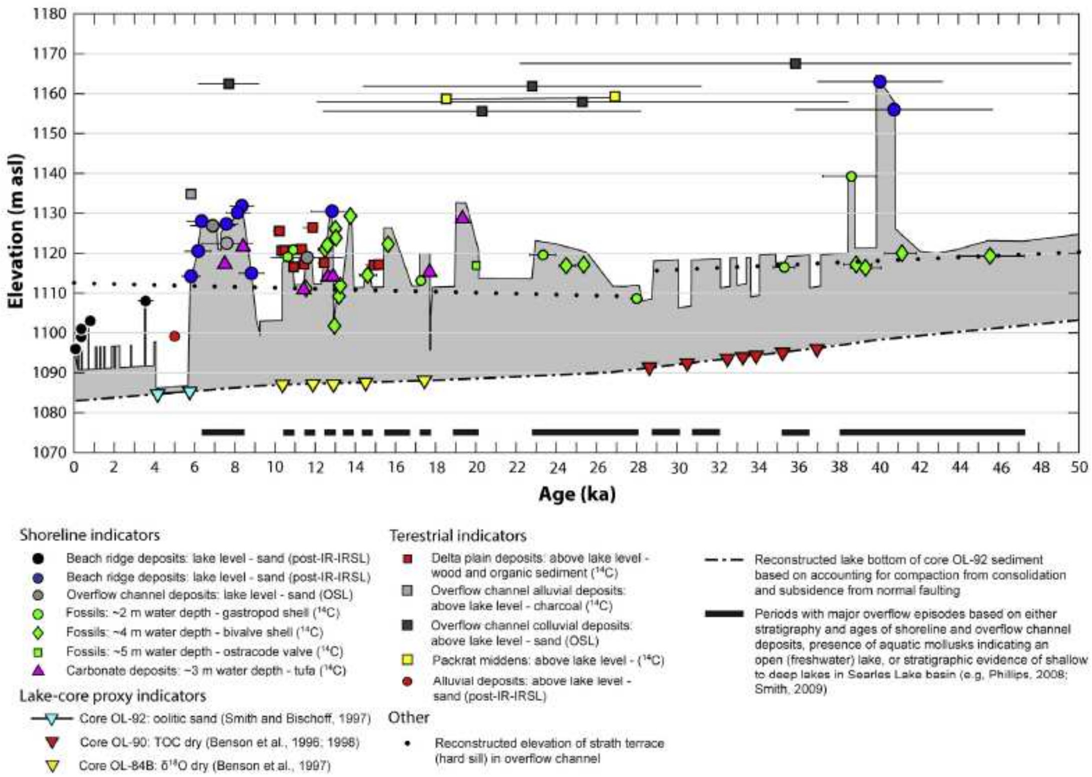
Elevation (m asl)
Age (ka)
Shoreline indicators
Beach ridge deposits: lake level - sand (post-IR-IRSL)
Beach ridge deposits: lake level - sand (post-IR-IRSL)
Overflow channel deposits: lake level - sand (OSL)
Fossils: ~2 m water depth - gastropod shell (14C)
Fossils: ~4 m water depth - bivalve shell (14C)
Fossils: ~5 m water depth - ostracode valve (14C)
Carbonate deposits: ~3 m water depth - tufa (14C)
Lake-core proxy indicators
Core OL-92: oolitic sand (Smith and Bischoff, 1997)
Core OL-90: TOC dry (Benson et al., 1996; 1998)
Core OL-84B: δ18O dry (Benson et al., 1997)
Terestrial indicators
Delta plain deposits: above lake level - wood and organic sediment (14C)
Overflow channel alluvial deposits: above lake level - charcoal (14C)
Overflow channel colluvial deposits: above lake level - sand (OSL)
Packrat middens: above lake level - (14C)
Alluvial deposits: above lake level - sand (post-IR-IRSL)
Other
Reconstructed elevation of strath terrace (hard sill) in overflow channel
Reconstructed lake bottom of core OL-92 sediment based on accounting for compaction from consolidation and subsidence from normal faulting
Periods with major overflow episodes based on either stratigraphy and ages of shoreline and overflow channel deposits, presence of aquatic mollusks indicating an open (freshwater) lake, or stratigraphic evidence of shallow to deep lakes in Searles Lake basin (e.g, Phillips, 2008; Smith, 2009)

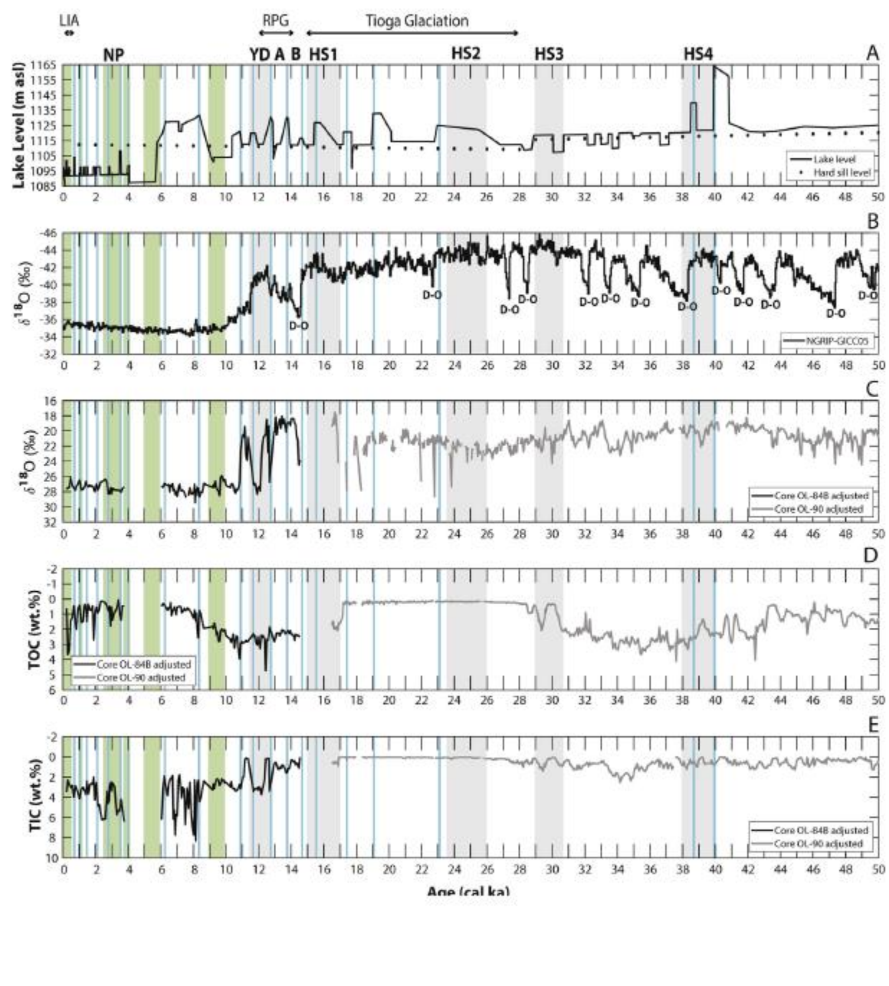
LIA
RPG
Tioga Glaciation
NP
YD A B HS1
HS2
HS3
HS4
A
Lake Level (m asl)
Lake level
Hard sill level
B
δ18O (‰)
D-O
NGRIP-GICC05
C
δ18O (‰)
Core OL-84B adjusted
Core OL-90 adjusted
D
TOC (wt.%)
E
TIC (wt.%)
Age (cal ka)